Measurement and Simulation of Environmental Controls on Vegetation Water Use for Selected Native Species in South Australia

BY

HAILONG WANG

As a requirement in full for the degree of

Doctor of Philosophy

National Centre for Groundwater Research and Training &

School of the Environment

Flinders University of South Australia

Submitted in October, 2014

Revised in March, 2015

To My Wife

YUNHUI GUO

And My Son

ZHIBIN WANG

Table of Contents

List of Tables

List of Tables in Appendix

List of Figures

List of Figures in Appendix

Summary

Plants need water to survive, so the distribution, structure and composition of plant communities are influenced by water availability, at the same time, plants are a major conduit for water to return to the atmosphere, and hence influence climate and exert strong effects on hydrologic fluxes in the land-atmosphere system. Ecohydrological studies typically focus on the understanding of the interactions between hydrologic and ecosystem processes, and how these processes are manifested across spatiotemporal scales. In recent years, ecohydrologists have increased emphasis on understanding the plant-water relations, especially the vegetation water use and mechanisms controlling the responses to environmental conditions. Understanding the species-specific patterns of plant water use and the connections with atmospheric conditions is useful for improving land and water management through afforestation/deforestation efforts. In this context, this thesis focuses on the vegetation water use (interchangeable with transpiration, E_c) of selected native species in South Australia and the responses to a series of environmental variables, including air temperature, vapour pressure deficit, solar radiation and soil water condition which is reflected by either plant stem water potential or the most commonly used volumetric soil water content. Some of the main issues in current ecohydrological studies are explored in this thesis, for example, the upscaling of water fluxes from the tree scale to stand or catchment scale, the transferability of information across temporal and spatial scales, and the effects of heterogeneity and complexity of land surface on vegetation water use and the responses to environmental conditions. Specifically, the following five projects have been conducted to form this thesis.

Transpiration (E_c) is often simulated in land surface models based on the relationship with environmental variables. According to the structure of E_c models, they can be categorized into "direct" and "indirect" ones. The latter refers mainly to the Penman-Monteith equation, with g_c correlated to environmental variables; while the former simulates E_c straightforward using environmental variables, omitting the calculation of g_c. Most g_c models are empirically developed by establishing relationship between g_c and different environmental variables; therefore, the g_c models and relevant parameters are highly site specific, i.e. the response functions and parameter values may change with species and climate conditions. The first part of this thesis is focused on species-specific model selections. An appropriate g_c model for one Australian native species Drooping Sheoak was determined by running an optimization model. In the meantime, the significance of temperature functions for canopy conductance modelling, which is often neglected in previous studies, was tested.

Once the appropriate g_c model was determined, in the second part of this thesis, it was applied in the ″indirect″ method for E_c modelling, and the simulation results were compared to two types of ″direct″ models, to determine which category of E_c models better reproduced sap flow measurement. Moreover, the environmental conditions that constrain tree water use can be divided into supply and demand variables. Soil water condition is the only supply variable that has been widely discussed. Transpiration from trees that grow at riparian sites and from trees that access groundwater is not limited by soil water condition. Rainfall influence soil water dynamics, and therefore tree water uptake differs among seasons accordingly. Therefore, whether and when soil water condition function has significant influence on tree water use simulations were determined by comparing the ″direct″ and ″indirect″ models at daily and hourly scales; and the transferability of parameterization across temporal scales was also discussed.

For water balance studies using sap flow techniques, the upscaling of sap flux from individual trees to forest or catchment scale transpiration is particularly important. The scaling issue is one of the most important research questions in ecohydrological studies. Sapwood area is the most common scalar to accomplish this, thus it is realized that quantification of sapwood area is crucial for accurate transpiration estimation. In the third part of this thesis, a recent developed geophysics based technique, electrical resistivity tomography (ERT), was applied to estimate sapwood width. Compared to incremental wood cores ERT is relatively non-destructive and efficient. ERT not only gives point estimation of sapwood width, but also provides spatial variation of sapwood sections, which is useful for sensor positioning at the beginning of sap flow measurements.

Complex terrain brings forth more challenges in understanding the plant-water relations, because terrain conditions lead to the variability of solar energy, soil water and microclimate, and hence further influence the tree growth and distribution. In the fourth part of this thesis, field measurements were presented for comparison of tree water use, micrometeorological conditions, and soil water dynamics on two slopes with contrasting aspects (north facing vs. south facing) in a small native forest stand in South Australia, in order to examine plant-water relations mediated by topography. Comparison among daily soil water content, transpiration and potential *ET* indicates that tree water use at the site was mainly controlled by soil water supply in summer and autumn and by evaporative demand in winter and spring. The total estimated transpiration in the study period was similar on both slopes, although difference was observed during dry and wet periods. The response of tree water use to vapour pressure deficit and solar radiation was similar on both slopes; the response to soil water content was slightly different. Trees on north facing slope suffered water stress longer than trees on the other slope.

Studies at a point or catchment scale provide important knowledge of the plant-water relations; they reveal how vegetation is influenced by and influences the local climate conditions through water and energy exchanges. However, water resource management usually requires the knowledge and the quantification of water components more importantly at regional scale. For large spatial scale water component estimation ground measurements are limited in spatial representativeness, temporal continuity, and the extrapolation from point measurements to large area quantity has big uncertainties. Satellite observations overcome some of these limitations of field measurement. Therefore, in the last part of this thesis, water budget was examined over continental Australia using data obtained from different satellite platforms, that is, rainfall from Tropical Rainfall Measuring Mission (TRMM), evapotranspiration from Moderate Resolution Imaging Spectroradiometer (MODIS), and water storage change from the Gravity Recovery and Climate Experiment (GRACE). Water budget was examined in rainfall-limited and runoff-limited regions of Australia, and particularly an internal drainage basin, Lake Eyre Basin. Application of the satellite products for the water balance study in Lake Eyre Basin reflects well the seasonal hydrological processes in terms of net groundwater flow, and gives a reasonable estimation of the maximum possible integrated error of the three products as well as the maximum net groundwater inflow to the basin. This part using remote sensing data on a much larger spatial scale than the previous sections does not contribute to the core of the thesis, so the study is attached as an appendix in the end.

Declaration of Originality

I certify that this thesis does not incorporate, without acknowledgment, any material previously submitted for a degree or diploma in any other university; and that to the best of my knowledge and belief it does not contain any material previously published or written by another person except where due reference is made in the text.

Hailong Wang

Acknowledgements

By three methods we may learn wisdom: first, by reflection, which is noblest; second, by imitation, which is easiest; and third by experience, which is the bitterest.

Confucius (551-479 B.C.)

Speaking of help and support, I must give thanks to the school staffs Gail Jackson, Jodie Walker, Suzanne Myers, Kaye Hampton, and people in both electronic and mechanical workshops, e.g., Brenton Perkins, Wayne Peacock, Andrew Dunn and Bill Drury, who have provided assistance in my field and laboratory experiments. Thanks are also going to Mr Langdon Badger, who has generously provided his farm land for my field experiments, and made our work easier by clearing the way down to the valley. Special thanks are given to my collaborators Prof David A. Lockington and Dr Adrien Guyot at the School of Civil Engineering in The University of Queensland, for passing the knowledge of scientific instrumentation and data analyses of Electrical Resistivity Tomography. To my co-workers in the field works, Hugo A. Gutiérrez-Jurado, Xiang Xu, Zijuan Deng, Robert Andrew, Yuting Yang and Yunquan Wang, I would like to say thank you for the help and your friendship. I enjoy my study and life in Adelaide with you all.

Last but not least, I must thank God and the Church in Adelaide for all the blessings, for being with me emotionally and spiritually.

When looking back to this period in the future, I would be more than grateful to all the people who have printed a mark in my mind, who make my life wonderful and colourful, who smile to me and laugh with me. It is for sure a very impressive experience that benefits me in every aspect of my life and career, through which I gain my wisdom.

1. Introduction

Background

Ecohydrology, a highly integrated discipline between ecology and hydrology, has attracted increasing research interests in the last decade, as it provides theoretical frameworks and methodological approaches for understanding the complex interactions between vegetation and hydrologic processes such as evapotranspiration and runoff (Asbjornsen et al., 2011). Ecohydrological studies typically focus on the understanding of the interactions between hydrologic and ecosystem processes, and how these processes are manifested across spatiotemporal scales (Asbjornsen et al., 2011; Eagleson, 2002). The plant-water relation is the central concern of ecohydrological studies.

In the matter of water exchanges, evapotranspiration (*ET*) is one of the most complicated components in terrestrial water cycle to estimate. Land cover and land use changes affect hydrological processes such as evapotranspiration and runoff, on the other hand, the changes of hydrological processes feedback to atmospheric processes (Pielke et al., 2011; Williams et al., 2012; Zhang et al., 2011). Much effort has been made in *ET* quantification at various spatial scales (e.g., from tree to stand, catchment, region, continent and global) (Asbjornsen et al., 2011; Jarvis and McNaughton, 1986), using in situ measurements, satellite observations and land surface modelling. Vegetation plays a critical role in surface energy and water partitioning (e.g., Guan et al., (2010)) and interactions between land surface and atmosphere (Betts et al., 1997; Ivanov et al., 2008; Palmer et al., 2010), because vegetation covers 70% of the land surface (Dolman et al., 2014), contributes up to 80% transpiration for the global terrestrial evapotranspiration (Miralles et al., 2011). A large proportion of transpiration in global evapotranspiration has also been confirmed using isotope data (Jasechko et al., 2013; Wang et al., 2010), although Schlaepfer et al. (2014) argued the number in Jasechko et al (2013) has been overestimated, transpiration still takes more or less half of total evapotranspiration according to their studies (Schlesinger and Jasechko, 2014). Accurate estimation and partitioning of evapotranspiration into soil and canopy evaporation and vegetation transpiration (*E$_c$*) is one of the most difficult topics in ecohydrology and climatology (Dolman et al., 2014; Kool et al., 2014).

Among the methods of quantifying transpiration from vegetation, sap flow measurement techniques are useful means at different temporal and spatial scales, and are particularly useful in mountainous regions (Kumagai et al., 2008), because their applicability is not limited by

complex terrain and spatial heterogeneity (Ford et al., 2007; Kumagai et al., 2007; Wilson et al., 2001). Extension of sap flow measurements from individual trees to a larger spatial scale, for instance stand scale, usually needs a scalar. The most common scalar is the sapwood area (A_s). Sapwood area is conventionally determined by taking increment wood cores and measuring the sapwood width either by visual inspection of colour (Vertessy et al., 1995) or by staining (Gebauer et al., 2008). These methods are accurate but relatively destructive, and the measurements usually are conducted at the end of sap flow measurements, which will result in errors due to tree growth when applied for long-term study. An efficient, non-destructive method for estimating A_s is important and desirable for transpiration estimation at the stand scale.

In addition to sap flow techniques, transpiration can also be modelled based on energy partitioning (Guan and Wilson, 2009; Shuttleworth and Wallace, 1985) and vegetation controls in response to environmental conditions, such as air temperature (T), vapour pressure deficit (D), solar radiation (R_s) and soil water condition (volumetric water content θ or water potential ψ) (Jarvis 1976). The relationships have been integrated into different land surface and atmospheric models, for example, the Weather Research and Forecasting model (Hong et al., 2009), the North American Land Data Assimilation System (Mitchell et al., 2004), and the High-Resolution Land Data Assimilation System (Chen et al., 2007). In those models, parameter values are prescribed universally for lumped vegetation categories, for example, evergreen needle-leaf trees, deciduous broad-leaf trees, etc. However, the empirical relationships between transpiration and environmental variables are climate and vegetation specific. One set of universal values is not necessarily applicable to different vegetation species. The environmental condition related E_c models in the literature can be divided into two categories: ″direct″ and ″indirect″. An ″indirect″ method calculates E_c from the Penman-Monteith (PM) equation, in which canopy conductance (g_c) is simulated from the environmental variables following the Jarvis-Stewart approach (Jarvis, 1976; Stewart, 1988); while a ″direct″ method links transpiration straightforward to environmental conditions, omitting the g_c calculations. For each variable, multiple response functions were developed in different case studies; it is likely that different combinations of the functions will lead to difference in E_c simulation results. However, a combination of response functions is often chosen somewhat arbitrary without giving quantitative evidence. Therefore, it is necessary to emphasize on the importance of selecting the most suitable response functions to improve transpiration estimation.

In addition, many studies neglected temperature functions in E_c/g_c models without testing its significance (Lhomme et al., 1998; Mascart et al., 1991). In fact, in some cases temperature function has been claimed to have negative effects on E_c modelling (Sommer et al., 2002;

Whitley et al., 2013), and in other case the response function of temperature is even different from the commonly used function (Wang et al., 2014). Moreover, most of the studies simulated E_c or g_c taking soil water content into account, while a few studies demonstrated that soil water condition function can be neglected (Bunce, 2000; Leuning, 1995; Whitley et al., 2013), because transpiration from trees that can access groundwater with deep roots (Eamus and Froend, 2006) or from trees that grow in riparian sites (O'Grady et al., 2006) is not limited by soil water condition. At such study sites, the soil water availability function can be omitted in E_t and g_c models. However, at other sites, it is difficult to determine the significance of soil water condition for transpiration or canopy conductance modelling without long-term monitoring on the relevant variables. Furthermore, soil water availability has seasonal dynamics (Findell and Eltahir, 1997), and transpiration is usually energy-limited when soil water is sufficient, so it would be useful to determine the time and temporal scales (such as daily and hourly) at which soil water condition is more important in constraining tree water use.

Other than the current issues in ecohydrological studies mentioned above, the plant-soil system on complex terrain introduces more challenges in the plant water use estimation, because complex terrain alters the energy and water distribution (Gutiérrez-Jurado and Vivoni, 2013; Tromp-van Meerveld and McDonnell, 2006) and nutrients condition on land surface (Tokuchi et al., 1999), resulting in differences in vegetation growth and species distribution (Barij et al., 2007; Liu et al., 2012; Luizão et al., 2004). Tree water use and its response to environmental conditions are well investigated and understood; however, the influence of complex terrain on tree water use and the response of tree water use to environmental conditions have not yet been well established, partly due to the difficulty to capture the nonlinear processes at various spatiotemporal scales. Understanding the coupling of terrain, vegetation and hydrological conditions can reveal important constraints on the distribution and adaptability of vegetation to a range of environmental conditions. Tree water use along a hill slope has been studied in several sites (Kumagai et al., 2008; Mitchell et al., 2012), but there is little information available for tree water use and the environmental controls on contrasting hill slopes.

Objectives

This thesis focuses on the measurement and simulation of water use of selected native species in South Australia and its responses to environmental variables, including air temperature, vapour pressure deficit, solar radiation and soil water condition. Some of the main issues in current ecohydrological studies are discussed, including the spatial upscaling strategy of water fluxes from tree scale to stand or catchment scale, the constraints of selected environmental variables

on tree water use at different temporal scales, and the effects of heterogeneity and complexity of land surface on vegetation water use and the responses to environmental conditions.

Specifically, the objectives of the thesis are

(1) to determine the appropriate canopy conductance model for a specific environment (species and climate), and test the effects of temperature function in canopy conductance modelling

(2) to compare different transpiration models (″direct″ and ″indirect″) and test the significance of soil water condition and air temperature at daily and hourly scales

(3) to estimate the sapwood area using a non-destructive geophysics based method, electrical resistivity tomography

(4) to examine the difference of tree water use and the environmental controls on contrasting hill slopes due to topographic effects

Structure

To present each of the main objectives regarding the corresponding issues in current ecohydrological studies, this thesis is divided into six chapters and one appendix. Refer to Figure 1.1 for the key content of each chapter.

Thesis main theme:
Measurement and simulation of environmental controls on vegetation water use

Chapter 1 Introduction of some main issues in current ecohydrological studies, and general background knowledge of this thesis
Chapter 2 Select the appropriate canopy conductance model in response to environmental variables for use in indirect models to improve transpiration estimation
Chapter 3 Determine which way of tree water use modelling is better: direct or indirect? Test the significance of soil water condition and air temperature functions in tree water use modelling at different temporal scales
Chapter 4 Describe a geophysics based method to improve the estimation of sapwood width for upscaling sap flow from individual trees to catchment transpiration
Chapter 5 Experimental exploration of tree water use and the responses to environmental conditions on contrasting hill slopes
Chapter 6 A summary of main conclusions that are drawn from the above chapters (2-5), and further research interests and possibilities beyond this thesis
Appendix Application of remote sensing data for large scale water balance study in the Australian continent

Figure 1.1 Structure of the thesis, and the main content of each chapter

Note: the seasons throughout the thesis are referred to the austral seasons, and defined as follows to avoid the confusions with the concept in the northern hemisphere: spring is from September to November, summer is from December to February, autumn is from March to May and winter is from June to August.

Publications

From Chapters 2-5 and Appendix in this thesis, the following five manuscripts were prepared for publication in peer-reviewed journals. It should be noted that the introduction section of each paper (and hence the corresponding thesis chapter) contains the relevant thorough literature review.

[1] Wang, H., Guan, H., Deng, Z. and Simmons, C.T., 2014. Optimization of canopy conductance models from concurrent measurements of sap flow and stem water potential on Drooping Sheoak in South Australia. *Water Resources Research*, 50(7): 6154-6167. DOI: 10.1002/2013WR014818

[2] Wang H., H. Guan, C.T. Simmons. Modelling environmental controls on tree water use at different temporal scales: the significance of soil water condition. To be submitted to *Agricultural and Forest*

Meteorology

[3] Wang H., H. Guan, A. Guyot, C.T. Simmons, D.A. Lockington. 2015. Quantifying sapwood areas for three Australian native species using electrical resistivity tomography. *Ecohydrology*: in press. DOI: 10.1002/eco.1612

[4] Wang H., H. Guan, H.A. Gutiérrez-Jurado and C.T. Simmons. Tree water use and the environmental controls on contrasting slopes in a Mediterranean native forest stand. To be submitted to *Agricultural and Forest Meteorology*

[5] Wang, H., Guan, H., Gutiérrez-Jurado, H.A. and Simmons, C.T., 2014. Examination of water budget using satellite products over Australia. *Journal of Hydrology*, 511(0): 546-554. DOI: 10.1016/j.jhydrol.2014.01.076

References

Asbjornsen, H., Goldsmith, G.R., Alvarado-Barrientos, M.S., Rebel, K., Van Osch, F.P., Rietkerk, M., Chen, J.Q., Gotsch, S., Tobon, C., Geissert, D.R., Gomez-Tagle, A., Vache, K. and Dawson, T.E., 2011. Ecohydrological advances and applications in plant-water relations research: a review. Journal of Plant Ecology, 4(1-2): 3-22.

Barij, N., Stokes, A., Bogaard, T. and Van Beek, R., 2007. Does growing on a slope affect tree xylem structure and water relations? Tree Physiology, 27(5): 757-764.

Betts, R.A., Cox, P.M., Lee, S.E. and Woodward, F.I., 1997. Contrasting physiological and structural vegetation feedbacks in climate change simulations. Nature, 387(6635): 796-799.

Bunce, J.A., 2000. Responses of stomatal conductance to light, humidity and temperature in winter wheat and barley grown at three concentrations of carbon dioxide in the field. Global Change Biology, 6(4): 371-382.

Chen, F., Manning, K.W., LeMone, M.A., Trier, S.B., Alfieri, J.G., Roberts, R., Tewari, M., Niyogi, D., Horst, T.W., Oncley, S.P., Basara, J.B. and Blanken, P.D., 2007. Description and evaluation of the characteristics of the NCAR high-resolution land data assimilation system. Journal of Applied Meteorology and Climatology, 46(6): 694-713.

Dolman, A.J., Miralles, D.G. and de Jeu, R.A.M., 2014. Fifty years since Monteith's 1965 seminal paper: the emergence of global ecohydrology. Ecohydrology, 7(3): 897-902.

Eagleson, P.S., 2002. Ecohydrology. Cambridge University Press.

Eamus, D. and Froend, R., 2006. Groundwater-dependent ecosystems: the where, what and why of GDEs. Australian Journal of Botany, 54(2): 91-96.

Findell, K.L. and Eltahir, E.A.B., 1997. An analysis of the soil moisture-rainfall feedback, based on direct observations from Illinois. Water Resources Research, 33(4): 725-735.

Ford, C.R., Hubbard, R.M., Kloeppel, B.D. and Vose, J.M., 2007. A comparison of sap flux-based evapotranspiration estimates with catchment-scale water balance. Agricultural and Forest Meteorology, 145(3-4): 176-185.

Gebauer, T., Horna, V. and Leuschner, C., 2008. Variability in radial sap flux density patterns and sapwood area among seven co-occurring temperate broad-leaved tree species. Tree Physiology, 28(12): 1821-1830.

Guan, H., Simunek, J., Newman, B.D. and Wilson, J.L., 2010. Modelling investigation of water partitioning at a semiarid ponderosa pine hillslope. Hydrological Processes, 24: 1095-1105.

Guan, H. and Wilson, J.L., 2009. A hybrid dual-source model for potential evaporation and transpiration partitioning. Journal of Hydrology, 377: 405-416.

Gutiérrez-Jurado, H.A. and Vivoni, E.R., 2013. Ecogeomorphic expressions of an aspect-controlled semiarid basin: II. Topographic and vegetation controls on solar irradiance. Ecohydrology, 6(1): 24-37.

Hong, S.B., Lakshmi, V., Small, E.E., Chen, F., Tewari, M. and Manning, K.W., 2009. Effects of vegetation and soil moisture on the simulated land surface processes from the coupled WRF/Noah model. Journal of Geophysical Research-Atmospheres, 114.

Ivanov, V.Y., Bras, R.L. and Vivoni, E.R., 2008. Vegetation-hydrology dynamics in complex terrain of semiarid areas: 1. A mechanistic approach to modeling dynamic feedbacks. Water Resources Research, 44. (3).

Jarvis, P.G., 1976. The interpretation of the variations in leaf water potential and stomatal conductance found in canopies in the field. Philosophical Transactions of the Royal Society of London. B, Biological Sciences, 273(927): 593-610.

Jarvis, P.G. and McNaughton, K.G., 1986. Stomatal Control of Transpiration-Scaling Up From Leaf to Region. Advances in Ecological Research, 15: 1-49.

Jasechko, S., Sharp, Z.D., Gibson, J.J., Birks, S.J., Yi, Y. and Fawcett, P.J., 2013. Terrestrial water fluxes dominated by transpiration. Nature, 496(7445): 347-+.

Kool, D., Agam, N., Lazarovitch, N., Heitman, J.L., Sauer, T.J. and Ben-Gal, A., 2014. A review of approaches for evapotranspiration partitioning. Agricultural and Forest Meteorology, 184(0): 56-70.

Kumagai, T., Aoki, S., Shimizu, T. and Otsuki, K., 2007. Sap flow estimates of stand transpiration at two slope positions in a Japanese cedar forest watershed. Tree Physiology, 27(2): 161-168.

Kumagai, T., Tateishi, M., Shimizu, T. and Otsuki, K., 2008. Transpiration and canopy conductance at two slope positions in a Japanese cedar forest watershed. Agricultural and Forest Meteorology, 148(10): 1444-1455.

Leuning, R., 1995. A Critical-Appraisal of A Combined Stomatal-photosynthesis Model for C-3 Plants. Plant Cell and Environment, 18(4): 339-355.

Lhomme, J.P., Elguero, E., Chehbouni, A. and Boulet, G., 1998. Stomatal control of transpiration: Examination of Monteith's formulation of canopy resistance. Water Resources Research, 34(9): 2301-2308.

Liu, H.Y., He, S.Y., Anenkhonov, O.A., Hu, G.Z., Sandanov, D.V. and Badmaeva, N.K., 2012. Topography-controlled soil water content and the coexistence of forest and steppe in northern China. Physical Geography, 33(6): 561-573.

Luizão, R.C.C., Luizão, F.J., Paiva, R.Q., Monteiro, T.F., Sousa, L.S. and Kruijt, B., 2004. Variation of carbon and nitrogen cycling processes along a topographic gradient in a central Amazonian forest. Global Change Biology, 10(5): 592-600.

Mascart, P., Taconet, O., Pinty, J.P. and Mehrez, M.B., 1991. Canopy Resistance Formulation and Its Effect in Mesoscale Models - a Hapex Perspective. Agricultural and Forest Meteorology, 54(2-4): 319-351.

Miralles, D.G., De Jeu, R.A.M., Gash, J.H., Holmes, T.R.H. and Dolman, A.J., 2011. Magnitude and variability of land evaporation and its components at the global scale. Hydrology and Earth System Sciences, 15(3): 967-981.

Mitchell, K.E., Lohmann, D., Houser, P.R., Wood, E.F., Schaake, J.C., Robock, A., Cosgrove, B.A., Sheffield, J., Duan, Q.Y., Luo, L.F., Higgins, R.W., Pinker, R.T., Tarpley, J.D., Lettenmaier, D.P., Marshall, C.H., Entin, J.K., Pan, M., Shi, W., Koren, V., Meng, J., Ramsay, B.H. and Bailey, A.A., 2004. The multi-institution North American Land Data Assimilation System (NLDAS): Utilizing multiple GCIP products and partners in a continental distributed hydrological modeling system. Journal of Geophysical Research-Atmospheres, 109(D7).

Mitchell, P.J., Benyon, R.G. and Lane, P.N.J., 2012. Responses of evapotranspiration at different

topographic positions and catchment water balance following a pronounced drought in a mixed species eucalypt forest, Australia. Journal of Hydrology, 440: 62-74.

O'Grady, A.P., Eamus, D., Cook, P.G. and Lamontagne, S., 2006. Comparative water use by the riparian trees Melaleuca argentea and Corymbia bella in the wet-dry tropics of northern Australia. Tree Physiology, 26(2): 219-228.

Palmer, A.R., Fuentes, S., Taylor, D., Macinnis-Ng, C., Zeppel, M., Yunusa, I. and Eamus, D., 2010. Towards a spatial understanding of water use of several land-cover classes: an examination of relationships amongst pre-dawn leaf water potential, vegetation water use, aridity and MODIS LAI. Ecohydrology, 3(1): 1-10.

Pielke, R.A., Pitman, A., Niyogi, D., Mahmood, R., McAlpine, C., Hossain, F., Goldewijk, K.K., Nair, U., Betts, R., Fall, S., Reichstein, M., Kabat, P. and de Noblet, N., 2011. Land use/land cover changes and climate: modeling analysis and observational evidence. Wiley Interdisciplinary Reviews-Climate Change, 2(6): 828-850.

Schlaepfer, D.R., Ewers, B.E., Shuman, B.N., Williams, D.G., Frank, J.M., Massman, W.J. and Lauenroth, W.K., 2014. Terrestrial water fluxes dominated by transpiration: Comment. Ecosphere, 5(5): 1-9.

Schlesinger, W.H. and Jasechko, S., 2014. Transpiration in the global water cycle. Agricultural and Forest Meteorology, 189-190: 115-117.

Shuttleworth, W.J. and Wallace, J.S., 1985. Evaporation from sparse crops - an energy combination theory. Quarterly Journal of the Royal Meteorological Society, 111(469): 839-855.

Sommer, R., Sa, T.D.D., Vielhauer, K., de Araujo, A.C., Folster, H. and Vlek, P.L.G., 2002. Transpiration and canopy conductance of secondary vegetation in the eastern Amazon. Agricultural and Forest Meteorology, 112(2): 103-121.

Stewart, J.B., 1988. Modeling surface conductance of pine forest. Agricultural and Forest Meteorology, 43(1): 19-35.

Tokuchi, N., Takeda, H., Yoshida, K. and Iwatsubo, G., 1999. Topographical variations in a plant-soil system along a slope on Mt Ryuoh, Japan. Ecological Research, 14(4): 361-369.

Tromp-van Meerveld, H.J. and McDonnell, J.J., 2006. On the interrelations between topography, soil depth, soil moisture, transpiration rates and species distribution at the hillslope scale. Advances in Water Resources, 29(2): 293-310.

Vertessy, R.A., Benyon, R.G., Osullivan, S.K. and Gribben, P.R., 1995. Relationships between Stem Diameter, Sapwood Area, Leaf-Area and Transpiration in a Young Mountain Ash Forest. Tree Physiology, 15(9): 559-567.

Wang, H., Guan, H., Deng, Z. and Simmons, C.T., 2014. Optimization of canopy conductance models from concurrent measurements of sap flow and stem water potential on Drooping Sheoak in South Australia. Water Resources Research, 50(7): 6154-6167.

Wang, L., Kelly K. Caylor, Juan Camilo Villegas, Barron-Gafford, G.A., Breshears, D.D. and Huxman, T.E., 2010. Partitioning evapotranspiration across gradients of woody plant cover: Assessment of a stable isotope technique. Geophysical Research Letters, 37.

Whitley, R., Taylor, D., Macinnis-Ng, C., Zeppel, M., Yunusa, I., O'Grady, A., Froend, R., Medlyn, B. and Eamus, D., 2013. Developing an empirical model of canopy water flux describing the common response of transpiration to solar radiation and VPD across five contrasting woodlands and forests. Hydrological Processes, 27(8): 1133-1146.

Williams, C.A., Reichstein, M., Buchmann, N., Baldocchi, D., Beer, C., Schwalm, C., Wohlfahrt, G., Hasler, N., Bernhofer, C., Foken, T., Papale, D., Schymanski, S. and Schaefer, K., 2012. Climate and vegetation controls on the surface water balance: Synthesis of evapotranspiration measured across a global network of flux towers. Water Resources Research, 48.

Wilson, K.B., Hanson, P.J., Mulholland, P.J., Baldocchi, D.D. and Wullschleger, S.D., 2001. A comparison of methods for determining forest evapotranspiration and its components:

sap-flow, soil water budget, eddy covariance and catchment water balance. Agricultural and Forest Meteorology, 106(2): 153-168.

Zhang, L., Zhao, F.F., Chen, Y. and Dixon, R.N.M., 2011. Estimating effects of plantation expansion and climate variability on streamflow for catchments in Australia. Water Resources Research, 47.

2. Choosing the appropriate canopy conductance model for a native Australian species (Drooping Sheoak)

2.1. Introduction

Vegetation plays an important role in land surface hydrological processes, and coordinates the land-atmosphere interactions in a wide range of spatial scales (Avissar and Pielke, 1989; Chen et al., 1996; Dickinson, 1987; LeMone et al., 2007). It regulates water transport in the soil-plant-atmosphere continuum by means of stomata behaviour (Alfieri et al., 2008; Rao and Agarwal, 1984). Among approaches of quantifying this regulation, the 'big leaf' model in the Penman-Monteith (PM) equation (Monteith, 1981) has been widely discussed and applied (Leuning and Foster, 1990; Lu et al., 2003). The PM equation represents bulk stomata behaviour as canopy resistance (r_c), and assumes that stomata and canopy resistance have the same influencing factors (Lhomme et al., 1998) including air temperature (T), vapour pressure deficit (D), solar radiation (R_s), CO_2 concentration, soil water content (θ), and leaf water potential (ψ_l) (Damour et al., 2010; Jarvis, 1976; Tuzet et al., 2003).

Response of canopy conductance to the influencing factors has been incorporated into land surface models for transpiration estimate, such as in Noilhan and Planton (1989). Many studies constructed canopy conductance model following the Jarvis-Stewart approach (Jarvis, 1976; Stewart, 1988), which calculated canopy conductance from a maximum stomatal conductance by applying different stress functions related to influencing factors. For example, Thorpe et al. (1980) presented stomatal conductance of apple trees in terms of photon flux density and leaf to air vapour pressure gradient; Ball et al. (1987) and Collatz et al. (1991) linked stomatal conductance to CO_2 assimilation using a function of intercellular CO_2 concentration and leaf-level relative humidity; White et al. (1999b) related canopy resistance to solar radiation, air temperature and vapour pressure deficit for eucalyptus trees; Lu et al. (2003) modelled grapevine canopy conductance with solar radiation and vapour pressure deficit. More similar studies can be found in a recent review paper by Damour et al. (2010).

The gradient of water potentials in soil, stem and leaf drives water transport in the soil-plant-atmosphere system (Vandegehuchte et al., 2014a). Plant water potential is a sensitive indicator for vegetation water status (Choné et al., 2001; Nortes et al., 2005) and is constrained by stomata regulation of transpiration (Meinzer et al., 2008). Leaf water potential has been discussed in stomata regulation of water transport in a few studies (Comstock and Mencuccini, 1998; Jarvis, 1976; Macfarlane et al., 2004; Misson et al., 2004). Plant water potential is less favourable in

vegetation water use and canopy conductance modelling, due to the difficulty in measuring leaf/stem water potential continuously. Many studies after Jarvis (1976) used soil water content (Gash et al., 1989; Stewart, 1988) instead of plant water potential. However, most soil water content measurements only cover shallow soil layers up to 2 m deep, commonly within 50 cm (Whitley et al., 2008). Those measurements can reflect water availability to vegetation with shallow root systems; however, it is doubted that they can capture the whole picture of water uptake for vegetation with deep roots, because the 'wet' zones in the soil are progressively deeper during soil drying cycles (White et al., 2003), and some vegetation can access groundwater storage in dry periods (Eamus and Froend, 2006; Murray et al., 2003). In addition, storage of water in trees can also contribute to a certain proportion of the daily sap flux, especially when soil dries up (Edwards and Jarvis, 1982; Meinzer et al., 2004; Phillips et al., 1996; Tyree and Yang, 1990). Predawn stem water potential (ψ_{pd}) can be taken as a good approximate of root zone soil water condition (Palmer et al., 2010), because water potential is in equilibrium within the entire soil-plant continuum (Richter, 1997) at predawn. Recent technical advance allows monitoring stem water potential continuously (Patankar et al., 2013; Vandegehuchte et al., 2014a; Vandegehuchte et al., 2014b; Yang et al., 2013), which makes it more feasible to investigate the relationship between vegetation water use and stem and root zone water potential.

The stress of each influencing factor on canopy conductance is site specific and has been expressed differently among studies. Selection of response functions in many studies is somewhat arbitrary, without an explanation on why they, not others, were chosen. We hypothesize that selecting the appropriate functions will lead to better simulations of canopy conductance. The primary objective of this study is therefore to test this hypothesis by comparing simulation results from various response functions. The effect of temperature on canopy conductance is often neglected without quantitative evidence (Lhomme et al., 1998; Mascart et al., 1991). Significance of the temperature effect is specifically examined in this study. Measurements of sap flow and stem water potential were conducted on Drooping Sheoak trees (*Allocasuarina verticillata*) in Adelaide South Australia. This species is endemic to Australia, and widely distributed from Queensland to Tasmania and westward to South Australia. Its ability to develop extensive root systems in poor coastal soils (including sand dunes) makes it a valuable soil-stabilizer. It is also valued for its provision of habitat for cockatoos (Chapman and Paton, 2007). The areal extent of Drooping Sheoak has dramatically decreased in South Australia since the European Settlement (Peeters et al., 2006). Although climate is known to cause Drooping Sheoak mortality (Peeters et al., 2006), little specific

research has been conducted on its water use in response to environmental variables.

2.2. Methodology

2.2.1. Site description

The study site is near the campus of Flinders University ($138^{o}34'28''$E, $35^{o}01'49''$S). Ground surface is covered by sparse trees with short shrubs and grass at substrate. Soil type is characterized as sandy mixed with gravel. This soil condition makes it difficult to bury soil moisture probes for water content measurement near the trees.

The site is in Mediterranean climate zone. Annual mean temperature is about 17°C, and annual rainfall is around 546 mm, most of which occurs in May to September (Guan et al., 2013). Three Drooping Sheoak trees were selected for sap flow and stem water potential measurements in this study. Measurements were conducted in March-May 2011 (31 days) on tree 1 (Yang et al., 2013), January-April and October-December 2012 (150 days) on tree 2, and April-June 2014 (27 days) on tree 3.

2.2.2. Sap flow and stem water potential measurements

Sap flow was monitored at 30-min intervals in the tree trunks at 1.3 m above ground using the compensation heat-pulse technique (HPV) (Green and Clothier, 1988) for tree 1 in 2011 and tree 2 in 2012, and heat ratio method (HRM) (Burgess et al., 2001) for tree 3 in 2014. For HPV method three thermocouples are embedded inside each temperature probe at the depths of 5, 15, and 25 mm underneath the cambium. One temperature probe was installed 10 mm above the heater and the other 5 mm below the heater. Two sets of such probes were installed in the south and north sides of tree trunks. For HRM method two thermocouples are embedded at 12.5mm and 27.5mm underneath the cambium. Two temperature probes were symmetrically installed at 5 mm above and below the heater probe. All temperature sensors were located in sapwood and captured sap flux of the three trees. Volumetric sap flow was calculated from heat transport velocity and corrected for wounding, sapwood area, volume fraction of wood and water following Green et al. (2003) and Burgess et al. (2001) for the two methods respectively. Transpiration was converted from volumetric sap flow by the corresponding projected canopy area.

Stem water potential (ψ_{st}) was measured at 15-min intervals with PSY1 Stem Psychrometers (ICT International Pty Ltd., NSW, Australia), which was developed by Dixon and Tyree (1984) and has become commercially available in the last a few years. PSY1 measures the temperature

of sapwood surface and chamber air, and stem water potential is corrected with the temperature gradient. Recently, PSY1 has been applied in studies on different species, such as drooping sheoak (Yang et al., 2013), two mangrove species (Vandegehuchte et al., 2014b) and two betula species (Patankar et al., 2013). Predawn stem water potential (ψ_{pd}) was taken from the average of ψ_{st} between 3:00 am and 5:00 am, with the assumption that water potentials in the tree and root-zone soil have reached an equilibration at this time after water redistribution in the plant-soil system.

2.2.3. Canopy conductance model construction

The main objective of this study is to select a proper canopy conductance model for a specific environment. Although a two-leaf model that calculates water, carbon and energy fluxes for both sunlit and shaded leaves (Wang and Leuning, 1998) is considered better than the big-leaf model, the latter is still the most commonly used one for transpiration estimate in land surface models. Therefore, we follow previous studies such as Lu et al. (2003) to calculate canopy conductance from the inversion of Penman-Monteith equation:

$$g_c = \frac{g_a \gamma \lambda k_e E_c \rho_w}{\Delta A_c + k_t \rho_a C_p D g_a - \lambda(\Delta + \gamma)k_e E_c \rho_w} \qquad (2\text{-}1)$$

where g_c is canopy conductance [m/s]; g_a is aerodynamic conductance [m/s]; γ is psychrometric constant [kPa/^{o}C]; λ is latent heat of vaporization [MJ/kg]; E_c is the tree transpiration calculated from sap flow measurements; Δ is the slope of saturation vapor pressure-temperature curve [kPa/^{o}C]; A_c is the available energy allocated to canopy [MJ/(m^{2}h)]; C_p is specific heat of air at constant pressure [MJ/(kg^{o}C)]; D is vapor pressure deficit [kPa]; ρ_a and ρ_w are the density for air and water respectively [kg/m^3]; k_t is for units conversion. When E_c is in mm/h, k_t = 3600 s/h; when E_c is in mm/day, k_t = 86400 s/day. k_e = 0.001 is used to convert E_c from mm/day (mm/h) to m/day (m/h), so that the unit of g_c is m/s.

The available energy was partitioned for canopy (A_c) and substrate according to Beer's law following Shuttleworth and Wallace (1985):

$$A_c = (R_n - G)(1 - e^{-\kappa \cdot LAI}) \qquad (2\text{-}2)$$

R_n is net radiation, G is ground heat flux, both in W/m^2; LAI is leaf area index; κ is extinction coefficient, prescribed as 0.7 following (Yang et al., 2013). Other variables in equation (2-1) are calculated according to FAO irrigation and drainage paper 56 (Allen et al., 1998).

We consider four factors that influence the canopy conductance, which are air temperature (T), vapour pressure deficit (D), solar radiation (R_s) and predawn stem water potential (ψ_{pd}). Canopy conductance is modelled following Jarvis-Stewart approach (Jarvis, 1976; Stewart, 1988).

$$g_c = g_{max} LAI \cdot f(D) f(T) f(R_s) f(\psi_{pd}) \qquad (2\text{-}3)$$

where g_{max} represents the stomata conductance of unstressed vegetation under optimal conditions [m/s].

Different formulae coexist in published studies for each stress function in equation (2-3). For instance, $f(D)$ is linearly expressed in Aphalo and Javis (1991), while exponentially in White et al. (1999a). In this study we focus on two commonly used functions for each factor (from Table 2-1 and studies cited in this section), and combine them in different ways, then the most appropriate model is determined by comparing simulation results.

Table 2-1 Response functions of vegetation conductance to a series of factors in the literature[a]

Sites	Species	Response functions	Source	Notations
Fetteresso Forest, U.K. & Cedar River Forest, Washington, U.S.A.	*Sitka spruce & Douglas fir*	$f(Q)=k_1k_2(Q-k_3)/[k_1+k_2(Q-k_3)]$ $f(T)=k_1(T-T_1)(T_h-T)^{k2}$ $f(D)=1-k_1D$ $f(\psi_1)=1-\exp[-k_1(\psi_1-\psi_m)]$	Jarvis (1976)	
	Golden Delicious apple trees	$f(Q)=1/(1+k_1/Q)$ $f(D)=1-k_2D$	Thorpe et al. (1980); Warrit et al. (1980)	k_x (x=1,2,…) is parameter for each equation Q: photon flux density T_h, T_1: high and low leaf temperature ψ_1: leaf water potential ψ_m: value of ψ_1 when $g_s=0$ ψ_{cr}: critical leaf water potential beyond which transpiration is strongly limited by water stress $\delta\theta$: soil moisture deficit $\delta\theta_m$: empirically determined maximum value of $\delta\theta$ Rsmin: minimum stomatal resistance T in Kelvin degree θ_{cr}: critical point moisture θ_{wp}: wilting point moisture Q_h: incident radiation at top of canopy Q_{50}: value of Q, when g_s is half of the maxima k_Q: light extinction coefficient ψ_{pd}: predawn leaf water potential
U.S. Water Conservation Laboratory in Phoenix, Arizona	*Anza wheat (Triticum aestivum, L., cv. Anza)*	$f(\psi_1)=[(1+\psi_1/\psi_{cr})^{k3}]^{-1}$	Choudhury and Idso (1985)	
Thetford Forest, Norfolk, England	*Scots pine (Pinus sylvestris (L.))*	$f1(Rs)=k_1(Rs-1000)+1$ $f1(D)=1-k_2D$ $f1(T)=k_3(T-30)+1$ $f1(\delta\theta)=1-k_4\delta\theta$ -- $f2(Rs)=(1000+k_1)Rs/1000/(k_1+Rs)$ $f2(D)=1-k_2D$ $f2(T)=k_3(T-T_1)(T_h-T)^{k4}$ $f2(\delta\theta)=1-\exp[k_4(\delta\theta-\delta\theta_m)]$	Stewart (1988)	
Southern Great Plains of the United States	*Grass, winter wheat*	$f(Rs)=(Rsmin/5000+f)/(1+f)$ $f=0.55Rs/k_1*2/LAI$ $f(D)=1-k_2D$ $f(T)=1-0.0016(T-298)^2$ $f(\theta)=1$, when $\theta> \theta_{cr}$ $f(\theta)=0$, when $\theta< \theta_{wp}$ $f(\theta)=(\theta-\theta_{wp})/(\theta_{cr}-\theta_{wp})$, $(\theta_{wp}\leq\theta\leq\theta_{cr})$	Alfieri et al. (2008)	
Frankfort State Forest, eastern Transvaal, South Africa	*Eucalyptus grandis*	$f(Q)=k_1k_2Q/(k_1+k_2Q)$ $f(D)=k_3\exp(k_4D)$	Dye and Olbrich (1993)	
	Eucalyptus grandis and other species (refer to references)	$f(D)=1/(1+D/k_1)$ $f(Q)=\ln\{(Q_h+Q_{50})/[Q_h\exp(-k_QLAI)+Q_{50}]\}$ /k_Q $f(Rs)=(1000+k_1)Rs/[1000(k_1+Rs)]$ $f(\psi_1)=[(1+\psi_1/\psi_{cr})^{k3}]^{-1}$ $f(D)=1-k_2D$	Leuning (1995) Lohammar et al. (1980) Kelliher et al. (1995) Leuning et al. (2008)	
south-east Tasmania	*Eucalyptus globulus and Eucalyptus nitens*	$f(Q)=k_1\{k_2Q+1-[(k_2Q+1)^2-k_3Q]^{0.5}\}$ $f(T)=k_4(T-T_1)(T_h-T)^{k5}$ $f(D)=1.1\exp(-0.63D)$ $f(\psi_{pd})=1.09\exp(-1.27\psi_{pd})$	White et al. (1999b)	
Liverpool Plains, north-western NSW	*Eucalyptus crebra and Callitris glaucophylla*	$f(Rs)=(1000+k_1)Rs/[1000(k_1+Rs)]$ $f(D)=\exp(-k_3D)$ $f(\theta)=1$, when $\theta> \theta_{cr}$ $f(\theta)=0$, when $\theta< \theta_{wp}$ $f(\theta)=(\theta-\theta_{wp})/(\theta_{cr}-\theta_{wp})$, $(\theta_{wp}\leq\theta\leq\theta_{cr})$	Whitley et al. (2009)	

[a]CO_2 concentration is not considered in this study, so carbon functions are not listed.

One of the solar radiation functions is adopted from Stewart (1988) in Eq. (2-4a), in which R_{sH} is

the approximate maximum solar radiation, and given 350 (W/m^2) for daily step calculations according to the measurements. Another response function that is widely used in land surface model is given in Eq. (2-4b) (Chen and Dudhia, 2001). In both equations, k_{Rs} is a fitting parameter [W/m^2].

$$f(R_s) = \frac{R_s}{R_s + k_{Rs}} \frac{R_{sH} + k_{Rs}}{R_{sH}} \qquad (2\text{-}4a)$$

$$f(R_s) = \frac{1/(g_{max} \times 5000) + f}{1 + f}, \ f = 0.55 \frac{R_s}{k_{Rs}} \frac{2}{LAI} \qquad (2\text{-}4b)$$

The effect of vapour pressure deficit is expressed exponentially (Eq. 2-5a) in Whitley et al. (2009), and linearly (Eq. 2-5b) in other models (Noilhan and Planton, 1989; Stewart, 1988). In both equations, k_D is a fitting parameter [kPa^{-1}].

$$f(D) = e^{-k_D D} \qquad (2\text{-}5a)$$

$$f(D) = 1 - k_D D \qquad (2\text{-}5b)$$

A second-order polynomial function of air temperature T (in ^{o}C) in Eq. (2-6a) is originally proposed by Jarvis (1976) and used in SiB model (Sellers et al., 1986), and extended by Dickinson (1987). Temperature function in Jarvis (1976) is essentially the same with that in Dickinson (1984; 1987), and it requires specification of the optimum, upper-limit and lower-limit temperatures. In this study, we choose the temperature function in Dickinson (1984). Eq. (2-6b) is a linear model used in Stewart (1988). T_o is the temperature [^{o}C] at which transpiration rate reaches the maximum. In equations (2-6a, b), k_T is a fitting parameter.

$$f(T) = 1 - k_T (T_o - T)^2 \qquad (2\text{-}6a)$$

$$f(T) = 1 - k_T (T_o - T) \qquad (2\text{-}6b)$$

For stem water potential, the relationship given in Eq. (2-7a) is adopted from Jarvis (1976) and that in Eq. (2-7b) is from Choudhury and Idso (1985) and Lhomme et al. (1998). Root water uptake model described by Feddes et al. (1978) gives a relationship between plant water stress and soil water potential: under extremely dry and wet conditions transpiration rate is assumed to be zero, and in a certain range of soil water potential, transpiration reaches the highest rate; and in other soil moisture conditions transpiration is linearly related to soil water potential.

Following this pattern, we propose an upper and a lower limit for stem water potential (ψ_u and ψ_l) at which tree transpires water at the maximum and zero rates respectively; when potential is between ψ_l and ψ_u, $f(\psi_{pd})$ is linearly interpolated. The function is given in Eq. (2-7c). Parameter ψ_m (MPa) in Eq. (2-7a) is the value of ψ_{pd} at which $f(\psi_{pd})$ extrapolates to 0; ψ_m in Eq. (2-7b) gives the water potential limit beyond which the transpiration is strongly limited by water stress (Lhomme et al., 1998). In both equations, k_ψ is a fitting parameter.

$$f(\psi_{pd}) = 1 - e^{-k_\psi (\psi_{pd} - \psi_m)} \tag{2-7a}$$

$$f(\psi_{pd}) = \frac{1}{1 + (\psi_{pd}/\psi_m)^{k_\psi}} \tag{2-7b}$$

$$f(\psi_{pd}) = \begin{cases} 0, & \psi_{pd} \leq \psi_l \\ \dfrac{\psi_{pd} - \psi_l}{\psi_u - \psi_l}, & \psi_l < \psi_{pd} < \psi_u \\ 1, & \psi_{pd} \geq \psi_u \end{cases} \tag{2-7c}$$

2.2.4. Model selection and parameter optimization

Canopy conductance models were examined at daily time step. Measurements on tree 2 in 2012 covered the longest period including both dry and wet days (mostly in dry warm season) compared to the other two trees. Data from tree 2 on rainy days were filtered out, the rest were divided into two groups (one contains data in the order of 1, 3, 5… and the other 2, 4, 6… respectively). The first group was used to train the model, and the second group was used to test the model. Data collected on tree 1 in 2011 and tree 3 in 2014 were also filtered and used for model testing.

Unlike some studies using only two or three response functions (examples in Table 2-1), we presume that four factors are all functioning significantly in regulating the canopy conductance. Therefore, we first examined 24 combinations of the functions (equation 2-4a~2-7c), and then tested the importance of temperature by setting $f(T)$ to 1 (giving 12 additional models) and comparing the results with those using equations 6a & 6b. The 36 model constructions are illustrated in Figure 2.1. Parameters for each g_c model were obtained using the DiffeRential Evolution Adaptive Metropolis (DREAM) model (Vrugt et al., 2009). DREAM runs multiple different chains simultaneously for global exploration and automatically tunes the scale and orientation of the proposal distribution in randomized subspaces during the search. More details about the model can be found in Vrugt et al. (2009). The DREAM is performed for each

conductance model by 20,000 iterations, in order to make it highly possible that the final results are at their global optimum.
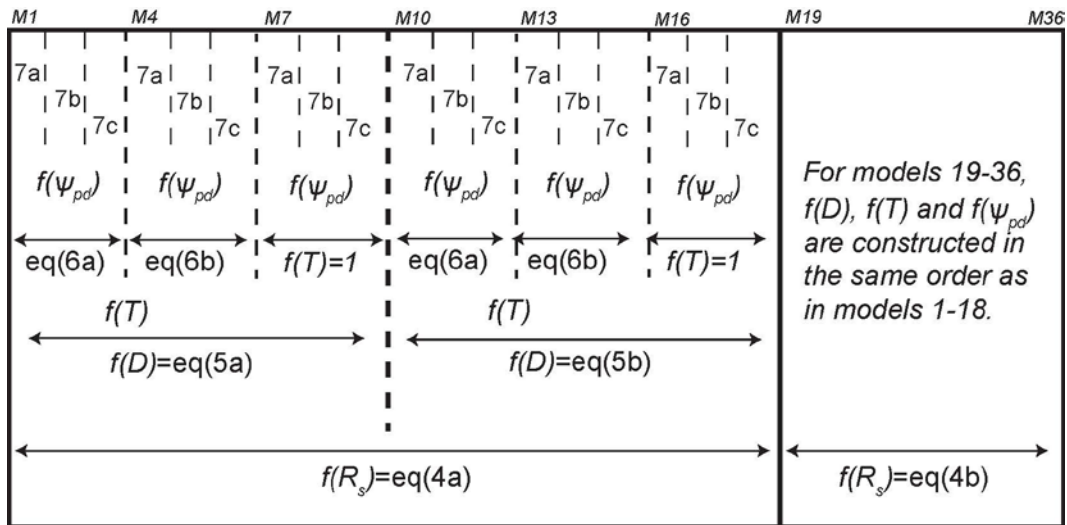
Figure 2.1 Illustration of 36 canopy conductance models comprised of different response functions for D, R_s, T and ψ_{pd}. Symbols on top indicate the model numbers ($M1$-$M36$).

2.3. Results and discussion

2.3.1. Microclimate, sap flow and stem water potential

Part of the measurement results for tree 2 is demonstrated in Figure 2.2 at half-hourly intervals. Daily data of sap flow, stem water potential and microclimate were calculated from the original 30-min and 15-min measurements. Daily mean temperature in the measurement periods of 2011, 2012 and 2014 was 17°C, 20°C and 15°C respectively. Most days in the measurement period for tree 3 were cloudy or rainy, which affected the data quality in this period.

Figure 2.3 shows that the changes of air temperature (T) and vapour pressure deficit (D) with time are similar. Stem water potential (ψ_{st}) responds to rainfall sensitively in dry periods. After rainfall occurs, ψ_{st} increases quickly to a high value within a short time range such as a few hours, which depends on the rainfall amount and duration. The relationship between stem water potential, solar radiation and tree water use indicates that tree water use is mainly constrained by water availability rather than energy in summer. Particularly, daily stem water potential decreased continuously from October to December of 2012 (Figure 2.3), when soil became drier. Transpiration rate also decreased during this period. Stem water potential data indicate that Sheoak recovers xylem water storage in night time and likely has reached an equilibrium state before predawn (Figure 2.2 and Figure 2.3). The daily average difference between the maximum stem water potential (around predawn) and minimum stem water potential (late afternoon 15:00-16:00) was around 1 MPa for clear days in dry season (Figure 2.3).
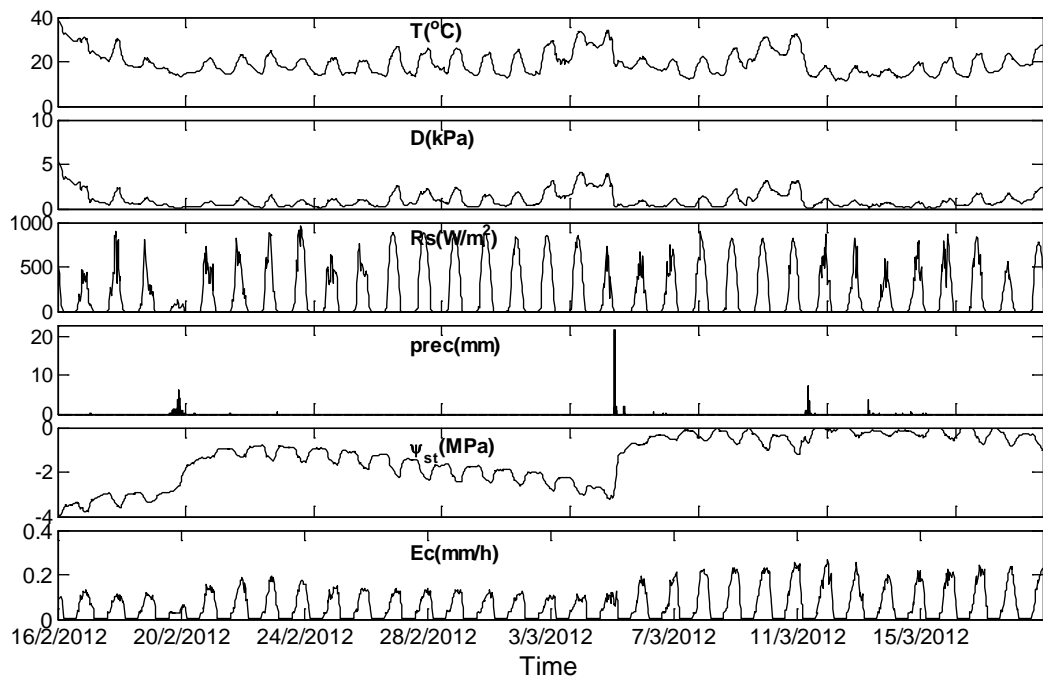
Figure 2.2 Part of microclimatic variables, tree water use and stem water potential data for tree 2 in 2012 at 30-minute intervals. *T* is air temperature, *D* is vapor pressure deficit, R_s is solar radiation, *prec* is rainfall, ψ_{st} is stem water potential, E_c is transpiration.
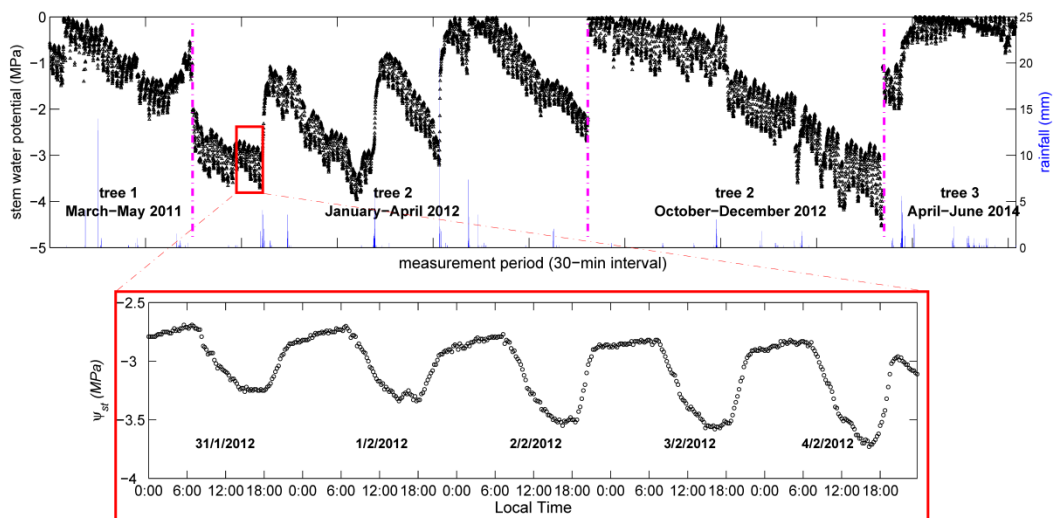
Figure 2.3 Part of rainfall and stem water potential measurements (30-minute intervals) for three trees. Bottom plot gives stem water potential data of tree 2 at 15-minute intervals for the part of data enclosed in red rectangle in the top plot.

Relationship between canopy conductance and the four influencing factors (*T*, *D*, R_s, and ψ_{pd}) is given in Figure 2.4 for three trees in different measurement periods. The calculated canopy conductance was larger in spring and autumn than in summer. The maximum canopy conductance was observed in early October 2012 after the rainy season, about 0.015 m/s.

19
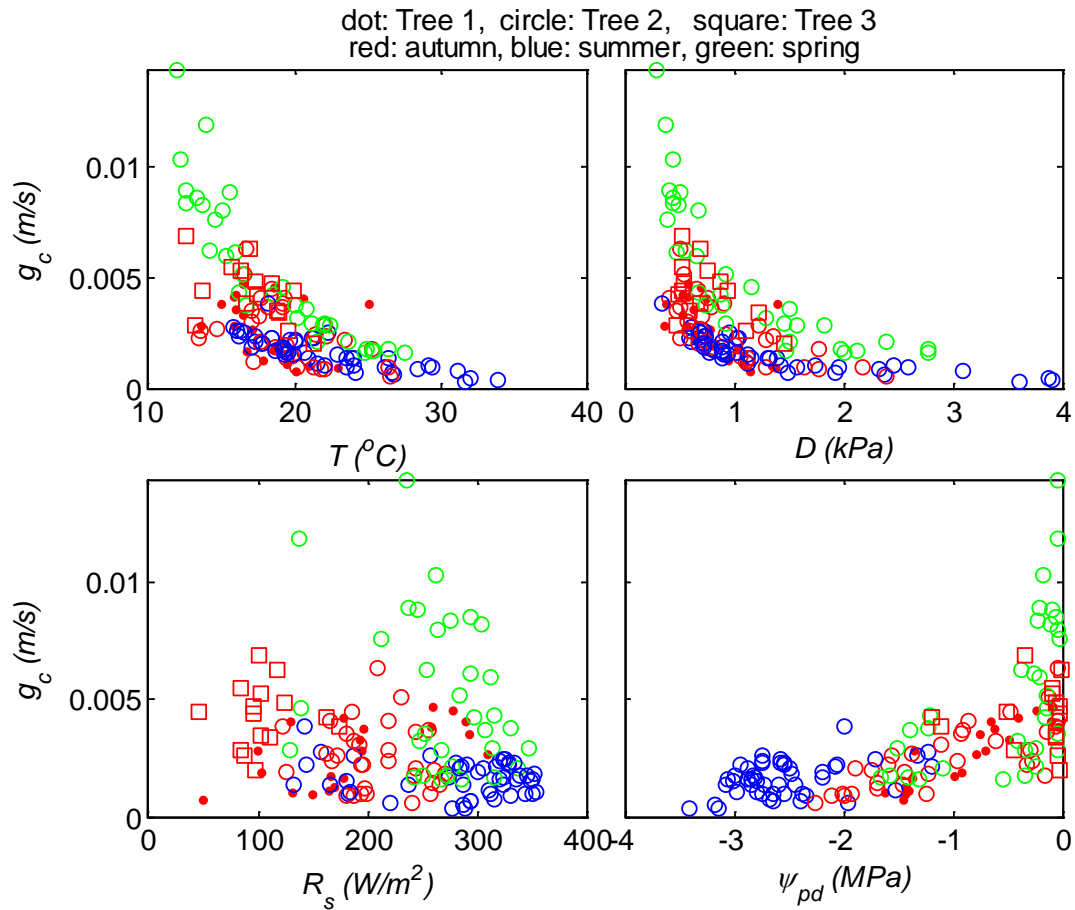
Figure 2.4 Relationship between canopy conductance and four influencing factors (T, D, R_s, and ψ_{pd}). Data include all measurements (excluding rainy days) for three trees in 2011, 2012 and 2014.

2.3.2. Model optimization and comparison

To compare the conductance models and determine the most appropriate one, we calculated correlation coefficient (r), root mean square error ($RMSE$) and slope of linear regression (with zero intercept) between simulated and calculated g_c from Eq. (2-1) for each model based on the training and testing datasets. Results are given in Figure 2.5. We notice that the results of model testing based on dataset of 2012, reflected in correlation coefficients, $RMSE$ and slopes, appear better than those from model calibration based on the training dataset of 2012, which is against our intuition. A careful check suggests that this is because some extreme large conductance values were accidentally allocated to the training dataset. The calibrated models with training data from tree 2 in 2012 were also applied for tree 1 in 2011 and tree 3 in 2014. Results showed consistent overestimation of canopy conductance for these two trees (fitting slopes larger than 1, Figure 2.5c). In this exercise, we assumed a constant g_{max} which was obtained from training data of tree 2 collected in spring, summer and early autumn, while the data of tree 1 and tree 3 were collected in mid and late autumn. In fact, as pointed out by Schulze et al. (1994), Ronda et al. (2001) and Alfieri et al. (2008), g_{max} is both time and site specific. Seasonal variability of g_{max}

likely interprets the consistent model overestimation for tree 1 in 2011 and tree 3 in 2014. Based on this result, sheoak trees likely have a lower g_{max} in autumn than that in spring and summer.
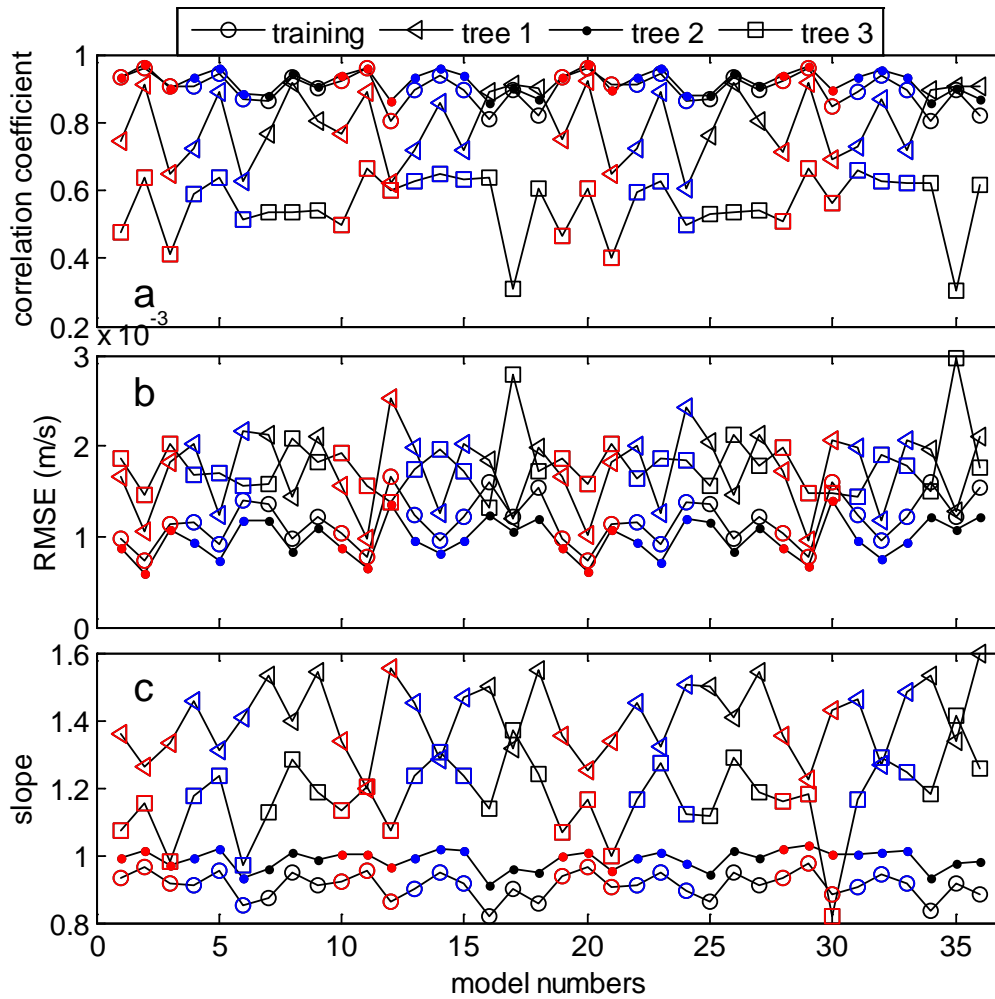
Figure 2.5 Comparison of model performance using training data in 2012 and testing data in 2011 (tree 1), 2012 (tree 2) and 2014 (tree 3). Slope in plot *c* is from linear regression between simulated and PM calculated g_c with zero intercept. Red color highlights models using Eq. (2-6a), blue stands for models using Eq. (2-6b), and black symbolizes models without temperature function. Refer to Figure 2.1 for model numbers and the relevant response functions.

Figure 2.5 and Figure 2.6 show the influence of stress function selection on model performance, and hence suggest the appropriate functions that better fit the calculated canopy conductance. When equations for *T*, *D* and R_s are the same, models using Eq. (2-7b) for predawn stem water potential (the middle one of each group of three models in the queue, Figure 2.5) give better results than models using Eq. (2-7a and c). For example, in models 1-3 the correlation coefficient of the training data is 0.94, 0.97 and 0.90, and the root mean square error is 0.0009, 0.0006 and 0.0011 m/s. This is particularly clear in Figure 2.6*d,* where the results from Eq. (2-7b) (pentagrams) appear to be better than those from Eq. (2-7a and c) (circles and dots) in terms of both $r_{testing}$ and *RMSE*. When equations for *D*, R_s and ψ_{pd} are the same, models with a

21

temperature function fit calculated g_c better than those without a temperature function. For example in Figure 2.5 models 2 and 5 give higher correlation coefficient and lower *RMSE* than model 8, and Figure 2.6*c* shows that results from Eq. (2-6a) (circles) are better than those from Eq. (2-6b) (pentagrams); results from models without temperature function (dots) appear to be the worst. Therefore, temperature plays a significant role in canopy conductance modelling and should not be neglected. Figure 2.6*b* shows that models using Eq. (2-5a) for vapour pressure deficit generate better results than those using Eq. (2-5b). Models using the two solar radiation functions give similar results, which implies that it does not matter much which of the two response functions, *i.e.* Eq. (2-4a) and Eq. (2-4b) symbolized by circles and dots in Figure 2.6*a*, is used in canopy conductance models.
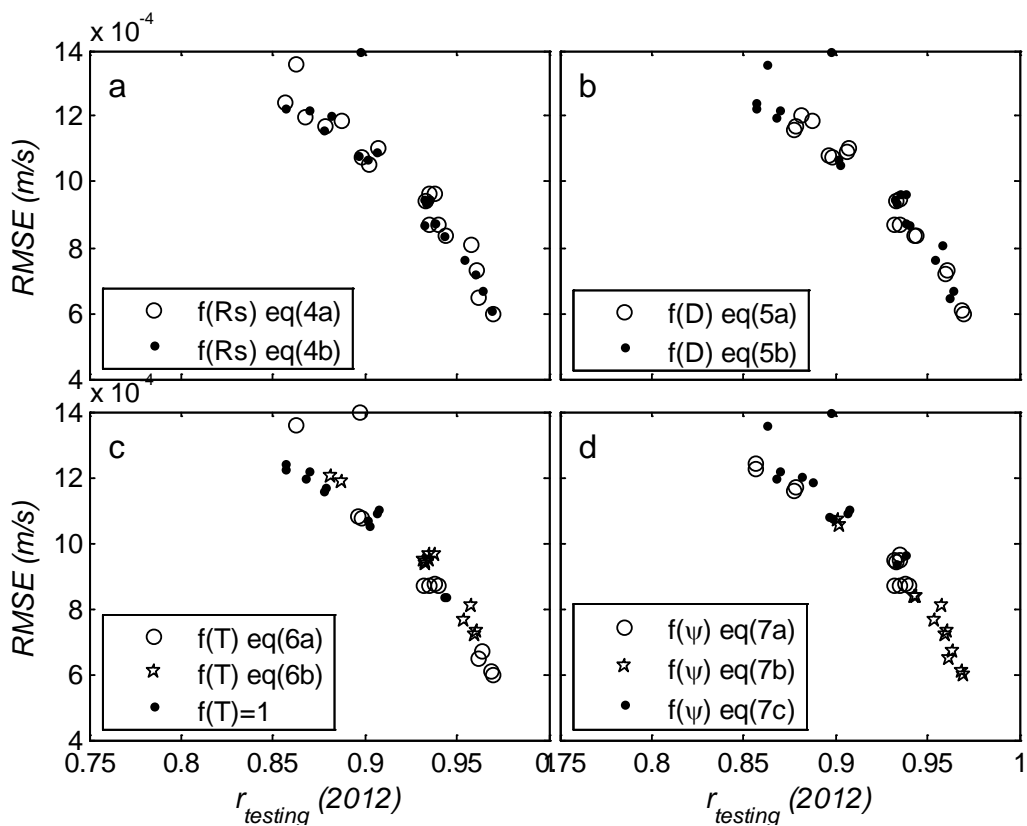
Figure 2.6 Significance tests of response functions for each influencing factor using *RMSE* and correlation coefficient based on data from tree 2 in 2012. *a*. simulations using Eq. (2-4a) for *f(R_s)* combined with other functions in comparison to simulations using Eq. (2-4b) for *f(R_s)* with other functions. It is the same in *b*, *c* & *d* for *f(D)*, *f(T)* and *f(ψ_pd)*. The four figures share the same axes tick labels.

From statistical results in Figure 2.5 and Figure 2.6, model 2 is considered the most suitable model in this study and given in Eq. (2-8). This model comprises Eq. (2-4a) for solar radiation, Eq. (2-5a) for vapour pressure deficit, Eq. (2-6a) for temperature and Eq. (2-7b) for predawn stem water potential.

$$g_c = 0.0076 \cdot LAI \cdot \left(\frac{R_s}{R_s + 4.6} \cdot \frac{350 + 4.6}{350} \right) \cdot \left\{ e^{-0.75D} \cdot \left[1 + 0.0128(20 - T)^2 \right] \right\} \cdot \frac{1}{1 + \left(\dfrac{\psi_{pd}}{-0.87} \right)^{0.74}} \quad (2\text{-}8)$$

Comparison between the calculated g_c from Eq. (2-1) and simulated g_c from model 2 for three trees is given in Figure 2.7. The maximum stomatal conductance g_{max} for this model is 0.0076 m/s; the equivalent minimum stomatal resistance for the Droop Sheoak trees is 132 s/m. This number is close to that used in Noah land surface model, which is one of the land surface models used in the Weather Research and Forecasting model (Hong et al., 2009), the North American Land Data Assimilation System (Mitchell et al., 2004), and the High-Resolution Land Data Assimilation System (Chen et al., 2007). In Noah, the minimum stomatal resistance for needle-leaf evergreen trees is 150 s/m (Chen and Dudhia, 2001; Kumar et al., 2011). Transpiration in this study is converted from volumetric sap flow by the projected canopy area. This area may underestimate the effective coverage of the tree for transpiration calculation, thus underestimate the canopy resistance. Nevertheless, this uncertainty of transpiration estimation does not change the model selection results.
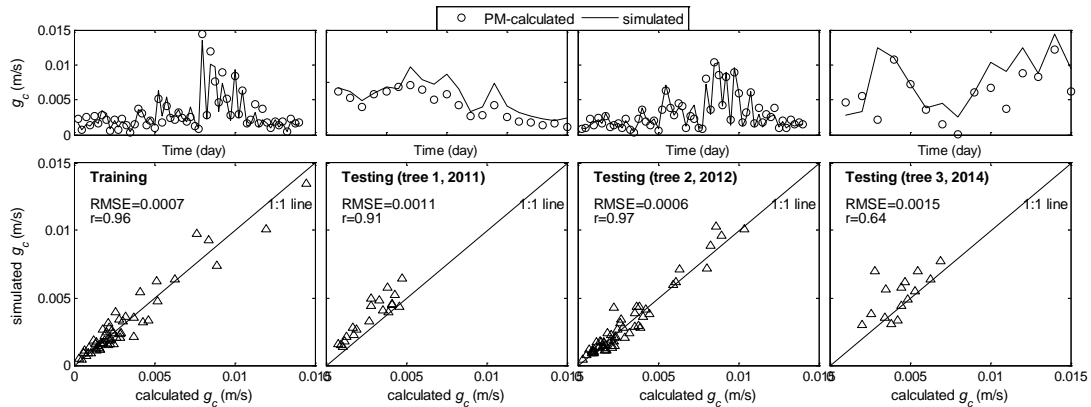
Figure 2.7 Comparison of canopy conductance calculated from Eq. (2-1) and simulated from the best model (model 2). Training data are from tree 2 in 2012, testing data are from tree 1 in 2011, tree 3 in 2014, and the other half of data from tree 2 in 2012.

2.3.3.   Parameter values

Relationship between parameters and correlation coefficient for the testing dataset ($r_{testing}$) from tree 2 in 2012 is examined and shown in Figure 2.8, so as to have a better view of the ranges of parameter values for each response function. Testing data in 2011 and 2014 are not plotted in the figure due to the overestimation of conductance for tree 1, and poor data quality for tree 3. Different response functions for each factor show different ranges of parameter values, indicated by the different symbols in the figure. The following discussion on parameter value range is

based on models that give correlation coefficient greater than 0.96, and *RMSE* smaller than 0.0008 m/s. For those models, g_{max} ranges from about 0.005 to 0.008 m/s (Figure 2.8*a*). k_D range from 0.66 to 0.77 kPa^{-1} for Eq. (2-5a), and from 0.24 to 0.32 kPa^{-1} for Eq. (2-5b) (Figure 2.8*c*). k_T values are negative, and does not vary much for Eq. (2-6a), but has large variability for Eq. (2-6b) (Figure 2.8*d*). k_ψ ranges from 0.50 to 0.78, and ψ_m ranges from -0.87 to -0.34 MPa for Eq. (2-7b), while k_ψ and ψ_m ranges from 0.39 to 0.17 and from -4.01 to -3.46 MPa for Eq. (2-7a) (Figure 2.8*e*, *f*). Correlation coefficient is always smaller than 0.95 when using Eq. (2-7a) for predawn stem water potential. The values of k_{Rs} ranges from 0 to 10 W/m^2 for both Eq. (2-4a) and (2-4b) (Figure 2.8*b*). The values of k_D for Eq. (2-5b) is less variable than that for Eq. (2-5a). The parameter values discussed above were derived based on daily data.
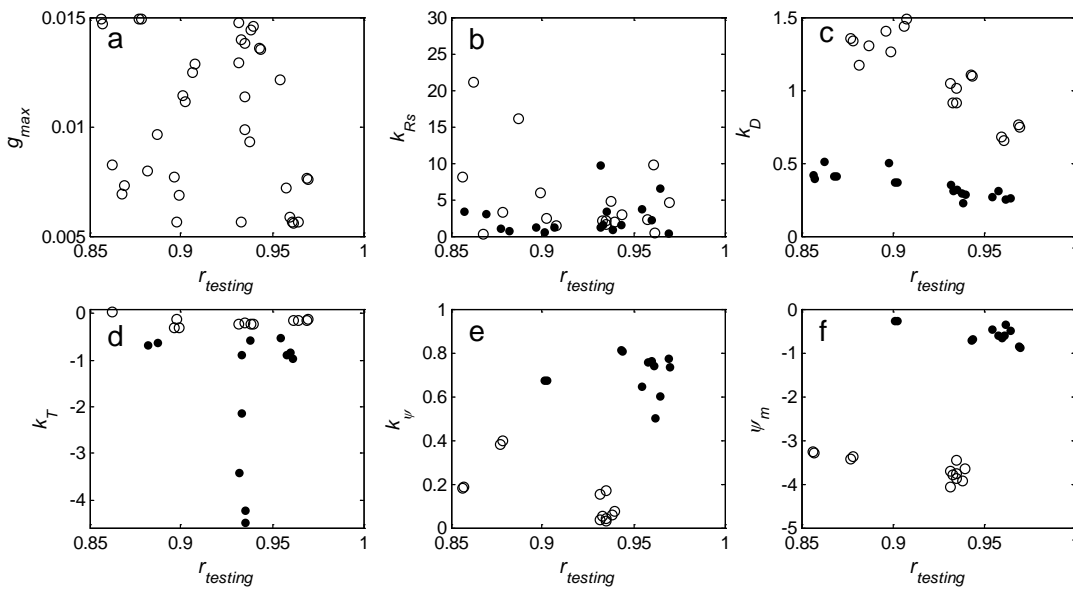
Figure 2.8 Parameter (g_{max}, k_{Rs}, k_D, k_T, k_ψ and ψ_m) value ranges for different response functions. a. results from all simulations; b. circles symbolize results from models using Eq. (2-4a), and dots Eq. (2-4b); c. circles symbolize results from models using Eq. (2-5a),

The simulation results of k_T for Eq. (2-6a) are negative for all models that use this temperature function (Figure 2.8*d*), for example, the one in Eq. (2-8) is -0.0128. This results in *f(T)* greater than 1, which is not compatible with the principle of Eq. (2-3) that *f(T)*, *f(R_s)*, *f(D)* and *f(ψ_pd)* should lie between 0 and 1 (Stewart, 1988). Figure 2.4 shows that the relationship between g_c and *T* is similar to g_c and *D*. This relationship is different from the ones illustrated in other studies such as Jarvis (1976) and White et al. (1999) in which the relationship fits the 'downward' parabolic curve, as is also shown in Noilhan and Planton (1989) and Chen et al. (1996) with k_T = 0.0016 for the same equation. The important assumption of analysing the relationship between canopy conductance and influencing factors is that the factors should be independent of each other (Macfarlane et al., 2004). However, it is difficult to distinguish the

effects of T and D on canopy conductance, because T and D are usually highly correlated (Alves and Pereira, 2000). This correlation is especially strong in this study, showing a linear correlation coefficient of 0.92, which explains the similar relationship between g_c-T and g_c-D (Figure 2.4). To examine if the negative k_T only applies to tree 2 in 2012 or it also applies on other sheoak trees in other years, we ran the DREAM optimization with data from tree 1 in 2011 and tree 3 in 2014. Results also gave negative k_T values.

The measurements and optimization results suggest that effects of air temperature on canopy conductance are not appropriately expressed by $f(T)$ in this study. We further examined the relationship between functions of temperature and vapour pressure deficit in model 2 (Figure 2.9) using all data from tree 2 in 2012, by comparing $f(T)$, $f(D)$ and $f(DT)$ which is the product of $f(T)$ and $f(D)$. The results show that when T is between 18$^{\rm o}$C and 22$^{\rm o}$C, $f(DT)$ is almost the same as $f(D)$, which implies that the influence of temperature on canopy conductance is very small in this temperature range. However, when T is below 18$^{\rm o}$C, $f(DT)$ is apparently larger than $f(D)$ but smaller than $f(T)$; when T is above 22$^{\rm o}$C, $f(DT)$ is also larger than $f(D)$, but to a small degree. Mostly, the values of $f(DT)$ lies between 0 and 1, consistent with the principle of a stress function (Stewart, 1988). Therefore, we suggest that the effect of vapour pressure deficit and air temperature should be combined into one, such as $f(DT)$.
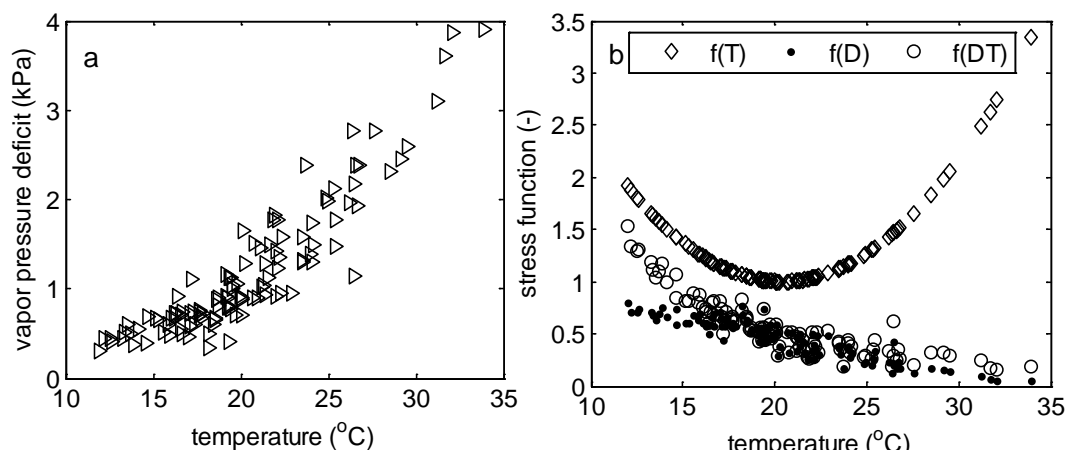
Figure 2.9 Relationship between temperature and vapor pressure deficit (a), and the response functions $f(T)$, $f(D)$, and $f(DT)$ [$=f(T) \times f(D)$] (b) of model 2.

2.4. Conclusions

Stomata regulation of water transport in the soil-plant-atmosphere continuum is vegetation and climate specific. Different models are used to quantify this regulation to help understand climate control on tree water use by relating stomata conductance to environment conditions. Different response functions are presented in literature for conductance modelling for different species and

climate conditions. We constructed canopy conductance models by combining the commonly used functions in different ways and selected the best one for our study species and climate. The method in this study shows a success in selecting the suitable canopy conductance model. This optimization method should also be applicable in other environment, even with different response functions, provided that enough data are collected for the targeted influencing factors.

Selection of response functions is very important for canopy conductance modelling. For Drooping Sheoak in this study, models that better simulate canopy conductance comprise a parabolic function of air temperature, an exponential function of vapour pressure deficit and a hyperbolic function of predawn stem water potential. Selection of either of the solar radiation functions does not make significant difference in the model performance. Canopy conductance models that take temperature functions into account resulted in better simulations than those without temperature function. Therefore, temperature effect should not be neglected in canopy conductance model. The resulted temperature stress function gives values greater than 1, which is considered to be associated with highly interdependence of air temperature and vapour pressure deficit. Combined stress function of air temperature and vapour pressure deficit suggests a sound physical meaning with the values between zero and unity.

2.5. References

Alfieri, J.G., Niyogi, D., Blanken, P.D., Chen, F., LeMone, M.A., Mitchell, K.E., Ek, M.B. and Kumar, A., 2008. Estimation of the Minimum Canopy Resistance for Croplands and Grasslands Using Data from the 2002 International H2O Project. Monthly Weather Review, 136(11): 4452-4469.

Allen, R.G., Pereira, L.S., Raes, D. and Smith, M., 1998. Crop evapotranspiration: guidelines for computing crop water requirements. FAO Irrigation and drainage paper 56, Rome, Italy.

Alves, I. and Pereira, L.S., 2000. Modelling surface resistance from climatic variables? Agricultural Water Management, 42(3): 371-385.

Aphalo, P.J. and Jarvis, P.G., 1991. Do stomata respond to relative humidity? Plant Cell and Environment, 14(1): 127-132.

Avissar, R. and Pielke, R.A., 1989. A parameterization of heterogeneous land surfaces for atmospheric numerical-models and its impact on regional meteorology. Monthly Weather Review, 117(10): 2113-2136.

Ball, J.H., L. E. Woodrow and Beny, J.A., 1987. A model predicting stomatal conductance and its contribution to the control of photosynthesis under different environmental conditions. In: J. Biggins (Editor), Progress in Photosynthesis research. Martinus Nijhoff, Providence, Rhode Island, USA, pp. 221-224.

Burgess, S.S.O., Adams, M.A., Turner, N.C., Beverly, C.R., Ong, C.K., Khan, A.A.H. and Bleby, T.M., 2001. An improved heat pulse method to measure low and reverse rates of sap flow in woody plants. Tree Physiology, 21(9): 589-598.

Chapman, T.F. and Paton, D.C., 2007. Casuarina ecology: factors limiting cone production in the drooping sheoak, Allocasuarina verticillata. Australian Journal of Botany, 55(2): 171-177.

Chen, F. and Dudhia, J., 2001. Coupling an advanced land surface-hydrology model with the

Penn State-NCAR MM5 modeling system. Part I: Model implementation and sensitivity. Monthly Weather Review, 129(4): 569-585.

Chen, F., Manning, K.W., LeMone, M.A., Trier, S.B., Alfieri, J.G., Roberts, R., Tewari, M., Niyogi, D., Horst, T.W., Oncley, S.P., Basara, J.B. and Blanken, P.D., 2007. Description and evaluation of the characteristics of the NCAR high-resolution land data assimilation system. Journal of Applied Meteorology and Climatology, 46(6): 694-713.

Chen, F., Mitchell, K., Schaake, J., Xue, Y.K., Pan, H.L., Koren, V., Duan, Q.Y., Ek, M. and Betts, A., 1996. Modeling of land surface evaporation by four schemes and comparison with FIFE observations. Journal of Geophysical Research-Atmospheres, 101(D3): 7251-7268.

Choné, X., eacute, Leeuwen, C.v., Dubourdieu, D., Gaudill, J., egrave and re, 2001. Stem Water Potential is a Sensitive Indicator of Grapevine Water Status. Annals of Botany, 87(4): 477-483.

Choudhury, B.J. and Idso, S.B., 1985. An empirical-model for stomatal-resistance of field-grown wheat. Agricultural and Forest Meteorology, 36(1): 65-82.

Collatz, G.J., Ball, J.T., Grivet, C. and Berry, J.A., 1991. Physiological and environmental regulation of stomatal conductance, photosynthesis and transpiration: a model that includes a laminar boundary layer. Agricultural and Forest Meteorology, 54(2–4): 107-136.

Comstock, J. and Mencuccini, M., 1998. Control of stomatal conductance by leaf water potential in Hymenoclea salsola (T & G), a desert subshrub. Plant Cell and Environment, 21(10): 1029-1038.

Damour, G., Simonneau, T., Cochard, H. and Urban, L., 2010. An overview of models of stomatal conductance at the leaf level. Plant Cell and Environment, 33(9): 1419-1438.

Dickinson, R.E., 1987. Evapotranspiration in global climate models. Advances in Space Research, 7(11): 17-26.

Dixon, M.A. and Tyree, M.T., 1984. A new stem hygrometer, corrected for temperature-gradients and calibrated against the pressure bomb. Plant Cell and Environment, 7(9): 693-697.

Dye, P.J. and Olbrich, B.W., 1993. Estimating transpiration from 6-year-old Eucalyptus grandis trees: development of a canopy conductance model and comparison with independent sap flux measurements. Plant Cell and Environment, 16(1): 45-53.

Eamus, D. and Froend, R., 2006. Groundwater-dependent ecosystems: the where, what and why of GDEs. Australian Journal of Botany, 54(2): 91-96.

Edwards, W.R.N. and Jarvis, P.G., 1982. Relations between water-content, potential and permeability in stems of conifers. Plant Cell and Environment, 5(4): 271-277.

Feddes, R.A., Kowalik, P.J. and Zaradny, H., 1978. Simulation of field water use and crop yield. Centre for Agricultural Publishing and Documentation, Wageningen, Netherlands.

Gash, J.H.C., Shuttleworth, W.J., Lloyd, C.R., Andre, J.C., Goutorbe, J.P. and Gelpe, J., 1989. Micrometeorological measurements in Les Landes forest during HAPEX-MOBILHY. Agricultural and Forest Meteorology, 46(1-2): 131-147.

Green, S., Clothier, B. and Jardine, B., 2003. Theory and practical application of heat pulse to measure sap flow. Agronomy Journal, 95(6): 1371-1379.

Green, S. and Clothier, B.E., 1988. Water-use of kiwifruit vines and apple-trees by the heat-pulse technique. Journal of Experimental Botany, 39(198): 115-123.

Guan, H.D., Zhang, X.P., Skrzypek, G., Sun, Z. and Xu, X., 2013. Deuterium excess variations of rainfall events in a coastal area of South Australia and its relationship with synoptic weather systems and atmospheric moisture sources. Journal of Geophysical Research-Atmospheres, 118(2): 1123-1138.

Hong, S.B., Lakshmi, V., Small, E.E., Chen, F., Tewari, M. and Manning, K.W., 2009. Effects of vegetation and soil moisture on the simulated land surface processes from the coupled WRF/Noah model. Journal of Geophysical Research-Atmospheres, 114.

Jarvis, P.G., 1976. The interpretation of the variations in leaf water potential and stomatal conductance found in canopies in the field. Philosophical Transactions of the Royal Society of London. B, Biological Sciences, 273(927): 593-610.

Kelliher, F.M., Leuning, R., Raupach, M.R. and Schulze, E.D., 1995. Maximum conductances for evaporation from global vegetation types. Agricultural and Forest Meteorology, 73(1-2): 1-16.

Kumar, A., Chen, F., Niyogi, D., Alfieri, J.G., Ek, M. and Mitchell, K., 2011. Evaluation of a Photosynthesis-Based Canopy Resistance Formulation in the Noah Land-Surface Model. Boundary-Layer Meteorology, 138(2): 263-284.

LeMone, M.A., Chen, F., Alfieri, J.G., Tewari, M., Geerts, B., Miao, Q., Grossman, R.L. and Coulter, R.L., 2007. Influence of land cover and soil moisture on the horizontal distribution of sensible and latent heat fluxes in southeast Kansas during IHOP_2002 and CASES-97. Journal of Hydrometeorology, 8(1): 68-87.

Leuning, R., 1995. A Critical-Appraisal of A Combined Stomatal-photosynthesis Model for C-3 Plants. Plant Cell and Environment, 18(4): 339-355.

Leuning, R. and Foster, I.J., 1990. Estimation of transpiration by single trees - comparison of a ventilated chamber, leaf energy budgets and a combination equation. Agricultural and Forest Meteorology, 51(1): 63-86.

Leuning, R., Zhang, Y.Q., Rajaud, A., Cleugh, H. and Tu, K., 2008. A simple surface conductance model to estimate regional evaporation using MODIS leaf area index and the Penman-Monteith equation. Water Resources Research, 44(10): -.

Lhomme, J.P., Elguero, E., Chehbouni, A. and Boulet, G., 1998. Stomatal control of transpiration: Examination of Monteith's formulation of canopy resistance. Water Resources Research, 34(9): 2301-2308.

Lohammar, T., Larsson, S., Linder, S. and Falk, S.O., 1980. Fast-simulation models of gaseous exchange in Scots pine. In: T. Persson (Editor), Structure and function of northern coniferous forests : an ecosystem study. Swedish Natural Science Research Council, Stockholm, pp. 505-523.

Lu, P., Yunusa, I.A.M., Walker, R.R. and Muller, W.J., 2003. Regulation of canopy conductance and transpiration and their modelling in irrigated grapevines. Functional Plant Biology, 30(6): 689-698.

Macfarlane, C., White, D.A. and Adams, M.A., 2004. The apparent feed-forward response to vapour pressure deficit of stomata in droughted, field-grown Eucalyptus globulus Labill. Plant Cell and Environment, 27(10): 1268-1280.

Mascart, P., Taconet, O., Pinty, J.P. and Mehrez, M.B., 1991. Canopy Resistance Formulation and Its Effect in Mesoscale Models - a Hapex Perspective. Agricultural and Forest Meteorology, 54(2-4): 319-351.

Meinzer, F.C., James, S.A. and Goldstein, G., 2004. Dynamics of transpiration, sap flow and use of stored water in tropical forest canopy trees. Tree Physiology, 24(8): 901-909.

Meinzer, F.C., Woodruff, D.R., Domec, J.C., Goldstein, G., Campanello, P.I., Gatti, M.G. and Villalobos-Vega, R., 2008. Coordination of leaf and stem water transport properties in tropical forest trees. Oecologia, 156(1): 31-41.

Misson, L., Panek, J.A. and Goldstein, A.H., 2004. A comparison of three approaches to modeling leaf gas exchange in annually drought-stressed ponderosa pine forests. Tree Physiology, 24(5): 529-541.

Mitchell, K.E., Lohmann, D., Houser, P.R., Wood, E.F., Schaake, J.C., Robock, A., Cosgrove, B.A., Sheffield, J., Duan, Q.Y., Luo, L.F., Higgins, R.W., Pinker, R.T., Tarpley, J.D., Lettenmaier, D.P., Marshall, C.H., Entin, J.K., Pan, M., Shi, W., Koren, V., Meng, J., Ramsay, B.H. and Bailey, A.A., 2004. The multi-institution North American Land Data Assimilation System (NLDAS): Utilizing multiple GCIP products and partners in a continental distributed hydrological modeling system. Journal of Geophysical Research-Atmospheres, 109(D7).

Monteith, J.L., 1981. Evaporation and surface-temperature. Quarterly Journal of the Royal Meteorological Society, 107(451): 1-27.

Murray, B., Zeppel, M., Hose, G. and Eamus, D., 2003. Groundwater dependent ecosystems in Australia: it's more than just water for rivers. Ecological Management & Restoration, 4: 109-113.

Noilhan, J. and Planton, S., 1989. A simple parameterization of land surface processes for meteorological models. Monthly Weather Review, 117(3): 536-549.

Nortes, P.A., Pérez-Pastor, A., Egea, G., Conejero, W. and Domingo, R., 2005. Comparison of changes in stem diameter and water potential values for detecting water stress in young almond trees. Agricultural Water Management, 77(1–3): 296-307.

Palmer, A.R., Fuentes, S., Taylor, D., Macinnis-Ng, C., Zeppel, M., Yunusa, I. and Eamus, D., 2010. Towards a spatial understanding of water use of several land-cover classes: an examination of relationships amongst pre-dawn leaf water potential, vegetation water use, aridity and MODIS LAI. Ecohydrology, 3(1): 1-10.

Patankar, R., Quinton, W.L. and Baltzer, J.L., 2013. Permafrost-driven differences in habitat quality determine plant response to gall-inducing mite herbivory. Journal of Ecology, 101(4): 1042-1052.

Peeters, P.J., T. Gerschwitz and Carpenter, R.J., 2006. Restoring Sheoak Grassy Woodlands on Lower Eyre Peninsula. , School of Earth and Environmental Sciences, Adelaide, South Australia.

Phillips, N., Oren, R. and Zimmermann, R., 1996. Radial patterns of xylem sap flow in non-, diffuse- and ring-porous tree species. Plant Cell and Environment, 19(8): 983-990.

Rao, P. and Agarwal, S.K., 1984. Diurnal-variation in leaf water potential, stomatal conductance, and irradiance of winter crop under different moisture levels. Biologia Plantarum, 26(1): 1-4.

Richter, H., 1997. Water relations of plants in the field: Some comments on the measurement of selected parameters. Journal of Experimental Botany, 48(306): 1-7.

Ronda, R.J., de Bruin, H.A.R. and Holtslag, A.A.M., 2001. Representation of the canopy conductance in modeling the surface energy budget for low vegetation. Journal of Applied Meteorology, 40(8): 1431-1444.

Schulze, E.D., Kelliher, F.M., Korner, C., Lloyd, J. and Leuning, R., 1994. Relationships among maximum stomatal conductance, ecosystem surface conductance, carbon assimilation rate, and plant nitrogen nutrition - a global ecology scaling exercise. Annual Review of Ecology and Systematics, 25: 629-&.

Sellers, P.J., Mintz, Y., Sud, Y.C. and Dalcher, A., 1986. A simple biosphere model (sib) for use within general-circulation models. Journal of the Atmospheric Sciences, 43(6): 505-531.

Shuttleworth, W.J. and Wallace, J.S., 1985. Evaporation from sparse crops - an energy combination theory. Quarterly Journal of the Royal Meteorological Society, 111(469): 839-855.

Stewart, J.B., 1988. Modeling surface conductance of pine forest. Agricultural and Forest Meteorology, 43(1): 19-35.

Thorpe, M.R., Warrit, B. and Landsberg, J.J., 1980. Responses of apple leaf stomata - a model for single leaves and a whole tree. Plant Cell and Environment, 3(1): 23-27.

Tuzet, A., Perrier, A. and Leuning, R., 2003. A coupled model of stomatal conductance, photosynthesis and transpiration. Plant Cell and Environment, 26(7): 1097-1116.

Tyree, M.T. and Yang, S.D., 1990. Water-storage capacity of thuja, tsuga and acer stems measured by dehydration isotherms - the contribution of capillary water and cavitation. Planta, 182(3): 420-426.

Vandegehuchte, M.W., Guyot, A., Hubau, M., De Groote, S.R.E., De Baerdemaeker, N.J.F., Hayes, M., Welti, N., Lovelock, C.E., Lockington, D.A. and Steppe, K., 2014a. Long-term versus daily stem diameter variation in co-occurring mangrove species: Environmental versus ecophysiological drivers. Agricultural and Forest Meteorology,

192–193(0): 51-58.

Vandegehuchte, M.W., Guyot, A., Hubeau, M., De Swaef, T., Lockington, D.A. and Steppe, K., 2014b. Modelling reveals endogenous osmotic adaptation of storage tissue water potential as an important driver determining different stem diameter variation patterns in the mangrove species Avicennia marina and Rhizophora stylosa. Annals of Botany.

Vrugt, J.A., ter Braak, C.J.F., Diks, C.G.H., Robinson, B.A., Hyman, J.M. and Higdon, D., 2009. Accelerating Markov Chain Monte Carlo Simulation by Differential Evolution with Self-Adaptive Randomized Subspace Sampling. International Journal of Nonlinear Sciences and Numerical Simulation, 10(3): 273-290.

Wang, Y.P. and Leuning, R., 1998. A two-leaf model for canopy conductance, photosynthesis and partitioning of available energy I: Model description and comparison with a multi-layered model. Agricultural and Forest Meteorology, 91(1-2): 89-111.

Warrit, B., Landsberg, J.J. and Thorpe, M.R., 1980. Responses of Apple Leaf Stomata to Environmental-Factors. Plant Cell and Environment, 3(1): 13-22.

White, D., Beadle, C.L., Sands, P.J., Worledge, D. and Honeysett, J.L., 1999a. Quantifying the effect of cumulative water stress on stomatal conductance of Eucalyptus globulus and Eucalyptus nitens: a phenomenological approach. Australian Journal of Plant Physiology, 26(1): 17-27.

White, D.A., Beadle, C.L., Sands, P.J., Worledge, D. and Honeysett, J.L., 1999b. Quantifying the effect of cumulative water stress on stomatal conductance of Eucalyptus globulus and Eucalyptus nitens: a phenomenological approach. Australian Journal of Plant Physiology, 26(1): 17-27.

White, R., Christy, B.P., Ridley, A.M., Okom, A.E., Murphy, S.R., Johnston, W.H., Michalk, D.L., Sanford, P., McCaskill, M.R., Johnson, I.R., Garden, D.L., Hall, D.J.M. and Andrew, M.H., 2003. SGS Water Theme: influence of soil, pasture type and management on water use in grazing systems across the high rainfall zone of southern Australia. Australian Journal of Experimental Agriculture, 43(7-8): 907-926.

Whitley, R., Medlyn, B., Zeppel, M., Macinnis-Ng, C. and Eamus, D., 2009. Comparing the Penman-Monteith equation and a modified Jarvis-Stewart model with an artificial neural network to estimate stand-scale transpiration and canopy conductance. Journal of Hydrology, 373(1-2): 256-266.

Whitley, R., Zeppel, M., Armstrong, N., Macinnis-Ng, C., Yunusa, I. and Eamus, D., 2008. A modified Jarvis-Stewart model for predicting stand-scale transpiration of an Australian native forest. Plant and Soil, 305(1-2): 35-47.

Yang, Y.T., Guan, H.D., Hutson, J.L., Wang, H.L., Ewenz, C., Shang, S.H. and Simmons, C.T., 2013. Examination and parameterization of the root water uptake model from stem water potential and sap flow measurements. Hydrological Processes, 27(20): 2857-2863.

3. Modelling the environmental controls on tree water use at different temporal scales: significance of soil water condition

3.1. Introduction

Vegetation covers 70% of the land surface (Dolman et al., 2014), playing an important role in land surface hydrological and climatological processes, and coordinating the land-atmosphere interactions in a wide range of spatial and temporal scales (Chen et al., 1996; Dickinson, 1987; LeMone et al., 2007). Vegetation affects water, carbon and energy transfer in the soil-atmosphere system by altering surface albedo, roughness, soil macroporosity, intercepting rainfall and transpiring water from deep soil layers (Ivanov et al., 2008). Up to 80% of total global evapotranspiration (ET) is contributed by transpiration from vegetation (E_c, interchangeable with "tree water use" throughout the text) (Miralles et al., 2011), which highlights the importance of the quantification of vegetation water use to the understanding of land-atmosphere interactions.

Transpiration at the tree and stand/forest scales can be estimated using the sap flow techniques (Ford et al., 2007; Hatton et al., 1995). Alternatively, transpiration can be estimated from potential transpiration by applying stress functions related to different environmental variables (Chen et al., 1996), such as temperature, vapour pressure deficit, solar radiation, CO_2 concentration (Ball et al., 1987), soil water content/potential and plant water potential (Damour et al., 2010; Jarvis, 1976; Tuzet et al., 2003; Wang et al., 2014). Such an approach can be applied over various spatial scales, thus has long been incorporated into land surface models (Noilhan and Planton, 1989) and atmospheric models (Dai et al., 2004; Dickinson et al., 1991). It should be noted that the reduction of potential E_c by environmental constraints in the land surface or atmospheric models is often realized by replacing the canopy conductance g_c (or resistance, $1/g_c$) under the optimal conditions in the Penman-Monteith equation with the one considering the environmental stresses. This way of E_c estimation can be categorized as "indirect" method, which involves the calculation of g_c. Numerous studies after Monteith (1965), Jarvis (1976) and Stewart (1988) have discussed the environmental controls on canopy conductance for different species and climate types, in order to improve transpiration estimates (Buckley et al., 2012; Comstock and Mencuccini, 1998; Kelliher et al., 1993). Apart from studies using the Penman-Monteith equation for transpiration estimates, there are several attempts to correlate E_c straightforward with environmental variables, avoiding the g_c calculation. This way of E_c modelling can be categorized as "direct" method. For example, Whitley et al. (2009; 2013)

developed an empirical model for tree water use estimation using vapour pressure deficit, solar radiation and volumetric soil water content; Buckley et al. (2012) developed a transpiration model only considering explicitly solar radiation and vapour pressure deficit. Such models contain reduced number of parameters and have great potential for use in land surface and atmospheric models.

The environmental variables that influence transpiration modelling can be divided into two groups, i.e. demand and supply. The environmental variables in the demand group include solar radiation, vapour pressure deficit and air temperature, etc. Temperature functions are often neglected in E_c (or g_c) models (Lhomme et al., 1998; Mascart et al., 1991). The corresponding environmental variable in the supply group is the root zone soil water condition, determined by root distribution, soil hydraulic properties and water content in root zones. It is worth mentioning that plants respond to soil water potential rather than soil water content (Gregory and Nortcliff, 2013; Marshall et al., 1996; Mullins, 2001; Verhoef and Egea, 2014); the latter in most studies was measured in shallow soil layers up to 2 m deep and usually 0.5 m (Whitley et al., 2009). Soil water availability can restrict plant water uptake (Chen et al., 2014), however, it is doubted whether the measurements of soil water content in shallow soil layers can represent the entire picture of root-zone water availability (Schulze et al., 1996), especially for the trees with deep root systems. The gradient of water potentials in soil, stem and leaf drives the water transport in the soil-plant system (Vandegehuchte et al., 2014). Plant water potential is a sensitive indicator for vegetation water status (Choné et al., 2001; Nortes et al., 2005) and can be in equilibrium in the whole soil-plant system at predawn (Palmer et al., 2010; Richter, 1997). Therefore, plant water potential is a good approximate of water availability in root-zone soil for vegetation transpiration. Previous studies have tested the feasibility of using stem water potential to simulate plant water stresses from a reduced soil moisture condition (Wang et al., 2014; Yang et al., 2013).

Despite the wealth of literature in considering soil water condition in E_c and g_c modelling, some studies showed the feasibility to simulate E_c and g_c without soil water condition functions (Bunce, 2000; Leuning, 1995; Whitley et al., 2013). Transpiration from trees that can access groundwater with deep roots (Eamus and Froend, 2006) or from trees that grow in riparian sites (O'Grady et al., 2006) is not limited by soil water condition. At such sites, the soil water stress function can be omitted in E_c and g_c models. However, at other sites, it is difficult to determine the significance ofC soil water condition for E_c or g_c modelling without long-term monitoring on the relevant variables. Furthermore, soil water availability has seasonal variations (Findell and Eltahir, 1997), which means the necessity to include a soil water stress function may vary

seasonally. As such, the time and temporal scales (such as daily and sub-daily) at which a soil water condition function is more important for transpiration modelling may vary.

In addition, models are usually only as good as the data on which they are based and have been tested (Silberstein, 2003). Parameter values in many land surface models are prescribed universally for lumped vegetation categories, for example, evergreen needle-leaf trees, deciduous broad-leaf trees, etc. (Chen and Dudhia, 2001), and they keep the same for various temporal scales. However, the empirical relationships between transpiration and environmental variables are climate and vegetation specific. One set of universal parameter values is not necessarily applicable to different climate-species.

Therefore, in this study, E_c was simulated for a Drooping Sheoak tree in South Australia at daily and hourly scales and in spring, summer and autumn using two categories of models. By comparing simulation results, this study was aimed to answer the following four questions: (1) which type of E_c model can better reproduce sap flow measurements in this study, ″direct″ or ″indirect″; (2) how significant is it to include soil water condition and temperature functions for E_c modelling; (3) when and at which time scale soil water condition function has stronger influence on E_c modelling; and (4) whether parameter values are applicable across different temporal scales (daily and hourly) for a certain E_c model.

3.2. Methodology

3.2.1. Site and measurements

The study site, in Mediterranean climate zone, is near the campus of Flinders University ($138°34′28″$E, $35°01′49″$S). Annual mean temperature is about 17 $°$C, and annual rainfall is around 546 mm, most of which occurs in May to September (Guan et al., 2013). Ground surface is covered by sparse trees with short shrubs and grass at substrate. Soil type in the site is characterized as sandy mixed with gravel. This soil condition makes it difficult to bury soil moisture probes in deep root zone soil layers near the tree. Therefore, as discussed in previous work (Wang et al., 2014; Yang et al., 2013) we used the stem water potential as an indicator for water availability. All measurements in this study were conducted on a drooping sheoak (*Allocasuarina verticillata*) tree in January-April and October-December 2012.

Sap flow was monitored at 30-min intervals in the tree trunks at 1.3 m above ground using the compensation heat-pulse technique (Green and Clothier, 1988). Three thermocouples are embedded inside each temperature probe at the depths of 0.5, 1.5, and 2.5 cm underneath the cambium. One temperature probe was installed 1.0 cm above the heater and the other 0.5 cm

below the heater. Two sets of such probes were installed in the south and north sides of the tree. Transpiration was calculated from heat transport velocity and corrected for wounding, sapwood area, volume fraction of wood and water following Green et al. (2003).

Stem water potential (ψ_{st}) was measured at 15-minute intervals with PSY1 Stem Psychrometer (*ICT International Pty Ltd., NSW, Australia*), which was developed by Dixon and Tyree (1984) and has become commercially available in the last a few years. PSY1 measures the temperature of sapwood surface and chamber air, and stem water potential is corrected with the temperature gradient (Dixon and Tyree, 1984). Predawn stem water potential (ψ_{pd}) was taken as the average of ψ_{st} between 3:00 am and 5:00 am, when water potentials in the tree and root-zone soil have reached an equilibrium state after water redistribution in the plant-soil system.

3.2.2. Models briefing

"Indirect" E_c model

The ″indirect″ model for transpiration estimate refers to the Penman-Monteith method (PM), equation (3-1); the canopy conductance g_c in PM equation is estimated from the environmental conditions following the Jarvis-Stewart (JS) approach in equation (3-2).

$$E_c = \frac{\Delta A_c + \rho_a C_p D g_a}{\lambda [\Delta + \gamma (1 + g_a / g_c)]}$$

(3-1)

$$g_c = g_{max} LAI \cdot f(D) f(T) f(R_s) f(\psi)$$

(3-2)

In equations (3-1) and (3-2), g_a is aerodynamic conductance [m/s]; γ is psychrometric constant [kPa/^{o}C]; λ is latent heat of vaporization [MJ/kg]; E_c is the tree water use calculated from sap flow measurements; Δ is the slope of saturation vapour pressure-temperature curve [kPa/^{o}C]; A_c is the available energy allocated to canopy [MJ/(m^{2}h)]; C_p is specific heat of air at constant pressure [MJ/(kg^{o}C)]; D is vapour pressure deficit in the air [kPa]; ρ_a is the density of air [kg/m^3]. g_{max} is the maximum stomatal conductance [m/s]. LAI is leaf area index. ψ is the stem water potential [MPa]; when used for daily E_c or g_c estimation, predawn stem water potential (ψ_{pd}) is used.

Here we denoted equation (3-2) as JS4 model, as it considers the effects of four environmental variables. In order to test the significance of stress functions of air temperature and soil water condition, we made modifications to JS4 by neglecting *f(T)* and *f(ψ)* respectively, and the relevant models were denoted as JSψ and JST. Equations (3-3~3-6) are the stress functions for each variable based on a previous study (Wang et al., 2014).

$$f(R_s) = \frac{R_s}{R_s + k_{Rs}} \cdot \frac{R_{sm} + k_{Rs}}{R_{sm}} \tag{3-3}$$

$$f(D) = e^{-k_D D} \tag{3-4}$$

$$f(T) = 1 - k_T (T_o - T)^2 \tag{3-5}$$

$$f(\psi) = \frac{1}{1 + (\psi / \psi_m)^{k_\psi}} \tag{3-6}$$

R_{sm} in equation (3-3) is the approximate maximum radiation, set as 1000 W/m^2 for hourly and 350 W/m^2 for daily simulations according to measurements. k_{Rs} [W/m^2], k_D [kPa^{-1}], k_T [-], T_o [^{o}C], k_ψ [-] and ψ_m [MPa] are fitting parameters.

"Direct" E_c models

The models described in this section omit the calculation of canopy conductance, and estimate tree water use straightforward from a set of environmental variables. From the available literature, we selected two "direct" models for comparison; they have simple structure and limited parameters.

Whitley et al.'s model (UTS)

Following the Jarvis-Stewart pattern, Whitley et al. (2009; 2013) developed an empirical model for tree water use estimation from environmental variables, bypassing the stomatal conductance. We supplemented a temperature function and replaced the soil water content function with a stem water potential function in equation (3-6), and further reduced one parameter for vapour pressure deficit function. The modified model is given in equation (3-7) and referred to as UTS4. In equations (3-7) and (3-8), E_{max} is the maximum transpiration rate [mm/h or mm/d]; k_D is a fitting parameter. D_{peak} [kPa] is the value of D at which E_c is maximized. $f(R_s)$, $f(T)$ and $f(\psi)$ are the same with equations (3-3), (3-5) and (3-6). To facilitate the model comparison, further modifications were made to UTS4 by neglecting $f(T)$ and $f(\psi)$, resulting in models UTSψ and UTST accordingly.

$$E_c = E_{max} f^\wedge(D) f(T) f(R_s) f(\psi) \tag{3-7}$$

$$f^\wedge(D) = \exp\left\{ -\frac{k_D (D - D_{peak})^2}{D} \right\} \tag{3-8}$$

Buckley et al. (2003; 2012) described a simple mechanism-based model for transpiration estimates, given in equation (3-9). Their model contains only solar radiation and vapour pressure deficit explicitly, thus has fewer parameters than the PM and UTS models. The parameter R_{s0} allows night time transpiration for sub-daily simulation which is the particular strength over other models. In this study, we assumed zero night-time transpiration, because the Jarvis-Stewart approach is incapable of capturing the nocturnal transpiration. Therefore, R_{s0} was prescribed as 0 for both hourly and daily scale simulations. E_{max} is the maximum transpiration rate, which includes the effect of soil water condition. D_s is the leaf to air vapour pressure deficit, which can be replaced with the air vapour pressure deficit (D) when canopy is coupled aerodynamically. We used D in this study.

$$E_c = \frac{E_{\max} D_s (R_s + R_{s0})}{k + bR_s + (R_s + R_{s0})D_s} \tag{3-9}$$

Buckley et al. (2012) also provided a canopy conductance model as follows:

$$g_c = \frac{E_m (R_s + R_{s0})}{k + bR_s + (R_s + R_{s0})D_s} \tag{3-10}$$

E_m, k and b are integrated model parameters.

Canopy conductance was also estimated from equation (3-10) and combined with the Penman-Monteith equation for transpiration estimate to compare with other modelling results.

3.2.3. Parameter optimization and model comparison

Data on rainy days were filtered out. For daily simulations, data were divided into two groups (one contains data in the order of 1, 3, 5… and the other 2, 4, 6… respectively). The first group was used to train the model, and the second group was used to test the model. For hourly simulations, we first used two-month data to train the model and tested the model with another two-month data. Furthermore, we grouped the data in spring (September, October and November), summer (December, January and February) and autumn (March, April and May), and then trained the model using 20 days of data in each season, and tested the model using another 20 days of data. Summer days in this study covered the hottest days in 2012, and early autumn was the driest in 2012.

Parameters were obtained using the DiffeRential Evolution Adaptive Metropolis (DREAM)

model (Vrugt et al., 2009). DREAM runs multiple different chains simultaneously for global exploration and automatically tunes the scale and orientation of the proposal distribution in randomized subspaces during the search. More details about the model can be found in Vrugt et al. (2009). The DREAM was performed for each model by 20,000 iterations. We evaluated the model performance using the slope (k) and coefficient of determination (R^2) of linear regression between the measured and simulated E_c, with zero intercepts, and the root mean square error ($RMSE$).

3.3. Results and discussion

3.3.1. Environmental conditions and tree water use

Part of the measurement results is demonstrated in Figure 3.1 at both hourly and daily scales. Daily data of tree water use and stem water potential, solar radiation, vapour pressure deficit and temperature were obtained from the original 30-minute and 15-minute measurements. Data in rainy days are not shown.
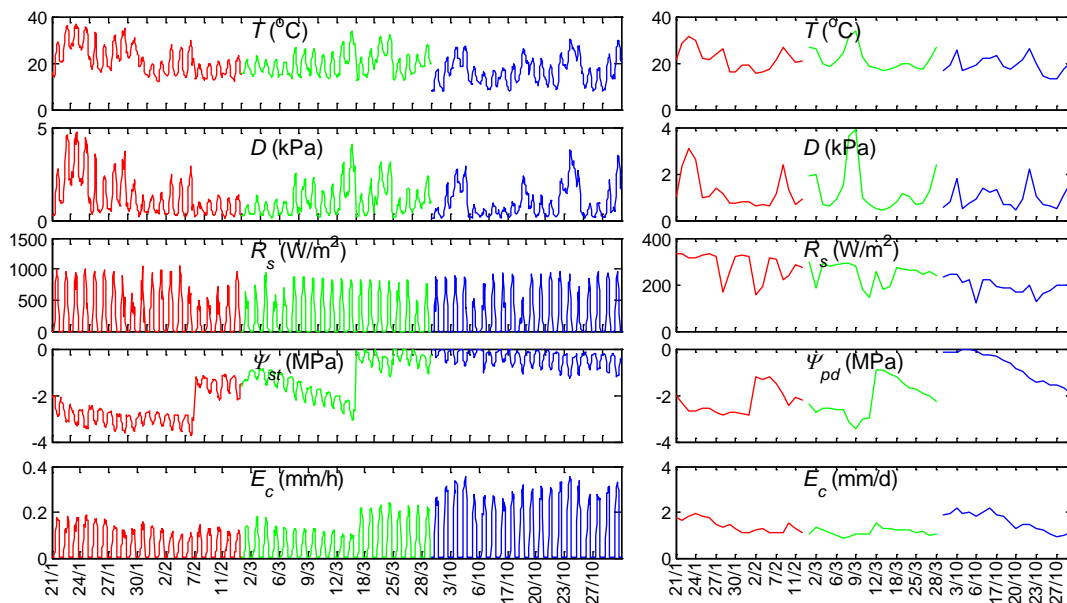
Figure 3.1 Environmental conditions and tree water use (E_c) at hourly (left panel) and daily (right panel) scales in the testing period. T: air temperature; D: vapor pressure deficit; R_s: solar radiation and ψ_{st}: stem water potential. ψ_{pd}: predawn stem water potential. X-axis labels are the measurement days in 2012. Red is for summer days, green is for autumn days and blue is for spring days.

The maximum transpiration and canopy conductance were observed in early spring (October) at a rate around 3.0 mm/d and 0.015 m/s respectively at daily scale. In this period, the rainy season just passed, so there was sufficient water storage in the soil for trees to transpire; in the meantime, solar energy was increasing, resulting in an optimal condition for tree water use and growth. In Figure 3.1, temperature has similar dynamics with vapour pressure deficit, which

reflects a high interdependency between these two variables. Transpiration increased when stem water potential increased. In December when the site became heating and drying, the stem water potential decreased, transpiration also decreased as soil water depletion increased. Stem water potential data indicate that Drooping Sheoak recovered xylem water storage in night-time and likely had reached an equilibrium state before predawn. The daily average difference between the maximum and minimum stem water potential was around 1.0 MPa for clear days in dry season.

3.3.2. Model comparisons

Hourly E_c modelling

We first evaluated the models at hourly scale by comparing simulated E_c with the sap flow measurements in 60 days in the testing period. Figure 3.2 shows the results from the "indirect" method (Penman-Monteith), in which g_c is simulated from models JS4, JST, JSψ and BTA. Figure 3.3 shows the results from the "direct" models UTS4, UTST, UTSψ and BTA. Overall, these models were able to reproduce the diurnal variation of E_c; the "direct" models gave relatively better fitting than the "indirect" models according to R^2 and *RMSE*. Both approaches overestimated E_c around midday of some days in summer and autumn when it was hot and dry, in particular PM(JST), PM(BTA) and UTST and BTA. In spring days transpiration was more underestimated by the "direct" models than the "indirect" methods.
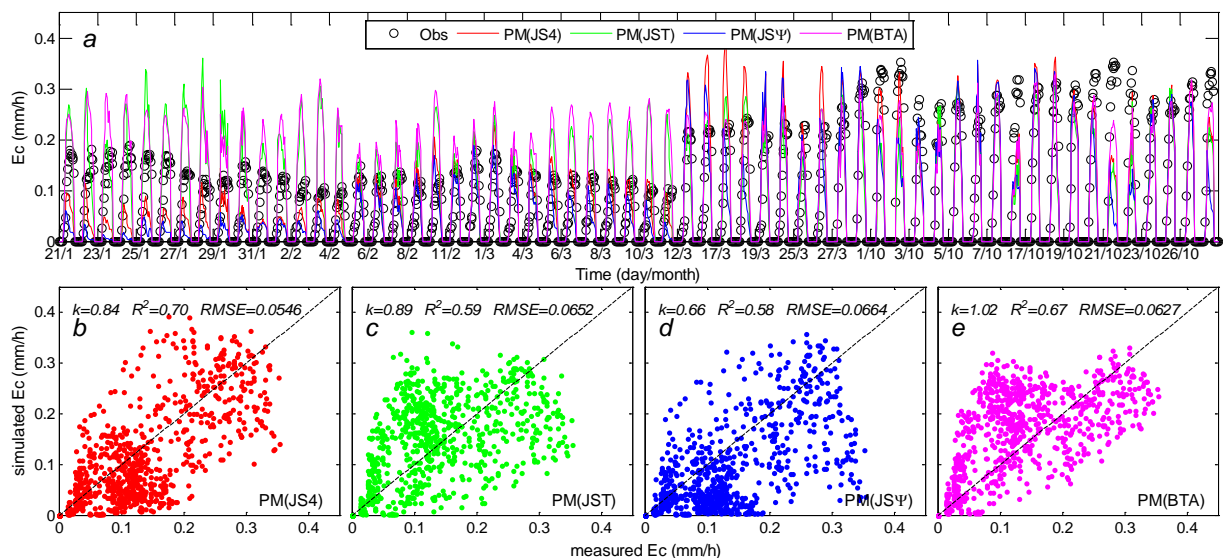
Figure 3.2 Comparison between sap flow measurements and E_c simulated by "indirect" models PM(JS4), PM(JST), PM(JSψ) and PM(BTA). *k* and R^2 are slope and coefficient of determination of the linear regression (with zero intercept) between simulated and measured E_c; *RMSE* is the root mean square error. *Obs* is the measured E_c. Dash lines in plots *b-e* are 1:1 lines.
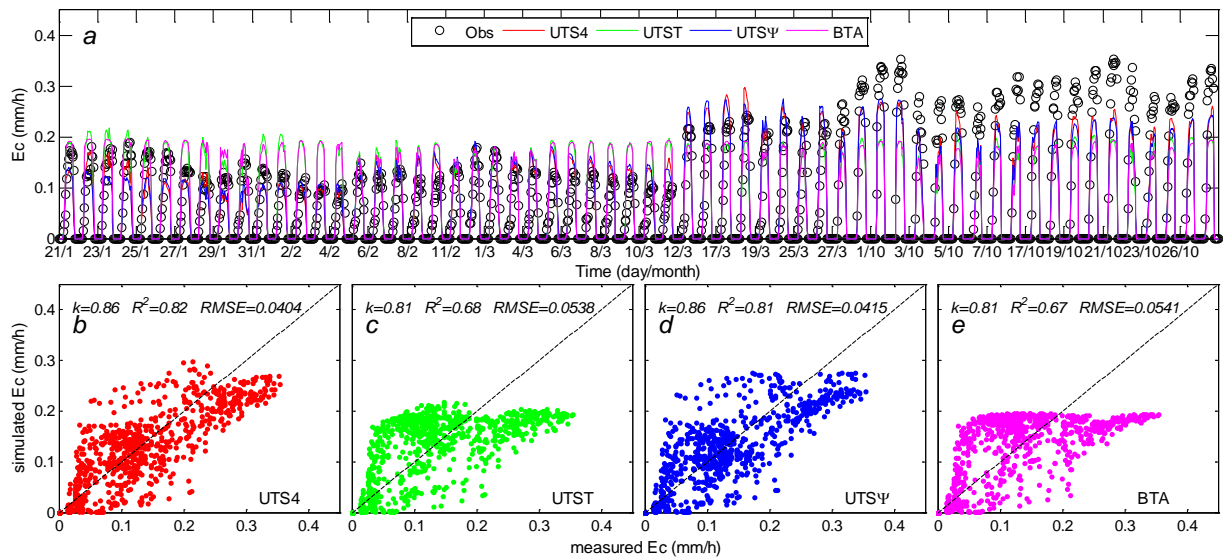
Figure 3.3 Same with Figure 3.2 but modelled by ″direct″ models UTS4, UTST, UTSψ and BTA

PM(JS4) among other ″indirect″ models gave the best simulations in comparison to the sap flow measurements, and UTS4 gave the best simulations among the ″direct″ models. Neglecting air temperature and/or soil water condition function worsened E_c models performance, reflected by the decreased k and R^2 and increased *RMSE* from the models that exclude *f(T)* and/or *f(ψ)* in comparison to PM(JS4) and UTS4 (Figure 3.2 and Figure 3.3). Therefore, at hourly scale, air temperature and soil water condition functions have positive effects on transpiration modelling. Comparing PM(JST) and PM(JSψ) and UTST and UTSψ indicates that the effect of soil water function was a little stronger than that of temperature function in ″direct″ models and the opposite in the ″indirect″ models. It should be noted that the day-to-day difference of E_c simulated from UTST and BTA were relatively small (Figure 3.3), which indicates that these two models were incapable of accounting for day-to-day variations of soil water availability.

Hourly E_c modelling in individual seasons

In order to examine the effects of soil water condition and air temperature functions on transpiration modelling in different seasons, we simulated E_c separately for spring, summer and autumn using all models. Results from the Penman-Monteith method are given in Figure 3.4 and Figure 3.5. Figure 3.4 shows a good fitting between the simulated (by ″indirect″ models) and measured E_c in all seasons, although overestimation around midday of a few days in each season was observed. The best agreement between the simulated and measured E_c appears in spring by PM(JS4) (Figure 3.5). Comparing the k, R^2 and *RMSE* given by PM(JS4) and PM(JST) shows that inclusion of *f(ψ)* resulted in great improvement on E_c simulation in autumn, but had little influence in spring and summer. Similarly, comparison between PM(JS4) and PM(JSψ) indicates

39

that inclusion of a temperature function improved model performance in spring, but deteriorated model performance in autumn. The negative impacts of temperature function on tree water use modelling have also been reported in other studies (Sommer et al., 2002; Whitley et al., 2013; Wright et al., 1995). The BTA model explicitly considers only the effects of solar radiation and vapour pressure deficit on canopy conductance, and embedded other factors (including the soil water condition) in the lumped parameters. BTA models were capable to reproduce diurnal variations of E_c with greater overestimation than other models especially in some autumn days (Figure 3.4c). This may be a result of the model structure which expresses the effects of soil water stress function through fixed parameter values, which cannot reflect the dynamics of soil water availability.
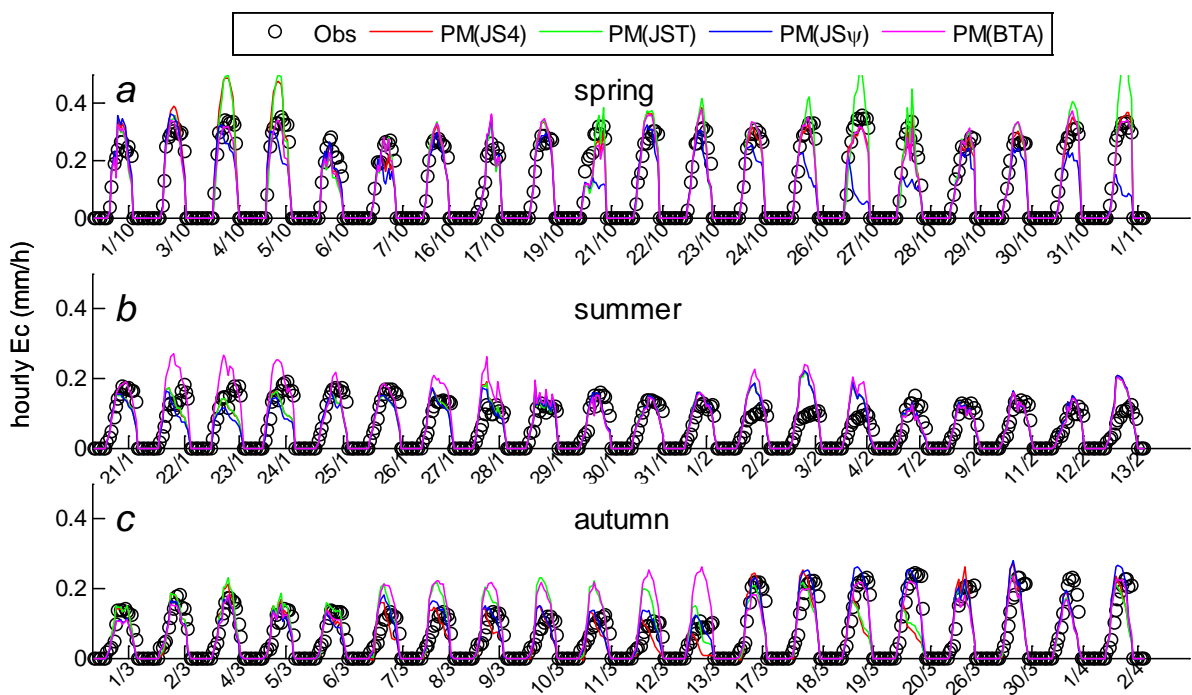
Figure 3.4 Hourly tree water use simulated from Penman-Monteith equation with g_c simulated by JS4, JST and JSψ models compared to sap flow measurements in (*a*) spring; (*b*) summer and (*c*) autumn.
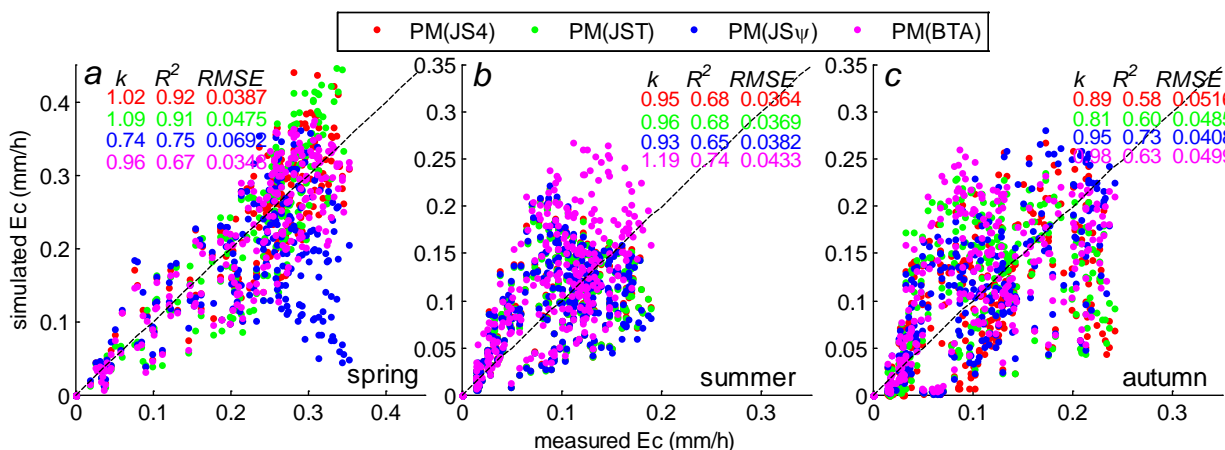
Figure 3.6 and Figure 3.7 show clearly that the ″direct″ models gave overall better simulations than the ″indirect″ models, reflected by the regression k, R^2 and *RMSE*. The best fitting between simulated (by ″direct″ models) and measured E_c was also in spring and the worst in autumn as is in Figure 3.4*c* and Figure 3.5*c* by the ″indirect″ models. The models counting in all four environmental variables did not show obvious superiority over the models without *f(T)* and/or *f(ψ)*. However, soil water function had a stronger influence on tree water use modelling in autumn than spring and summer (Figure 3.7*c*). E_c in Figure 3.6 underestimated the maximum sap flow measurements around midday in some days. Using other days of data to train and test the models did not eliminate the phenomenon. We checked on the rainfall and solar radiation data on those days and the days before, and found that the underestimation occurred on cloudy days or with rainfall on previous days, when solar radiation was not saturated as on clear days. This implies that the models need to be improved for explicit interpretation of transpiration under light-unsaturated conditions. BTA E_c model gave very similar simulations with other three models, which is encouraging because it requires the minimum number of input variables and parameters.
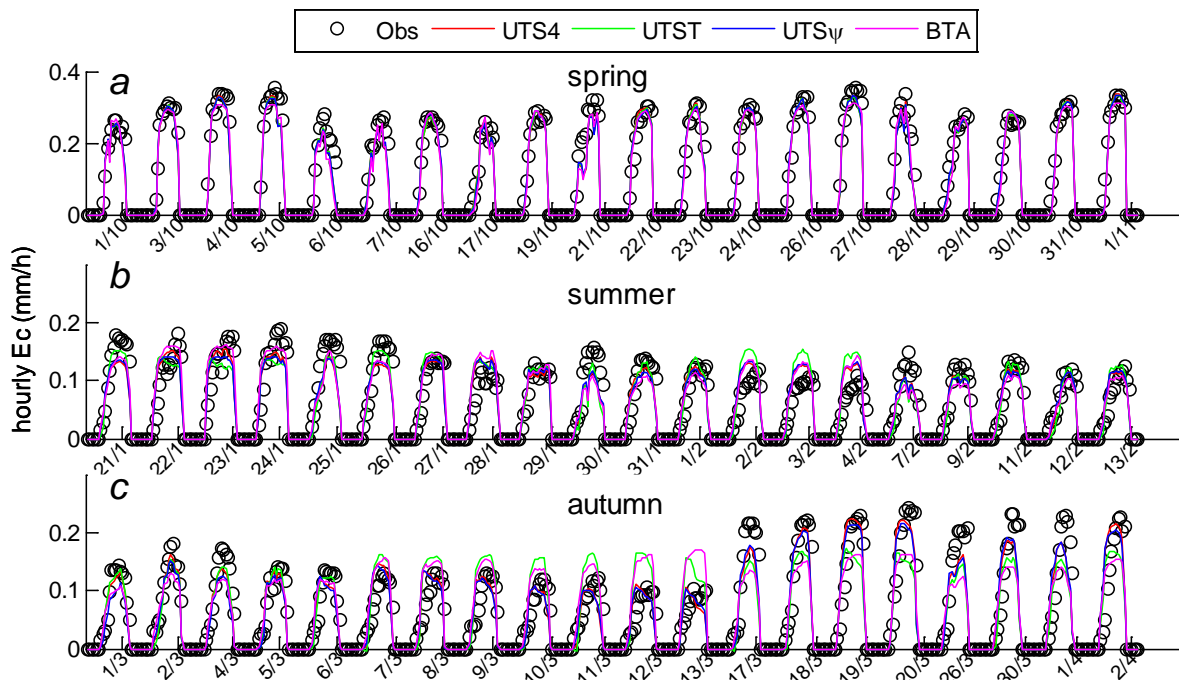
Figure 3.6 Tree water use simulated from the ″direct″ models (UTS, UTST, UTSψ and BTA) in comparison to sap flow measurements at hourly scale for (*a*) spring, (*b*) summer and (*c*) autumn.
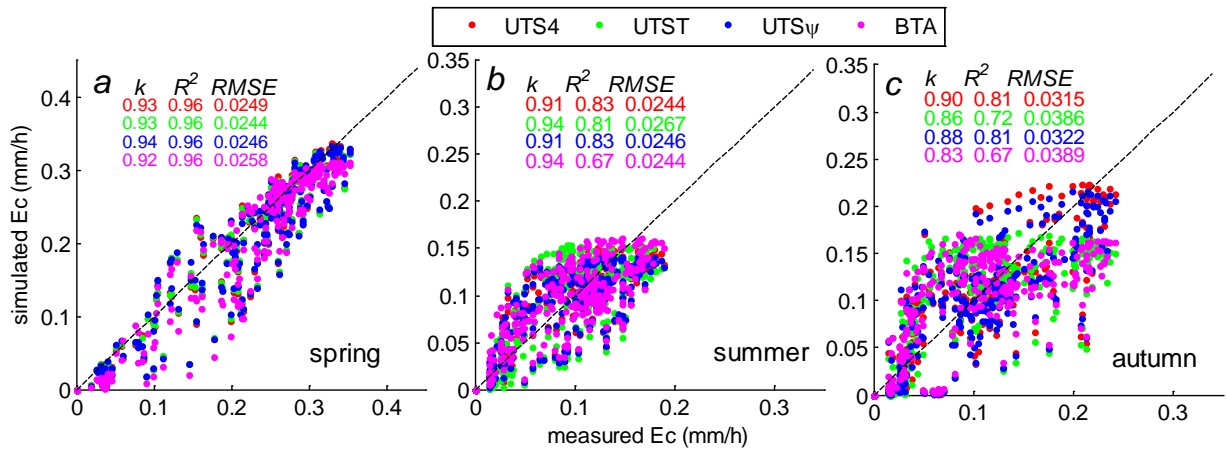
Figure 3.7 Same with Figure 3.6. Dash lines are 1:1 lines.

The surveyed tree was likely under optimal conditions for water uptake in spring, because most of rainfall occurred in May to September in the study site (Guan et al., 2013), resulting in sufficient water storage in the root zone for trees to transpire, and the energy also began to increase in this season. On the other hand, from the relationships between transpiration and the four environmental variables we observed that the data points in spring formed the upper envelope bounds (Figure 3.8). The stress functions in equations (3-6~3-8) were empirically developed by fitting the data that are located on the upper bounds, assuming that they represent the optimal conditions (Macfarlane et al., 2004; Whitley et al., 2013). This also partly explains why simulations fitted sap flow measurements the best in spring.
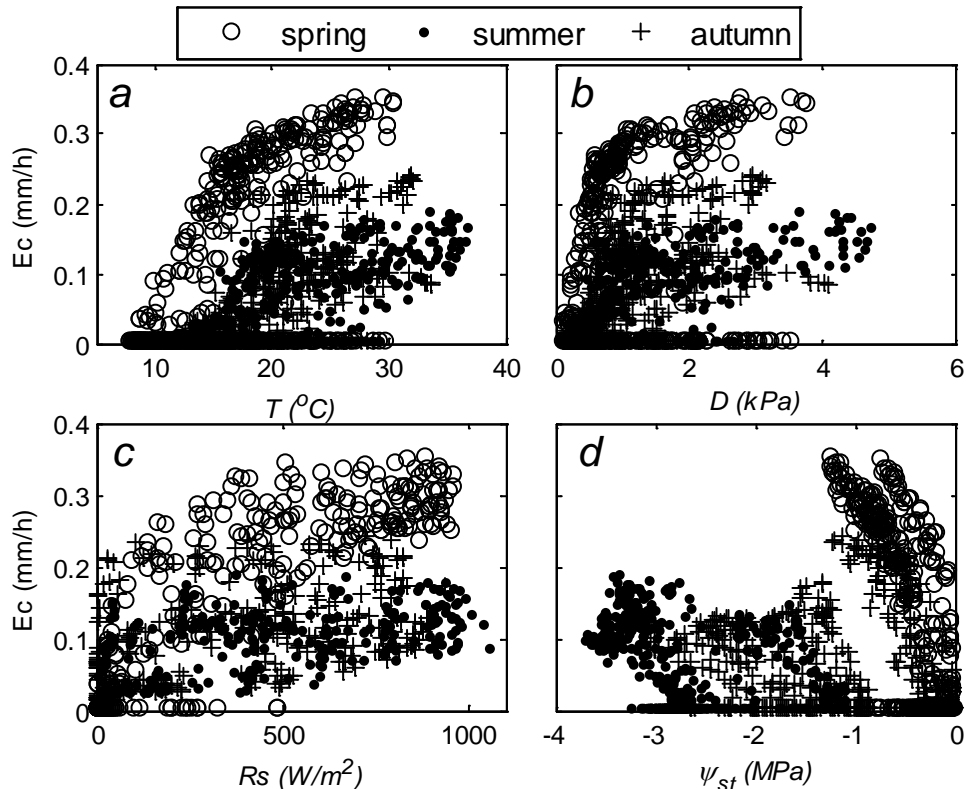
Figure 3.8 Relationship between tree water use and each environmental variable at hourly scale using the same data in Figure 3.1

Figure 3.2-3.7 suggest that both the ″direct″ and ″indirect″ methods for E_c estimation were capable to reproduce the sap flow measurements at hourly scale in three seasons, and the ″direct″ models are apparently better than the ″indirect″ ones. In fact, the Penman-Monteith method contained more parameters throughout the calculations. First g_c was calculated from the sap flow data using the inversed PM equation, and then parameters in equations (3-2~3-6) were optimized, after which E_c was back-calculated using the PM equation. More approximations involved (e.g., aerodynamic resistance, net radiation, etc) in the whole process likely resulted in the relatively poor degree of matching between simulated and measured E_c. On the contrary, models that simulated E_c straightforward from environmental variables avoided many of these approximations, which led to better simulation results than the PM models.

Implications for water balance study

In order to evaluate the applicability of the models for water balance study, we summed up the hourly transpiration from Figure 3.2, Figure 3.3, and from Figure 3.4 & Figure 3.6 to daily values, and then compared the total E_c amounts to sap flow measurements, which equals 107.5 mm. Results are shown in Figure 3.9. Most models slightly underestimated total E_c, except that PM(JST) overestimated E_c by 4.0% (sum of three seasons from Figure 3.4), PM(BTA) by 19.5% and 7.5% (sum from Figure 3.2 and Figure 3.4 respectively). Therefore, most models should be acceptable for transpiration quantification in short-term (within a year) water balance study, exceptions are PM(JSψ) in Figure 3.2 (27.3% underestimation) and PM(BTA) in Figure 3.2 (19.5% overestimation).
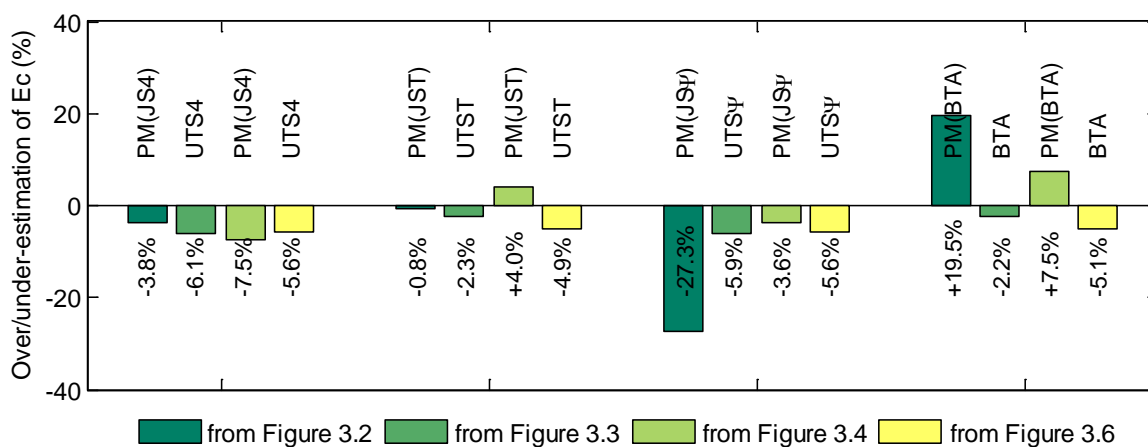
Figure 3.9 Total E_c summed up from each simulation compared to sap flow measurements. Percentage below the bars is the over/underestimated rate by each model.

Daily E$_c$ modelling

Simulated daily transpiration from both the ″direct″ and ″indirect″ methods in comparison to sap flow measurements is given in Figure 3.10. Clearly, models that contain four environmental variables gave the best simulations. Models that contain a *f(ψ)* generated better simulations than those without a *f(ψ)*. Soil water stress function had stronger effects on transpiration modelling at daily scale than hourly scale, which can be implied by comparing results in Figure 3.2, Figure 3.4 and Figure 3.10.The PM(JST), PM(BTA) and UTST and BTA models were not able to capture the daily variation of transpiration. It should be noted that the *k* and R^2 were obtained through linear regression with zero intercept.

The fitting of daily sap flow measurements by simulations from PM(JST) and UTST degraded dramatically compared to PM(JS4) and UTS4, which implies that soil water function had a very strong influence on daily E_c modelling. In addition, PM(JS4) resulted in *k*=0.96, R^2=0.69 and *RMSE*=0.3535, better than those given by PM(JSψ), while UTS4 gave similar simulations than UTSψ, which indicates that the influence *f(T)* on E_c modelling is more significant in the Penman-Monteith method than the ″direct″ models. This is the same with that at hourly scale.
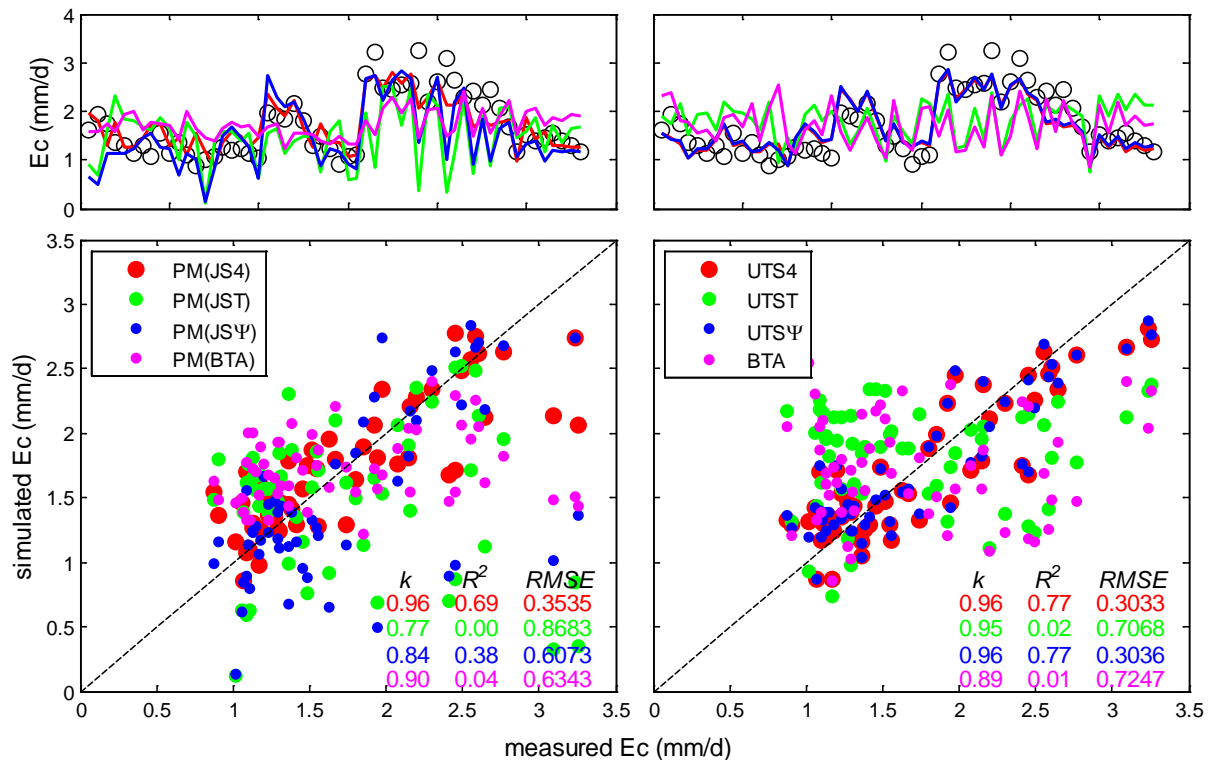
Figure 3.10 Comparison between simulated and measure transpiration at daily scale

3.3.3. Parameter values

By comparing the values of each parameter in the same model at different scales, we examined

the universality of parameter values (Table 3-1). Transpiration simulation in current land surface models is often based on the Jarvis-Stewart type approach, so in this part we only compared the parameters in PM(JS4), PM(JST), PM(JSψ) and UTS4, UTST and UTSψ which are variants of the Jarvis-Stewart approach.

Table 3-1 Parameter[*] values for different models at hourly and daily scales

Model	Scale	g_{max}	k_{Rs}	k_D	k_T	T_o	k_ψ	ψ_m	
PM(JS4)	daily	0.0102	41	0.92	-0.0141	19	0.66	-0.75	
	hourly	0.0245	166	1.12	-0.0204	18	2.44	-1.28	
	spring	0.0241	84	0.65	-0.0126	17	2.21	-0.83	
	summer	0.0086	40	0.52	-0.0012	26	0.08	-1.32	
	autumn	0.0159	42	0.99	0.0078	25	2.89	-1.91	
PM(JST)	daily	0.0104	42	2.01	-0.0273	18			
	hourly	0.0138	232	1.17	-0.0338	20			
	spring	0.0178	168	0.92	-0.0404	18			
	summer	0.0038	40	0.48	-0.0013	29			
	autumn	0.0116	43	0.93	0.0052	27			
PM(JSP)	daily	0.0148	41	1.17			0.82	-0.69	
	hourly	0.0333	89	1.11			2.02	-0.84	
	spring	0.0303	60	0.72			2.96	-0.62	
	summer	0.0095	40	0.57			0.01	-0.36	
	autumn	0.0053	40	0.31			2.92	-2.00	
		E_{max}	k_{Rs}	k_D	D_{peak}	k_T	T_o	k_ψ	ψ_m
UTS4	daily	3.25	111	0.01	3.7	-0.0007	20	0.98	-2.05
	hourly	0.32	159	0.02	5.6	-0.0040	26	1.90	-2.42
	spring	0.34	285	0.03	2.2	0.0010	29	4.99	-3.37
	summer	0.28	40	0.02	6.0	-0.0016	29	0.06	-3.87
	autumn	0.23	40	0.01	4.7	0.0033	30	4.01	-2.48
UTST	daily	3.00	82	0.03	4.0	0.0019	15		
	hourly	0.20	149	0.01	6.0	-0.0023	30		
	spring	0.34	264	0.02	2.9	0.0011	26		
	summer	0.20	40	0.02	6.0	0.0008	15		
	autumn	0.20	40	0.20	1.0	0.0039	30		
UTSP	daily	3.37	126	0.01	3.8			0.98	-2.09
	hourly	0.32	149	0.01	5.9			1.72	-2.43
	spring	0.34	272	0.01	5.4			4.39	-3.77
	summer	0.30	40	0.01	6.0			0.09	-1.08
	autumn	0.23	40	0.02	5.4			3.43	-2.46

[*] Refer to Section 3.3.2 for the unit of each parameter

The maximum transpiration rate E_{max} in UTS4, UTST and UTSψ models was similar at both daily scale (3.25, 3.00 and 3.37 mm/d) and hourly scale (0.32, 0.20 and 0.32 mm/h). At hourly scale in each season E_{max} also did not vary too much. The maximum stomatal conductance g_{max} in PM(JS4), PM(JST) and PM(JSψ) was similar at daily scale and varying at hourly scale. For

the rest of the fitting parameters such as k_{Rs}, k_D and D_{peak} in UTS4, UTST and UTSψ models, greater values were obtained at hourly scale than daily scale. k_{Rs} varied greatly between spring and the other two seasons at hourly scale, ranging from about 40 to 285 W/m^2; values in summer and autumn at hourly scale were similar. Parameter ψ_m was relatively stable within each model group and across temporal scales.

The difference of daily and hourly parameter values in each model raises the attention for model applications at different temporal scales. Models need to be recalibrated when applied at a different temporal scale from which they are tuned initially. To demonstrate this scale issue of parameters visually, we simulated hourly E_c with daily parameter values, and daily E_c with hourly parameter values using the Penman-Monteith method. The ″direct″ models were not tested because an obvious difference of E_{max} existed at hourly and daily scales, which will lead to a big difference in simulated hourly E_c using daily parameter values or vice versa. Results demonstrated that using hourly scale parameter values for daily E_c simulation and the other way around was not able to reproduce the daily sap flow measurements (Figure 3.11). Applying daily parameter values for hourly E_c modelling underestimated daily E_c by about 45% based on PM(JS4) model, while applying hourly parameter values for daily E_c modelling overestimated daily E_c by about 52% based on the same model.
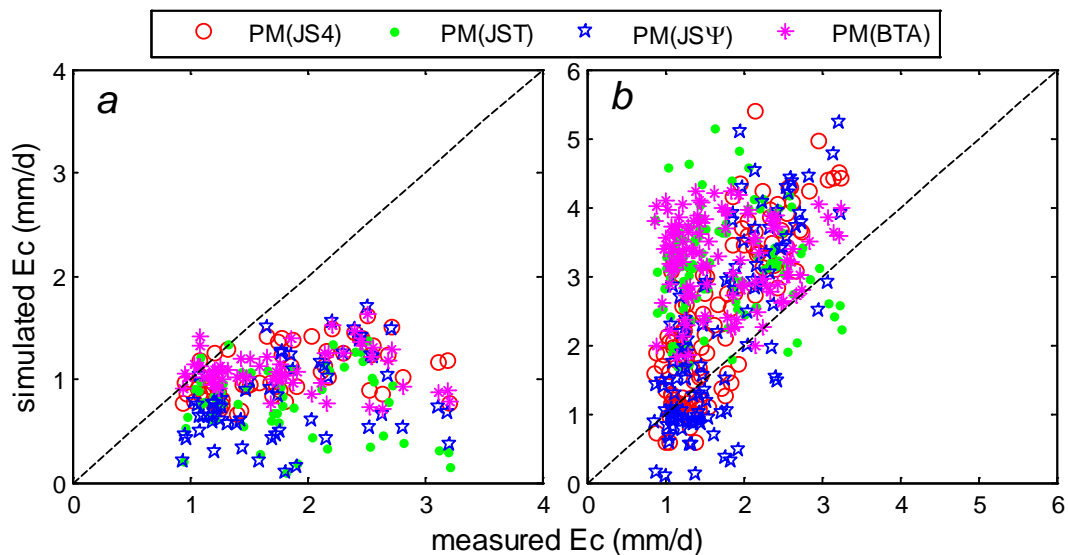
Figure 3.11 Comparison of simulated and measured E_c. (a) Applying daily parameter values for hourly simulation and sum the hourly E_c to daily values; (b) applying hourly parameter values for daily simulation.

3.4. Conclusions

Models for transpiration estimation were divided into two categories (″direct″ and ″indirect″) based on the way of linking with environmental variables. We tested comprehensively the two

categories of models for transpiration estimates and the roles of soil water condition and air temperature functions in the transpiration modelling at different temporal scales. The ″direct″ models gave better simulations than the Penman-Monteith method. Influence of both soil water condition and air temperature functions on transpiration modelling was more prominent at daily scale than hourly scale. At hourly scale, inclusion of a temperature function in the PM method had negative impacts on transpiration modelling in autumn, positive impacts in spring and little impacts in summer. The influence of soil water function was stronger in autumn than in spring. Results indicate that for hourly transpiration modelling soil water condition and temperature functions can be omitted under certain conditions, such as in wet and sunny periods when soil water is sufficient for vegetation transpiration. Parameters in each model varied across different time scales, calling for the attention to model applicability across various temporal scales. The major advantage of the ″direct″ models is the simplicity in terms of measurements and parameter calibration. This allows for wide applications, for instance, replacing the current transpiration calculation schemes in land surface models, with increased computing efficiency and limited sacrifice of accuracy.

3.5. References

Ball, J.H., L. E. Woodrow and Beny, J.A., 1987. A model predicting stomatal conductance and its contribution to the control of photosynthesis under different environmental conditions. In: J. Biggins (Editor), Progress in Photosynthesis research. Martinus Nijhoff, Providence, Rhode Island, USA, pp. 221-224.

Buckley, T.N., Mott, K.A. and Farquhar, G.D., 2003. A hydromechanical and biochemical model of stomatal conductance. Plant Cell and Environment, 26(10): 1767-1785.

Buckley, T.N., Turnbull, T.L. and Adams, M.A., 2012. Simple models for stomatal conductance derived from a process model: cross-validation against sap flux data. Plant Cell and Environment, 35(9): 1647-1662.

Bunce, J.A., 2000. Responses of stomatal conductance to light, humidity and temperature in winter wheat and barley grown at three concentrations of carbon dioxide in the field. Global Change Biology, 6(4): 371-382.

Chen, D.Y., Wang, Y.K., Liu, S.Y., Wei, X.G. and Wang, X., 2014. Response of relative sap flow to meteorological factors under different soil moisture conditions in rainfed jujube (Ziziphus jujuba Mill.) plantations in semiarid Northwest China. Agricultural Water Management, 136: 23-33.

Chen, F. and Dudhia, J., 2001. Coupling an advanced land surface-hydrology model with the Penn State-NCAR MM5 modeling system. Part I: Model implementation and sensitivity. Monthly Weather Review, 129(4): 569-585.

Chen, F., Mitchell, K., Schaake, J., Xue, Y.K., Pan, H.L., Koren, V., Duan, Q.Y., Ek, M. and Betts, A., 1996. Modeling of land surface evaporation by four schemes and comparison with FIFE observations. Journal of Geophysical Research-Atmospheres, 101(D3): 7251-7268.

Choné, X., eacute, Leeuwen, C.v., Dubourdieu, D., Gaudill, J., egrave and re, 2001. Stem Water Potential is a Sensitive Indicator of Grapevine Water Status. Annals of Botany, 87(4): 477-483.

Comstock, J. and Mencuccini, M., 1998. Control of stomatal conductance by leaf water potential in Hymenoclea salsola (T & G), a desert subshrub. Plant Cell and Environment, 21(10): 1029-1038.

Dai, Y.J., Dickinson, R.E. and Wang, Y.P., 2004. A two-big-leaf model for canopy temperature, photosynthesis, and stomatal conductance. Journal of Climate, 17(12): 2281-2299.

Damour, G., Simonneau, T., Cochard, H. and Urban, L., 2010. An overview of models of stomatal conductance at the leaf level. Plant Cell and Environment, 33(9): 1419-1438.

Dickinson, R.E., 1987. Evapotranspiration in global climate models. Advances in Space Research, 7(11): 17-26.

Dickinson, R.E., Henderson-Sellers, A., Rosenzweig, C. and Sellers, P.J., 1991. Evapotranspiration Models with Canopy Resistance for Use in Climate Models - a Review. Agricultural and Forest Meteorology, 54(2-4): 373-388.

Dixon, M.A. and Tyree, M.T., 1984. A new stem hygrometer, corrected for temperature-gradients and calibrated against the pressure bomb. Plant Cell and Environment, 7(9): 693-697.

Dolman, A.J., Miralles, D.G. and de Jeu, R.A.M., 2014. Fifty years since Monteith's 1965 seminal paper: the emergence of global ecohydrology. Ecohydrology, 7(3): 897-902.

Eamus, D. and Froend, R., 2006. Groundwater-dependent ecosystems: the where, what and why of GDEs. Australian Journal of Botany, 54(2): 91-96.

Findell, K.L. and Eltahir, E.A.B., 1997. An analysis of the soil moisture-rainfall feedback, based on direct observations from Illinois. Water Resources Research, 33(4): 725-735.

Ford, C.R., Hubbard, R.M., Kloeppel, B.D. and Vose, J.M., 2007. A comparison of sap flux-based evapotranspiration estimates with catchment-scale water balance. Agricultural and Forest Meteorology, 145(3-4): 176-185.

Green, S., Clothier, B. and Jardine, B., 2003. Theory and practical application of heat pulse to measure sap flow. Agronomy Journal, 95(6): 1371-1379.

Green, S. and Clothier, B.E., 1988. Water-use of kiwifruit vines and apple-trees by the heat-pulse technique. Journal of Experimental Botany, 39(198): 115-123.

Gregory, P.J. and Nortcliff, S., 2013. Index, Soil Conditions and Plant Growth. Blackwell Publishing Ltd, pp. 449-461.

Guan, H.D., Zhang, X.P., Skrzypek, G., Sun, Z. and Xu, X., 2013. Deuterium excess variations of rainfall events in a coastal area of South Australia and its relationship with synoptic weather systems and atmospheric moisture sources. Journal of Geophysical Research-Atmospheres, 118(2): 1123-1138.

Hatton, T.J., Moore, S.J. and Reece, P.H., 1995. Estimating stand transpiration in a Eucalyptus populnea woodland with the heat pulse method: measurement errors and sampling strategies. Tree Physiology, 15(4): 219-27.

Ivanov, V.Y., Bras, R.L. and Vivoni, E.R., 2008. Vegetation-hydrology dynamics in complex terrain of semiarid areas: 1. A mechanistic approach to modeling dynamic feedbacks. Water Resources Research, 44. (3).

Jarvis, P.G., 1976. The interpretation of the variations in leaf water potential and stomatal conductance found in canopies in the field. Philosophical Transactions of the Royal Society of London. B, Biological Sciences, 273(927): 593-610.

Kelliher, F.M., Leuning, R. and Schulze, E.D., 1993. Evaporation and canopy characteristics of coniferous forests and grasslands. Oecologia, 95(2): 153-163.

LeMone, M.A., Chen, F., Alfieri, J.G., Tewari, M., Geerts, B., Miao, Q., Grossman, R.L. and Coulter, R.L., 2007. Influence of land cover and soil moisture on the horizontal distribution of sensible and latent heat fluxes in southeast Kansas during IHOP_2002 and CASES-97. Journal of Hydrometeorology, 8(1): 68-87.

Leuning, R., 1995. A Critical-Appraisal of A Combined Stomatal-photosynthesis Model for C-3 Plants. Plant Cell and Environment, 18(4): 339-355.

Lhomme, J.P., Elguero, E., Chehbouni, A. and Boulet, G., 1998. Stomatal control of

transpiration: Examination of Monteith's formulation of canopy resistance. Water Resources Research, 34(9): 2301-2308.

Macfarlane, C., White, D.A. and Adams, M.A., 2004. The apparent feed-forward response to vapour pressure deficit of stomata in droughted, field-grown Eucalyptus globulus Labill. Plant Cell and Environment, 27(10): 1268-1280.

Marshall, T.J., Holmes, J.W. and Rose, C.W., 1996. Soil physics. Cambridge University Press, New York, USA, 21-28 pp.

Mascart, P., Taconet, O., Pinty, J.P. and Mehrez, M.B., 1991. Canopy Resistance Formulation and Its Effect in Mesoscale Models - a Hapex Perspective. Agricultural and Forest Meteorology, 54(2-4): 319-351.

Miralles, D.G., De Jeu, R.A.M., Gash, J.H., Holmes, T.R.H. and Dolman, A.J., 2011. Magnitude and variability of land evaporation and its components at the global scale. Hydrology and Earth System Sciences, 15(3): 967-981.

Monteith, J.L., 1965. Evaporation and environment. *The State and Movement of Water in Living Organisms*. Symposium of the Society for Experimental Biology, 19: 205-34.

Mullins, C.E., 2001. Matric potential. In: C.E. Mullins and K.A. Smith (Editors), Soil and Environmental Analysis: Physical Methods. Marcel Dekker, Inc., New York, pp. 65-93.

Noilhan, J. and Planton, S., 1989. A simple parameterization of land surface processes for meteorological models. Monthly Weather Review, 117(3): 536-549.

Nortes, P.A., Pérez-Pastor, A., Egea, G., Conejero, W. and Domingo, R., 2005. Comparison of changes in stem diameter and water potential values for detecting water stress in young almond trees. Agricultural Water Management, 77(1–3): 296-307.

O'Grady, A.P., Eamus, D., Cook, P.G. and Lamontagne, S., 2006. Comparative water use by the riparian trees Melaleuca argentea and Corymbia bella in the wet-dry tropics of northern Australia. Tree Physiology, 26(2): 219-228.

Palmer, A.R., Fuentes, S., Taylor, D., Macinnis-Ng, C., Zeppel, M., Yunusa, I. and Eamus, D., 2010. Towards a spatial understanding of water use of several land-cover classes: an examination of relationships amongst pre-dawn leaf water potential, vegetation water use, aridity and MODIS LAI. Ecohydrology, 3(1): 1-10.

Richter, H., 1997. Water relations of plants in the field: Some comments on the measurement of selected parameters. Journal of Experimental Botany, 48(306): 1-7.

Schulze, E.D., Mooney, H.A., Sala, O.E., Jobbagy, E., Buchmann, N., Bauer, G., Canadell, J., Jackson, R.B., Loreti, J., Oesterheld, M. and Ehleringer, J.R., 1996. Rooting depth, water availability, and vegetation cover along an aridity gradient in Patagonia. Oecologia, 108(3): 503-511.

Silberstein, R.P., 2003. Why collect data when we can model it? Modsim 2003: International Congress on Modelling and Simulation, Vols 1-4: 915-920.

Sommer, R., Sa, T.D.D., Vielhauer, K., de Araujo, A.C., Folster, H. and Vlek, P.L.G., 2002. Transpiration and canopy conductance of secondary vegetation in the eastern Amazon. Agricultural and Forest Meteorology, 112(2): 103-121.

Stewart, J.B., 1988. Modeling surface conductance of pine forest. Agricultural and Forest Meteorology, 43(1): 19-35.

Tuzet, A., Perrier, A. and Leuning, R., 2003. A coupled model of stomatal conductance, photosynthesis and transpiration. Plant Cell and Environment, 26(7): 1097-1116.

Vandegehuchte, M.W., Guyot, A., Hubau, M., De Groote, S.R.E., De Baerdemaeker, N.J.F., Hayes, M., Welti, N., Lovelock, C.E., Lockington, D.A. and Steppe, K., 2014. Long-term versus daily stem diameter variation in co-occurring mangrove species: Environmental versus ecophysiological drivers. Agricultural and Forest Meteorology, 192–193(0): 51-58.

Verhoef, A. and Egea, G., 2014. Modeling plant transpiration under limited soil water: Comparison of different plant and soil hydraulic parameterizations and preliminary implications for their use in land surface models. Agricultural and Forest Meteorology,

191: 22-32.

Vrugt, J.A., ter Braak, C.J.F., Diks, C.G.H., Robinson, B.A., Hyman, J.M. and Higdon, D., 2009. Accelerating Markov Chain Monte Carlo Simulation by Differential Evolution with Self-Adaptive Randomized Subspace Sampling. International Journal of Nonlinear Sciences and Numerical Simulation, 10(3): 273-290.

Wang, H., Guan, H., Deng, Z. and Simmons, C.T., 2014. Optimization of canopy conductance models from concurrent measurements of sap flow and stem water potential on Drooping Sheoak in South Australia. Water Resources Research, 50(7): 6154-6167.

Whitley, R., Medlyn, B., Zeppel, M., Macinnis-Ng, C. and Eamus, D., 2009. Comparing the Penman-Monteith equation and a modified Jarvis-Stewart model with an artificial neural network to estimate stand-scale transpiration and canopy conductance. Journal of Hydrology, 373(1-2): 256-266.

Whitley, R., Taylor, D., Macinnis-Ng, C., Zeppel, M., Yunusa, I., O'Grady, A., Froend, R., Medlyn, B. and Eamus, D., 2013. Developing an empirical model of canopy water flux describing the common response of transpiration to solar radiation and VPD across five contrasting woodlands and forests. Hydrological Processes, 27(8): 1133-1146.

Wright, I.R., Manzi, A.O. and Darocha, H.R., 1995. Surface conductance of amazonian pasture - model application and calibration for canopy climate. Agricultural and Forest Meteorology, 75(1-3): 51-70.

Yang, Y.T., Guan, H.D., Hutson, J.L., Wang, H.L., Ewenz, C., Shang, S.H. and Simmons, C.T., 2013. Examination and parameterization of the root water uptake model from stem water potential and sap flow measurements. Hydrological Processes, 27(20): 2857-2863.

4. Quantifying sapwood width for three Australian native species using electrical resistivity tomography

4.1. Introduction

Vegetation covers a considerable portion of the earth surface, and significantly influences climate (Betts *et al.,* 1997; Palmer *et al.,* 2010) and hydrological processes (Ivanov *et al.,* 2008) over a range of spatiotemporal scales, mainly by altering surface albedo, roughness, soil macroporosity, intercepting rainfall and transpiring water from deep soil layers (Ivanov *et al.,* 2008). Quantification of vegetation water use and its response to environmental conditions are important to the understanding of land-atmosphere interaction and ecosystem development and conservation.

Sap flow measurement techniques are useful means to quantify vegetation water use at different temporal and spatial scales, and are particularly useful in mountainous regions (Kumagai *et al.,* 2008), because their applicability is not limited by complex terrain and spatial heterogeneity (Ford et al., 2007; Kumagai et al., 2007; Wilson et al., 2001). Various heat-based sap flow techniques have been successfully applied in ecohydrological studies, as they can be used to estimate watershed transpiration through up-scaling sap flow from individual trees (Čermák et al., 2004; Swanson, 1994; Vandegehuchte and Steppe, 2013; Wullschleger et al., 1998). The up-scaling procedure can be difficult due to the spatial variability of sap flux density in individual trees (Hatton et al., 1995; Wullschleger and King, 2000), and inter-tree variability of the sap flux density (Wullschleger *et al.,* 2001) and determination of the conductive sapwood area, A_s (Kumagai *et al.,* 2005). The latter requires the identification of the sapwood-heartwood boundary (S-H) in the trunk cross-section. Inaccuracy in estimating A_s will transfer to transpiration estimates, and may be especially significant for species that have wide sapwood sections (Čermák *et al.,* 2004; Kume *et al.,* 2010).

Methods of identifying sapwood and heartwood depend on being able to differentiate the two woods by differences in their physical properties. The common methods used and their major disadvantages are summarized in Table 4-1 (Part 1). These methods are destructive to varying degrees and some are fatal to the trees. Therefore, they are usually conducted at the end of the sap flow measurement period, and are not appropriate for a large number of samples. Uncertainties in transpiration can be large when insufficient numbers of trees are sampled for sap flow and sapwood width measurements (Rust, 1999; Vertessy et al., 1997). In addition, the stem sizes will increase as trees grow, so a single survey of sapwood area at the end of a sap flow

measurement period can introduce errors in the transpiration estimate (Steppe *et al.,* 2006), especially for long-term studies such as on seasonal and annual scales (Liu *et al.,* 2012) on fast growing species. Therefore, an efficient, non-destructive method for estimating sapwood width and hence A_s is important and desirable for transpiration estimation at the stand scale.

Table 4-1 A summary of conventional methods for identifying sapwood and heartwood and recent studies using the electrical resistivity tomography (ERT)

	Methods	Wood physics	Disadvantages	Reference
PART ONE	Staining	Water conductance	Overestimating sapwood width; needs felling trees or on-site tree cuts	(Gebauer *et al.,* 2008)
	Resistance to penetration	Hardness	Only applicable to trees with large moisture contrast between sapwood and heartwood, or in frozen stems	(Rust, 1999)
	Visual inspection of wood cores	Color/Transparency	Big uncertainty when the contrast is not obvious	(Vertessy *et al.,* 1995)
	Bifocal microscopic assessing of tissues	Microscopic structure	Destructive; time consuming to prepare and analyze core sample slices	(Pfautsch *et al.,* 2010)
	Computer tomographic (CT) imaging / X-ray scanning	Density	Not sensitive when little change of density exists along the cambium-pith direction	(Longuetaud *et al.,* 2006; Tomazello *et al.,* 2008)

	Method	Wood physics	Species	S-H determination method	Reference
PART TWO	Electrical resistivity tomography (ERT)	Mainly wood moisture content and/or electrolyte concentration	Olive & oak at different ages	ERT configuration on trees; no quantitative method for S-H boundary demarcation was provided	(al Hagrey, 2007)
			Quercus robur	Visual checking of the R_s images; no mathematical method described	(Bieker and Rust, 2010a)
			Scots pine (*Pinus sylvestris* L.)	Pointing out S-H boundary coincides with the steepest rise in R_s from outer to inner wood sections; no clear description on the method	(Bieker and Rust, 2010b)
			Japanese cedar, Taiwania, and Luanta fir	Linear relationship was found between the sum of maximum and minimum R_s and R_s at S-H boundary; prior knowledge of S-H boundary is required to establish the relationship	(Lin *et al.,* 2012)
			Pinus elliottii Engelm var. *elliottii*; *Pinus caribaea* Morelet var. *hondurensis*	S-H boundary was defined as the average of the largest gradient of R_s profiles in four cardinal directions along a central path of a cross section (10mm wide). Analyses were done in ArcGIS.	(Guyot *et al.,* 2013)

Electrical resistivity tomography (ERT) for sapwood and heartwood differentiation is based on the variation of electrical resistivity (R_s) attributed to differences in wood moisture content mainly; although in some species (e.g. English oak) electrolyte concentration can be the main contributor (Bieker and Rust, 2010a). ERT is considered reasonably non-destructive because it only requires inserting small nails through the bark until a firm contact with sapwood (approximately 2 mm into sapwood), with the nails removed after the measurement. ERT has been applied in a few studies to determine sapwood width (Table 4-1 Part 2). These studies provide insights into the causal relationship between R_s distribution and wood properties including moisture content, density, electrolyte concentration (K^+, Mg^{2+}, Na^+ etc.) and pH. They identify the sapwood-heartwood boundary using ERT by looking for the steepest change of R_s from sapwood to heartwood sections. However, the description of R_s data processing and the S-H boundary positioning in these studies is not extensively detailed.

To estimate stand scale transpiration from sap flow meters efficiently, it would be useful to establish a relationship between sapwood area (A_s) and other more readily measured tree parameters such as DBH (trunk diameter measured at 130 cm above ground) (Wullschleger *et al.,* 1998). In Australia, eucalypts are a dominant part of the flora and tree water use and response to environmental conditions have been well documented, particularly for the most cultivated species (Benyon, 2002; Quentin et al., 2012; Whitehead and Beadle, 2004). A number of relationships between A_s and DBH have been reported, for example linear relationships for *Eucalyptus marginate* (Macfarlane *et al.,* 2010) and *Eucalyptus crebra* (Zeppel and Eamus, 2008), a power relationship for *Eucalyptus regnans* (Vertessy *et al.,* 1995), and other curvilinear relationships for other eucalyptus species such as *Eucalyptus miniata* (Kelley *et al.,* 2007). The A_s-DBH relationship for eucalypts and other genera has been synthesized by Zeppel (2013). However, there is little available information in the literature about the water use and A_s-DBH relationship for two eucalyptus species which are mainly distributed in South Australia and western Victoria. They are *Eucalyptus leucoxylon* and *Eucalyptus viminalis ssp. cygnetensis*.

In this study, we measured electrical resistivity in tree cross-sections from 30 trees of three Australian native species (*Eucalyptus leucoxylo*, *Eucalyptus viminalis ssp. cygnetensis* and *Allocasuarina verticillata*). The primary goal is to present in detail an objective method of processing the electrical resistivity data for sapwood width estimation. The second objective is to establish the relationship between sapwood area and tree diameter for these three species. Advantages and limitations of using the ERT technique are also discussed.

4.2. Materials and methods

4.2.1. Sites and trees

The trees in this study were selected from two field sites. The majority of measurements were conducted in a natural woody stand located 45 km south of Adelaide, South Australia (35°12'47"S, 138°38'15"E). This site has two contrasting aspects (south and north) and is surrounded by pastures and patches of vineyards. Stands like this provide important habitats for local wild animals such as kangaroos, koalas, birds, and lizards etc. The dominant plant species at the site are *Eucalyptus leucoxylon* on the north facing slope, and *Eucalyptus viminalis ssp. cygnetensis* on the south facing slope. Ten trees of each eucalyptus species were selected for ERT and wood core survey. Another ten drooping sheoak trees (*Allocasuarina verticillata*) near the campus of Flinders University of South Australia (35°1'49"S, 138°34'28"E) were also included in the survey. The typical spatial distribution of the three species is mainly in South Australia and west Victoria. Drooping sheoak extends further north to New South Wales and south to Tasmania.

The climate of the sites is Mediterranean, with hot dry summers and cool wet winters. Most rainfall occurs in May to September (Guan *et al.,* 2013). The selected trees have different diameters, and the stems at measurement level are relatively circular. The circular stems allow the assumption of symmetry of tree trunk cross-sections in ERT configuration used in this study.

4.2.2. Measurements

Measurements include DBH, bark thickness, sapwood width from increment cores, and cross-sectional electrical resistivity from ERT. Measurements on 20 eucalypts and 7 drooping sheoak trees were conducted in the afternoon on sunny days after several consecutive sunny days in October 2013 to March 2014, so as to avoid the issue of sap flow irrelevant moisture in the cross-sections. Measurements on another 3 drooping sheoak trees were conducted on an afternoon after previous rainy days in late May 2014, allowing us to test the capability of ERT for sapwood-heartwood demarcation under wet conditions.

Following Guyot et al. (2013), any dry bark at the trunk surface was removed prior to ERT measurements. Thickness of dry bark was accounted for in determining the relationship between sapwood area and tree diameter. Bark thickness was measured in four cardinal directions. Core samples from the same trees along the north-south or west-east directions were taken out using an increment borer (0.5 cm in diameter) immediately after ERT measurements. The distinct color difference (white and brown from outer to inner woods, Figure 4.1) along wood cores of the

three species allowed us to measure sapwood width in the field by visual inspection (Hatton *et al.,* 1995).
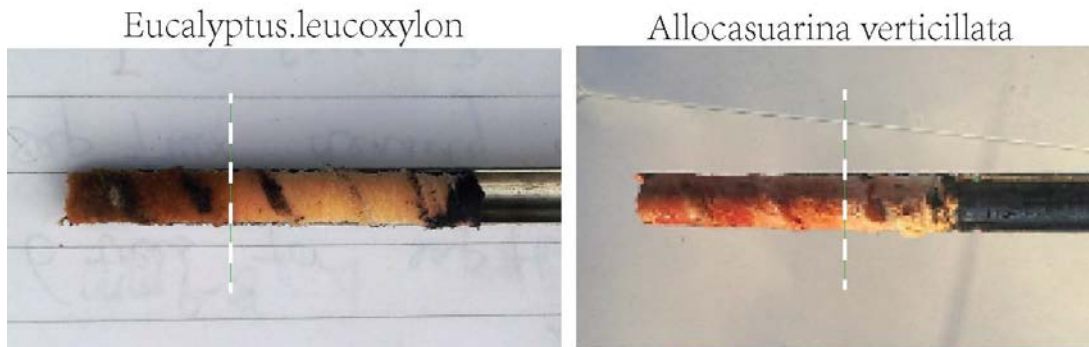
Figure 4.1 Two examples of wood cores for Eucalyptus and Allocasuarina for colour comparison

A multichannel, multi-electrode resistivity system (*Picus TreeTronic, Argus Electronic GmbH, Germany*) was deployed for ERT measurement following the configuration described in Guyot et al. (2013). Electrically conductive nails were tapped into the trunk until a firm contact with sapwood was established. The nails were evenly spaced at the same level (130 cm) around the trunk. The number of nails being used varies with tree size. Spacing of nails determines the R_s resolution. Most of the selected trees had circumference ranging from 24.0 to 66.0 cm, but three trees had circumference greater than 80.0 cm. The median circumference was 54.9 cm and the mean was 58.3 cm. The minimum number of nails employed in this study was 10 and the maximum was 24, which is the capacity of one unit of the instrument.

4.2.3. Theory and method of S-H differentiation using ERT

The phenomenon that the electrical resistivity of wood decreases with increasing moisture content was first quantitatively described by Stamm (1927). The theory that explains the strong moisture dependency of electrical resistivity of wood was proposed in the 1950's and has been reviewed extensively since then (Hearle, 1953; Skaar, 1988). In general, the moisture content of sapwood is significantly higher than that of heartwood in most species, resulting in lower electrical resistivity in sapwood than that in heartwood (Bieker and Rust, 2010b; Lin et al., 2012; Skaar, 1988). Some tree species (*Quercus robur L.*) are exceptions (Bieker and Rust, 2010a).
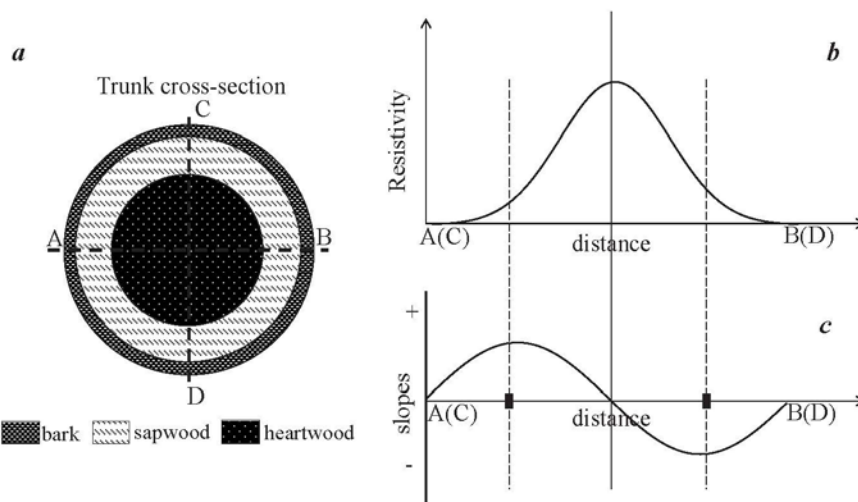
Figure 4.2 (*a*) schematic illustration of an undamaged tree trunk cross-section; (*b*) the electrical resistivity distribution along the centerline of the tree trunk cross-section, and (*c*) the slopes of the electrical resistivity distribution curve. Vertical solid line in plots (*b*) and (*c*) is the center of the trunk; two dash lines and rectangles indicate the sapwood and heartwood boundaries.

Summarized from the studies using ERT for S-H differentiation, theoretically, R_s along a cross-section diameter (e.g. A-B in Figure 4.2*a*) should present a distribution illustrated in Figure 1*b* for an undamaged tree. The S-H boundaries can be determined by locating the two steepest changes of the fitted R_s data on both sides of the trunk center (Figure 4.2*c*). However, ERT generates gridded R_s data over the cross-section, which means there are limited data points along a tree diameter for fitting R_s data and locating the steepest change points. The order of polynomial function used to fit R_s data also influences the sapwood width estimation. To reduce the errors in S-H demarcation induced by the limited number of data points and the fitting order of a polynomial function, in this study, we extracted R_s data within a narrow band enclosing the data along the diameter of a cross-section; the bandwidth *h* ranges from 0.4 to 4.0 cm. And then the extracted data were fitted with polynomial functions of different orders, with the order *n* ranging from 4 to 7. From the data fitting results, e.g. the largest coefficient of determination between the extracted and fitted R_s data, the appropriate *h* and *n* are determined for each tree. Figure 2 and Figure 3 give an example of bandwidth, fitting order selection and slopes of the fitted curve for tree sp2.6 (tree labels are given in Table 4-2). The same procedures were performed for all the sampled trees. Trees of similar size have the same number of electrodes and thus the same values of *h* and *n*. The final sapwood width is taken as the average of the results from north-south or west-east directional analyses.
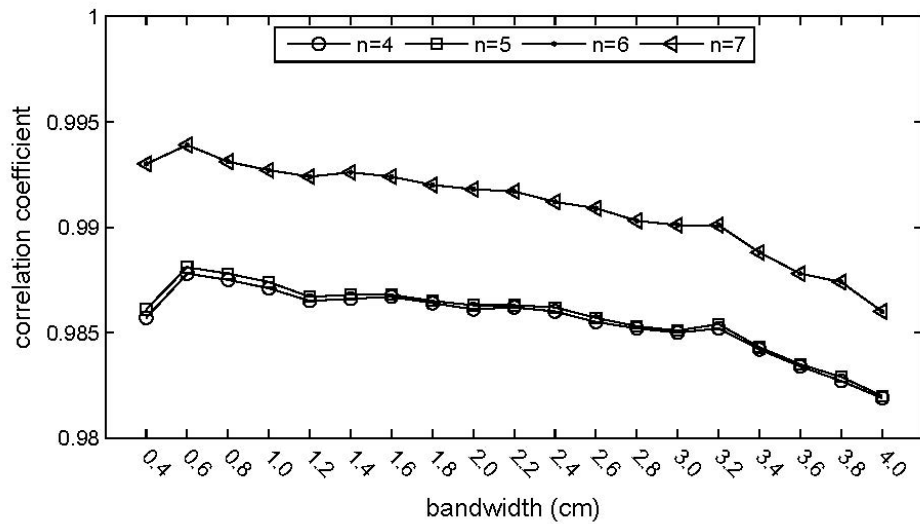
Figure 4.3 Comparison between the extracted and fitted resistivity data for determining the proper values of bandwidth *h* and fitting order *n* (example of tree sp2.6, *Eucalyptus viminalis ssp. cygnetensis*)
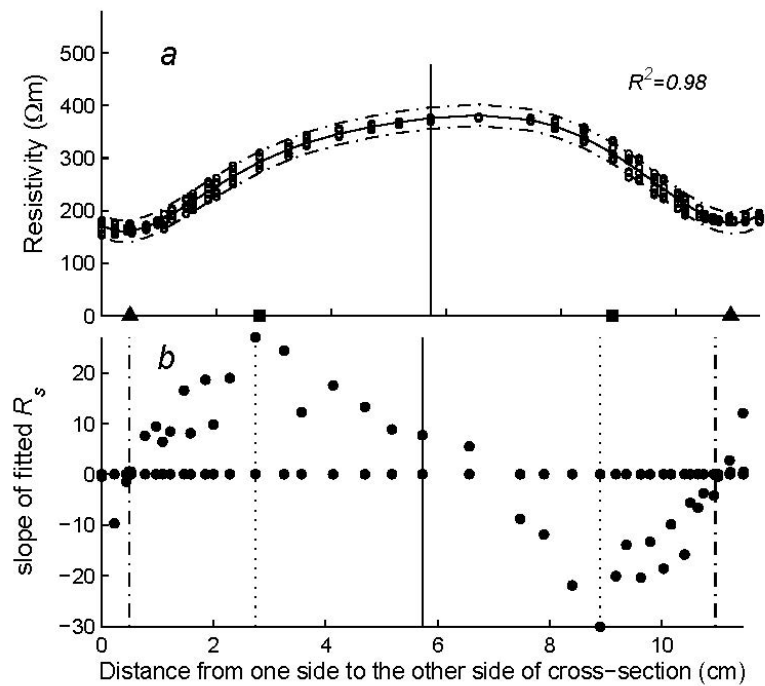
Figure 4.4 Example of electrical resistivity within a narrow band along the west-east diameter of cross-section (*a*) and slopes of the fitted curve (*b*) for sp2.6 of *Eucalyptus viminalis ssp. cygnetensis*. Bandwidth *h*=0.6 cm and fitting order *n*=7. Solid lines in the figure are the center of the tree trunk. Dash lines in plot *a* indicate 95% confidence of the data fitting. Triangles on the x-axis indicate the inner wet bark positions; squares indicate the S-H boundaries. Dash lines in plot *b* mark the relevant bark-sapwood and S-H boundaries. Dry bark is not included in the figure.

4.3. Results and discussion

4.3.1. Tree parameters measurement results

Measurements of tree parameters are given in Table 4-2. The bark of *Eucalyptus leucoxylon* is thick and wet. A layer of dry bark lies above the wet bark of *Eucalyptus viminalis ssp. cygnetensis* (about 20% of the total bark thickness on average) and *Allocasuarina verticillata* (about 16% of the total bark thickness on average). Generally, for trees of similar size, the bark of *Allocasuarina verticillata* is thinner and sapwood is wider than the two eucalyptus species. Most of the eucalyptus trees surveyed have sapwood width less than 3.0 cm.

Table 4-2 Measurements of parameters for 30 trees of 3 species

Species	Tree label	DBH (cm)	[a]Bark thickness (cm)	[b]Sapwood width (cm)	Sapwood area (cm^2)
Eucalyptus leucoxylon	sp1.1	16.4	1.5	1.8	48.5
	sp1.2	18.2	1.2	1.9	68.4
	sp1.3	22.8	1.2	1.6	82.3
	sp1.4	34.6	2.0	1.8	140.0
	sp1.5	15.3	1.3	2.2	54.8
	sp1.6	20.2	1.8	1.4	50.8
	sp1.7	18.6	1.4	2.2	74.3
	sp1.8	23.5	1.4	1.6	81.9
	sp1.9	21.7	1.6	1.5	64.9
	sp1.10	22.0	1.3	1.8	84.9
Eucalyptus viminalis ssp. cygnetensis	sp2.1	13.8	1.0	2.4	57.1
	sp2.2	19.6	1.5	3.1	117.4
	sp2.3	34.3	2.5	3.0	219.4
	sp2.4	15.5	1.4	2.4	56.8
	sp2.5	28.5	1.5	1.8	122.5
	sp2.6	13.5	1.0	2.2	57.1
	sp2.7	21.0	1.6	2.3	97.7
	sp2.8	23.6	1.6	2.3	110.3
	sp2.9	22.7	1.7	2.9	118.8
	sp2.10	16.4	1.5	2.1	54.6
Allocasuarina verticillata	sp3.1	21.4	1.8	4.2	153.4
	sp3.2	16.8	1.4	3.9	109.1
	sp3.3	9.2	0.7	2.3	32.5
	sp3.4	12.4	0.7	2.8	61.4
	sp3.5	14.4	0.6	2.9	83.0
	sp3.6	13.0	0.7	2.8	67.0
	sp3.7	8.8	0.6	1.9	28.3
	sp3.8	11.1	0.6	2.4	47.3
	sp3.9	15.2	0.9	2.9	84.5
	sp3.10	12.5	0.7	2.7	61.4

4.3.2. Electrical resistivity spatial variation

Electrical resistivity for one selected tree of each species is given in Figure 4.5. The same typical R_s spatial distribution pattern is observed for each tree as illustrated by al Hagrey (2006). That is, high R_s in the trunk center (heartwood) decreasing toward the outer layers (sapwood and wet bark). These trees have different diameters which can be observed from the axes. The drooping sheoak (Figure 4.5*c*) gave the greatest range of electrical resistivity (1049 Ωm) compared to the two selected eucalypts (1046 and 163 Ωm, Figure 4.5*a, b*). Figure 4*b* shows smaller R_s values and range, which indicates that the stem of tree sp2.9 on the south facing slope had more

moisture than the stems of sp1.4 and sp3.4 at their corresponding measurement time. Due to the wide time span of measurements on all sample trees, electrical resistivity had different ranges resulted from wood moisture content variations; they were not all shown in this paper.
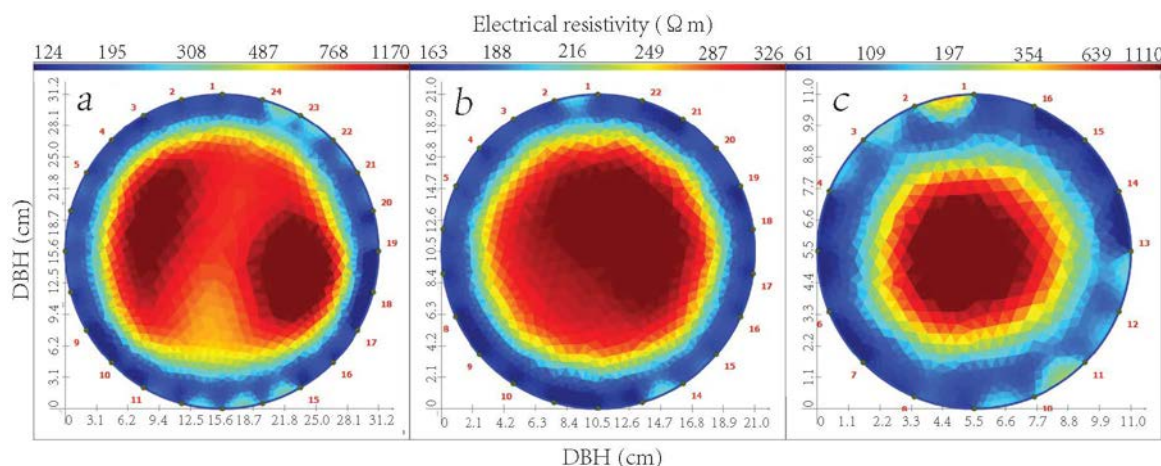
Figure 4.5 Examples of electrical resistivity distribution for three trees. (*a*) *Eucalyptus leucoxylon* (sp1.4)*,* (*b*) *Eucalyptus viminalis ssp. cygnetensis* (sp2.9)*,* and (*c*) *Allocasuarina verticillata* (sp3.4). Color bars on the top are for electrical resistivity, unit in Ωm. Horizontal and vertical axes are for the tree trunk dimensions, in cm. Red numbers around the cross sections indicate the positions of electrodes. Electrode 1 is always in the north as it was configured in the field. sp1.4 does not have dry bark; dry bark for sp2.9 and sp3.4 is not included in the figure.

Increasing the number of electrodes can increase the resolution of inversion results (al Hagrey, 2006). Ideally, the spacing between each two adjacent electrodes should be smaller than the actual sapwood width (Guyot *et al.,* 2013). The number of electrodes in this study was 16 for most of the trees. We did not use 24 electrodes for all trees because we found the ERT imaging resulted from 16 electrodes was already able to show distinct boundaries between wet and dry wood (example in Figure 4.5*c*).

4.3.3. Sapwood width, area and the relation with other tree parameters

Sapwood width (d_{sw}) was measured from wood cores and also estimated from ERT. Sapwood area was then calculated as the area between the concentric circles of bark-sapwood and sapwood-heartwood boundaries using equation (4-1), where *r* is stem radius, *l* is bark thickness, and r_h is heartwood radius, calculated from equation (4-2). In this study, the sapwood area was not directly obtained from ERT imaging or gridded data which are the two data formats that ERT generates. However, there are two potential ways of calculating sapwood area directly from ERT gridded or imaging data. One is to increase the directional analyses of R_s data, e.g., 36 directions (with an angle interval of 10°) instead of only two directions provided in this study, so that more estimates of sapwood width can be obtained on different locations around a trunk cross-section,

improving the accuracy of A_s calculation. The other way is to develop a method to determine which mesh triangles (Figure 4.5) are in sapwood section by establishing the relationship between electrical resistivity and wood moisture content (or electrolyte concentration in some cases), and then calculate total area of the triangles located in sapwood. This method would not need the assumption of circular tree trunks and is independent of bark thickness. In this study, for the purpose of demonstrating the capability of ERT for sapwood width estimation, we only conducted data analysis in two directions corresponding to the wood core sampling positions.

$$A_s = \pi (r - l)^2 - \pi r_h^{\,2} \qquad (4\text{-}1)$$

$$r_h = r - l - d_{sw} \qquad (4\text{-}2)$$

Comparison between sapwood width, sapwood area and heartwood radius from core sample analyses and ERT measurements for the three species is given in Figure 4.6 and Figure 4.7 in terms of slope (k), intercept (b) and coefficient of determination (R^2) from linear regression. Overall, we observe that sapwood widths and sapwood areas estimated from both methods agree well, showing k close to 1. ERT slightly overestimated sapwood areas compared to core sample analyses. Coefficient of determination for sapwood widths from the two methods is 0.62, 0.56 and 0.83 for *E. leucoxylon*, *E. viminalis*, and *A. verticillata* respectively, which indicates a wide spread of sapwood widths, and hence large uncertainty. The uncertainty arises from both core sample analyses and ERT data interpretation (Guyot *et al.,* 2013). Regression slopes and intercepts of heartwood radius from the two methods are similar for *E. leucoxylon* and *E. viminalis* (k=0.96 and 0.94; b=0.16 and 0.20 in Figure 4.7*c*). Heartwood radius was underestimated by ERT for *A. verticillata* (k=0.77 and R^2=0.74). This is likely due to the measurements on the three trees under wet conditions (Figure 4.7*c* and Figure 4.8*f*). Because under wet conditions, moisture content is high in both sapwood and heartwood, and the wetting front moves inward into the outer part of heartwood, forming a transition zone of moisture content, which causes the ERT-detected S-H boundaries further than the actual positions. The size of the three wet drooping sheoak trees was relatively small (average diameter 16 cm), so the overestimation of sapwood width and area is not so much and obvious. The overestimation of sapwood width has also been observed when using staining solutions (Bieker and Rust, 2010b). The results indicate that ERT is not able to accurately differentiate sapwood and heartwood under wet tree conditions.
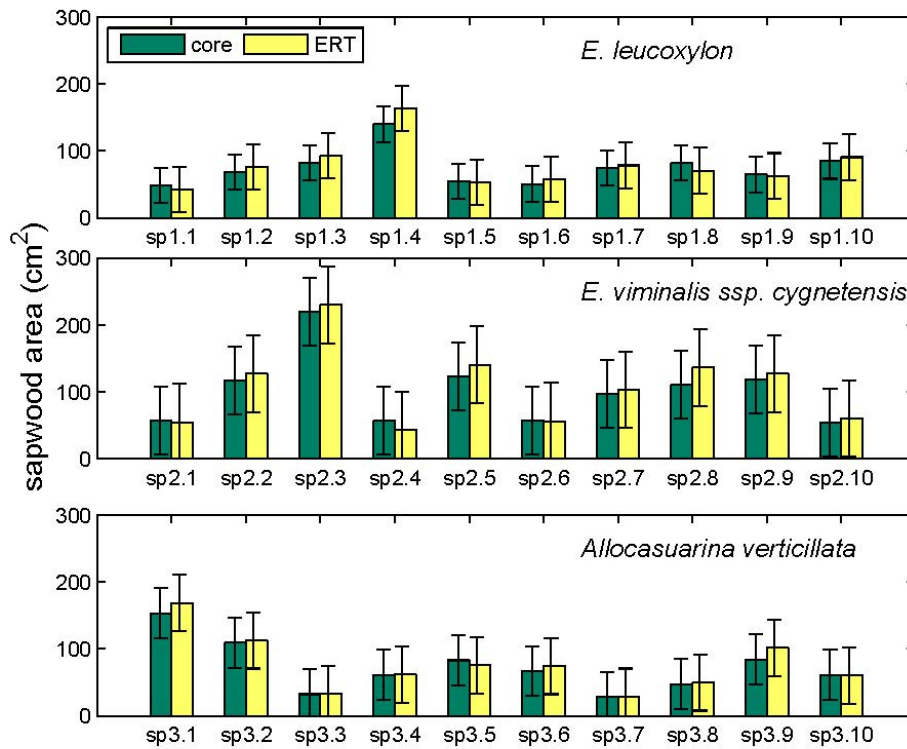
Figure 4.6 Comparison between sapwood areas derived from core samples and ERT for three species. Error bars are one standard deviation of each group.
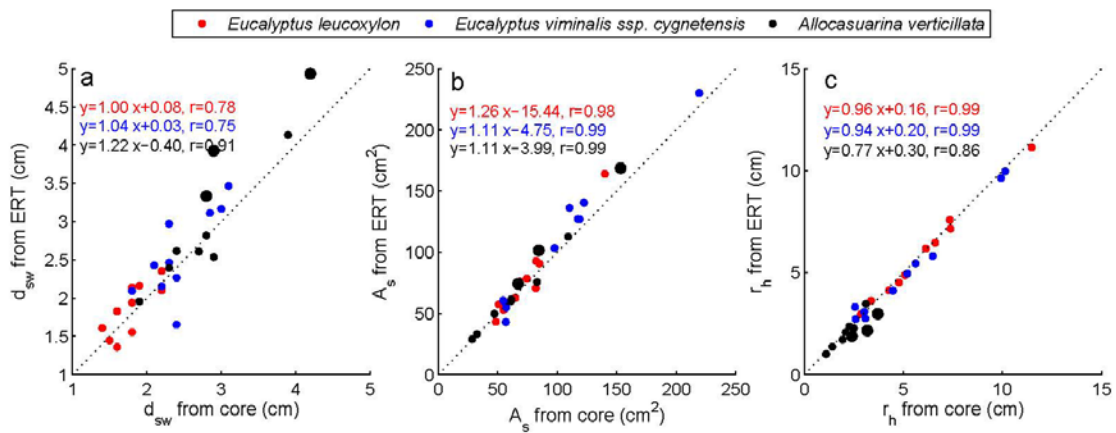
Figure 4.7 Relationships between sapwood widths (d_{sw}), sapwood areas (A_s) and heartwood radius (r_h) obtained from ERT and core samples for three species. Equations are the results of linear regression. Dash lines are 1:1 lines. Black symbols with a bigger size stand for the three trees measured under wet conditions.

Both sapwood area and heartwood radius have strong linear relationship with DBH for all species (Figure 4.8). *E. leucoxylon* has smaller sapwood area than *E. viminalis* when tree diameter is the same. There is limited information in the literature about the water use and A_s-DBH relationship for the two eucalyptus species in this study.
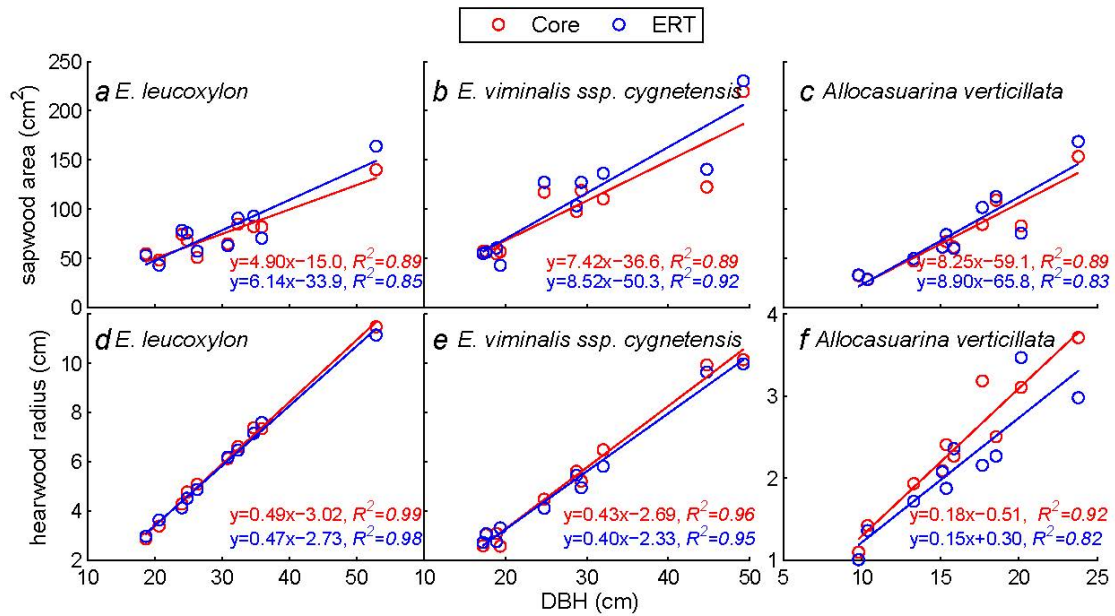
Figure 4.8 Relationships between sapwood area and tree diameter, and between heartwood radius and tree diameter for three species. Lines are linearly fitted. Equations are from the linear regression. Plots *a-c* and *d-e* share the same vertical axes; *a* & *d*, *b* & *e*, *c* & *f* share the same horizontal axes. Solid circles in plots *c* and *f* stand for the three trees measured under wet conditions.

We collected some published DBH and sapwood area data for different eucalypts, and compared the A_s-DBH relationship. Results are given in Figure 4.9. Species differ in the slopes of the linear A_s-DBH relationship, particularly, *E. marginata* (Macfarlane et al., 2010) and *E. crebra* (Zeppel and Eamus, 2008) diverge from other species. The relationship for *E. regnans* from Vertessy et al. (1997) and from Pfautsch et al. (2010) shares the same slope with slightly different intercepts. Same slopes also exist between *E. marginata* (Macfarlane *et al.,* 2010) and *E. crebra* (Zeppel and Eamus, 2008). For trees of diameter ranging from 20.0 to 30.0 cm, sapwood area of the two eucalyptus species in this study is larger than *E. crebra* (Zeppel and Eamus, 2008), *E. marginata* (Macfarlane *et al.,* 2010) and *E. grandis* (Dye and Olbrich, 1993). The DBH ranges from about 10.0 to 110.0 cm in Figure 4.9, while the two species in this study mainly contribute to the portion with DBH less than 40.0 cm. The A_s-DBH relationship in this study extends the data pool synthesized by Zeppel (2013) in terms of species.
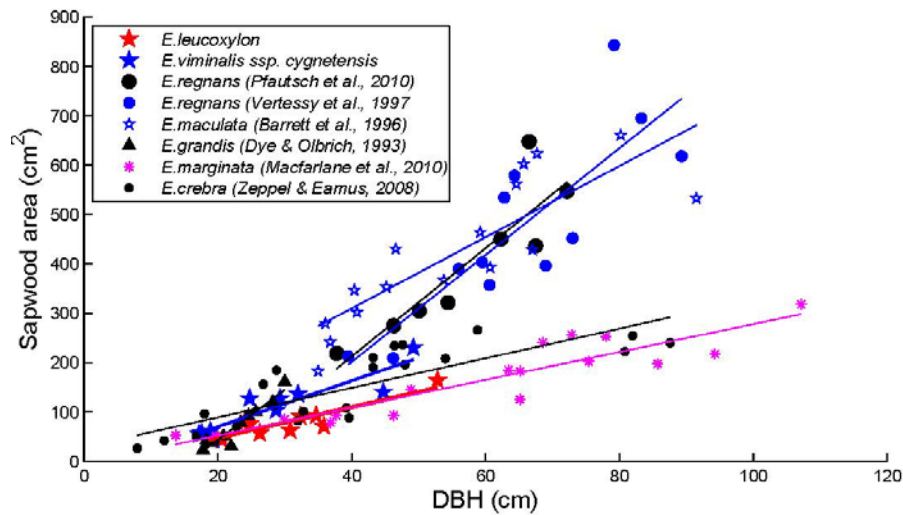
Figure 4.9 Relationship between sapwood area and DBH for different eucalypts species. Sapwood area of the two eucalyptus species in this study (*E. leucoxylon* and *E. viminalis*) in this figure were estimated using the ERT technique.

4.3.4. Advantages and limitations of ERT technique

ERT shows advantages over conventional methods in the following aspects. First, ERT measurements can give straightforward spatial distribution of sapwood in a whole trunk cross-section (Figure 4.5), while many conventional methods only give results at the specific measurement points. An advanced quantitative method is needed to estimate sapwood area directly from imaging or gridded resistivity data, and the method should be able to avoid the influences of bark thickness and tree trunk shape. Second, it is relatively non-destructive. ERT only requires inserting nails into the tree trunks at a shallow depth (approximately 2 mm into sapwood) and the nails are removed after measurements. Third, ERT is reasonably portable and efficient to use. It only takes 15 to 30 minutes to finish one measurement per tree (Bieker and Rust, 2010b; Guyot et al., 2013; Lin et al., 2012). Therefore, it is suitable for measurement on a large number of trees. In addition, ERT can be used for comprehensive measurement of tree hydraulics, e.g., it can be used to detect preferential flow path (Wu *et al.,* 2009) and can give 3-dimentional mapping of wood moisture distribution in a tree trunk when several sets of instrument are used concurrently at different levels of a tree. If the relationship between wood moisture content and electrical resistivity is established, ERT could also be used to estimate diurnal and seasonal stem water storage variation, which would benefit water uptake models that consider the tree hydraulic capacitance (Čermák *et al.,* 2007).

Despite the advantages of ERT the method presented in this study has limitations. First, the trunk cross section configuration could induce errors in estimating sapwood width. We chose carefully the trees and assumed that they have circular trunks, which is not always the case in reality.

Second, the device is more expensive than increment borers and staining solutions. Furthermore, ERT is not applicable to trees under extremely wet conditions, as is shown in this study for three *A.verticillata* trees. The steepest change of electrical resistivity still exists under wet conditions and can be determined by the method in this study, but the positions are expected to be further in the woods than the true sapwood-heartwood boundaries.

4.4. Conclusions

Sapwood width estimation and the relationship between sapwood area and tree diameter are significant in watershed transpiration estimation from sap flow measurements. We described a rigorous method of data processing for the use of electrical resistivity tomography to differentiate sapwood and heartwood for three Australian native species. Sapwood width and hence areas estimated from this method were in good agreement with those obtained from wood core analyses. Strong linear relationships were observed between sapwood area and diameter and between heartwood radius and diameter for all species. Results for the two eucalyptus species extend the literature pool in terms of the A_s-DBH relationship and species. ERT overestimated sapwood width for drooping sheoak under wet conditions, which indicates that ERT technique for sapwood and heartwood differentiation is limited under wet conditions. ERT has potential in estimating stem water storage change and characterizing hydraulic architecture of tree trunks.

4.5. References

al Hagrey, S.A., 2006. Electrical resistivity imaging of tree trunks. Near Surface Geophysics, 4(3): 179-187.

al Hagrey, S.A., 2007. Geophysical imaging of root-zone, trunk, and moisture heterogeneity. Journal of Experimental Botany, 58(4): 839-854.

Benyon, R.G., 2002. Water use by tree plantations in the Green Triangle: a review of current knowledge., CSIRO Forestry and Forest Products, Hamilton Victoria, Australia.

Betts, R.A., Cox, P.M., Lee, S.E. and Woodward, F.I., 1997. Contrasting physiological and structural vegetation feedbacks in climate change simulations. Nature, 387(6635): 796-799.

Bieker, D. and Rust, S., 2010a. Electric resistivity tomography shows radial variation of electrolytes in Quercus robur. Canadian Journal of Forest Research-Revue Canadienne De Recherche Forestiere, 40(6): 1189-1193.

Bieker, D. and Rust, S., 2010b. Non-Destructive Estimation of Sapwood and Heartwood Width in Scots Pine (Pinus sylvestris L.). Silva Fennica, 44(2): 267-273.

Čermák, J., Kucera, J., Bauerle, W.L., Phillips, N. and Hinckley, T.M., 2007. Tree water storage and its diurnal dynamics related to sap flow and changes in stem volume in old-growth Douglas-fir trees. Tree Physiology, 27(2): 181-198.

Čermák, J., Kučera, J. and Nadezhdina, N., 2004. Sap flow measurements with some thermodynamic methods, flow integration within trees and scaling up from sample trees to entire forest stands. Trees-Structure and Function, 18(5): 529-546.

Dye, P.J. and Olbrich, B.W., 1993. Estimating transpiration from 6-year-old Eucalyptus grandis trees: development of a canopy conductance model and comparison with independent sap

flux measurements. Plant Cell and Environment, 16(1): 45-53.

Ford, C.R., Hubbard, R.M., Kloeppel, B.D. and Vose, J.M., 2007. A comparison of sap flux-based evapotranspiration estimates with catchment-scale water balance. Agricultural and Forest Meteorology, 145(3-4): 176-185.

Gebauer, T., Horna, V. and Leuschner, C., 2008. Variability in radial sap flux density patterns and sapwood area among seven co-occurring temperate broad-leaved tree species. Tree Physiology, 28(12): 1821-1830.

Guan, H.D., Zhang, X.P., Skrzypek, G., Sun, Z. and Xu, X., 2013. Deuterium excess variations of rainfall events in a coastal area of South Australia and its relationship with synoptic weather systems and atmospheric moisture sources. Journal of Geophysical Research-Atmospheres, 118(2): 1123-1138.

Guyot, A., Ostergaard, K.T., Lenkopane, M., Fan, J. and Lockington, D.A., 2013. Using electrical resistivity tomography to differentiate sapwood from heartwood: application to conifers. Tree Physiology, 33(2): 187-194.

Hatton, T.J., Moore, S.J. and Reece, P.H., 1995. Estimating stand transpiration in a Eucalyptus populnea woodland with the heat pulse method: measurement errors and sampling strategies. Tree Physiology, 15(4): 219-27.

Hearle, J.W.S., 1953. The electrical resistance of textile materials: IV. Theory. Journal of the Textile Institute Transactions, 44(4): T177-T198.

Ivanov, V.Y., Bras, R.L. and Vivoni, E.R., 2008. Vegetation-hydrology dynamics in complex terrain of semiarid areas: 1. A mechanistic approach to modeling dynamic feedbacks. Water Resources Research, 44. (3).

Kelley, G., O'Grady, A.P., Hutley, L.B. and Eamus, D., 2007. A comparison of tree water use in two contiguous vegetation communities of the seasonally dry tropics of northern Australia: the importance of site water budget to tree hydraulics. Australian Journal of Botany, 55(7): 700-708.

Kumagai, T., Aoki, S., Shimizu, T. and Otsuki, K., 2007. Sap flow estimates of stand transpiration at two slope positions in a Japanese cedar forest watershed. Tree Physiology, 27(2): 161-168.

Kumagai, T., Nagasawa, H., Mabuchi, T., Ohsaki, S., Kubota, K., Kogi, K., Utsumi, Y., Koga, S. and Otsuki, K., 2005. Sources of error in estimating stand transpiration using allometric relationships between stem diameter and sapwood area for Cryptomeria japonica and Chamaecyparis obtusa. Forest Ecology and Management, 206(1-3): 191-195.

Kumagai, T., Tateishi, M., Shimizu, T. and Otsuki, K., 2008. Transpiration and canopy conductance at two slope positions in a Japanese cedar forest watershed. Agricultural and Forest Meteorology, 148(10): 1444-1455.

Kume, T., Tsuruta, K., Komatsu, H., Kumagai, T., Higashi, N., Shinohara, Y. and Otsuki, K., 2010. Effects of sample size on sap flux-based stand-scale transpiration estimates. Tree Physiology, 30(1): 129-138.

Lin, C.J., Chung, C.H., Yang, T.H. and Lin, F.C., 2012. Detection of Electric Resistivity Tomography and Evaluation of the Sapwood-Heartwood Demarcation in Three Asia Gymnosperm Species. Silva Fennica, 46(3): 415-424.

Liu, C.W., Du, T.S., Li, F.S., Kang, S.Z., Li, S.E. and Tong, L., 2012. Trunk sap flow characteristics during two growth stages of apple tree and its relationships with affecting factors in an arid region of northwest China. Agricultural Water Management, 104: 193-202.

Longuetaud, F., Mothe, F., Leban, J.M. and Makela, A., 2006. Picea abies sapwood width: Variations within and between trees. Scandinavian Journal of Forest Research, 21(1): 41-53.

Macfarlane, C., Bond, C., White, D.A., Grigg, A.H., Ogden, G.N. and Silberstein, R., 2010. Transpiration and hydraulic traits of old and regrowth eucalypt forest in southwestern Australia. Forest Ecology and Management, 260(1): 96-105.

Palmer, A.R., Fuentes, S., Taylor, D., Macinnis-Ng, C., Zeppel, M., Yunusa, I. and Eamus, D., 2010. Towards a spatial understanding of water use of several land-cover classes: an examination of relationships amongst pre-dawn leaf water potential, vegetation water use, aridity and MODIS LAI. Ecohydrology, 3(1): 1-10.

Pfautsch, S., Bleby, T.M., Rennenberg, H. and Adams, M.A., 2010. Sap flow measurements reveal influence of temperature and stand structure on water use of Eucalyptus regnans forests. Forest Ecology and Management, 259(6): 1190-1199.

Quentin, A.G., O'Grady, A.P., Beadle, C.L., Mohammed, C. and Pinkard, E.A., 2012. Interactive effects of water supply and defoliation on photosynthesis, plant water status and growth of Eucalyptus globulus Labill. Tree Physiology, 32(8): 958-967.

Rust, S., 1999. Comparison of three methods for determining the conductive xylem area of Scots pine (Pinus sylvestris). Forestry, 72(2): 103-108.

Skaar, C., 1988. Wood-Water Relations. Springer Series in Wood Science. Springer-Verlag, Berlin Heidelberg.

Stamm, A.J., 1927. The electrical resistance of wood as a measure of its moisture content. Industrial and Engineering Chemistry, 19(1): 1021-1025.

Steppe, K., De Pauw, D.J.W., Lemeur, R. and Vanrolleghem, P.A., 2006. A mathematical model linking tree sap flow dynamics to daily stem diameter fluctuations and radial stem growth. Tree Physiology, 26(3): 257-273.

Swanson, R.H., 1994. Significant Historical Developments in Thermal Methods for Measuring Sap Flow in Trees. Agricultural and Forest Meteorology, 72(1-2): 113-132.

Tomazello, M., Brazolin, S., Chagas, M.P., Oliveira, J.T.S., Ballarin, A.W. and Benjamin, C.A., 2008. Application of X-ray technique in nondestructive evaluation of eucalypt wood. Maderas-Ciencia Y Tecnologia, 10(2): 139-149.

Vandegehuchte, M.W. and Steppe, K., 2013. Sap-flux density measurement methods: working principles and applicability. Functional Plant Biology, 40(3): 213-223.

Vertessy, R.A., Benyon, R.G., Osullivan, S.K. and Gribben, P.R., 1995. Relationships between Stem Diameter, Sapwood Area, Leaf-Area and Transpiration in a Young Mountain Ash Forest. Tree Physiology, 15(9): 559-567.

Vertessy, R.A., Hatton, T.J., Reece, P., Osullivan, S.K. and Benyon, R.G., 1997. Estimating stand water use of large mountain ash trees and validation of the sap flow measurement technique. Tree Physiology, 17(12): 747-756.

Whitehead, D. and Beadle, C.L., 2004. Physiological regulation of productivity and water use in Eucalyptus: a review. Forest Ecology and Management, 193(1-2): 113-140.

Wilson, K.B., Hanson, P.J., Mulholland, P.J., Baldocchi, D.D. and Wullschleger, S.D., 2001. A comparison of methods for determining forest evapotranspiration and its components: sap-flow, soil water budget, eddy covariance and catchment water balance. Agricultural and Forest Meteorology, 106(2): 153-168.

Wu, H., Zhou, Q., Liu, H. and Tang, M., 2009. Application of electrical resistivity tomography in studying water uptake process in tree trunk (in Chinese). Chinese Journal of Ecology, 28(02): 350-356.

Wullschleger, S.D., Hanson, P.J. and Todd, D.E., 2001. Transpiration from a multi-species deciduous forest as estimated by xylem sap flow techniques. Forest Ecology and Management, 143(1-3): 205-213.

Wullschleger, S.D. and King, A.W., 2000. Radial variation in sap velocity as a function of stem diameter and sapwood thickness in yellow-poplar trees. Tree Physiology, 20(8): 511-518.

Wullschleger, S.D., Meinzer, F.C. and Vertessy, R.A., 1998. A review of whole-plant water use studies in trees. Tree Physiology, 18(8-9): 499-512.

Zeppel, M., 2013. Convergence of tree water use and hydraulic architecture in water-limited regions: a review and synthesis. Ecohydrology, 6(5): 889-900.

Zeppel, M. and Eamus, D., 2008. Coordination of leaf area, sapwood area and canopy conductance leads to species convergence of tree water use in a remnant evergreen

woodland. Australian Journal of Botany, 56(2): 97-108.

5. Tree water use and response to environmental conditions on contrasting slopes

5.1. Introduction

Evapotranspiration is one of the most challenging components of the terrestrial water cycle to measure. Its quantification has been attempted using a wide variety of methods at various spatial scales (from tree to stand, catchment, region, continent and global) (Asbjornsen et al., 2011) using in situ measurements, satellite observations and land surface modelling. Partitioning evapotranspiration into soil evaporation and plant transpiration is challenging but important for biomass production assessment and water resources allocation (Kool et al., 2014). Vegetation covers 70% of the land surface (Dolman et al., 2014), and transpiration contributes up to 80% of the total global evapotranspiration (Miralles et al., 2011), stressing the significant role of vegetation in the water and carbon transfer from soil to the atmosphere. This makes the study of vegetation water use of prime significance in the global change context (Aranda et al., 2012). Transpiration has been claimed to highly correlate with environmental variables, including solar radiation, vapour pressure deficit, temperature, soil water content, and CO_2 concentration. Influence of those variables on tree water use varies from site to site. Following Jarvis (1976) and Stewart (1988), many studies examine the response of tree water use or canopy/stomatal conductance to environmental conditions in a wide range of climate and species (Damour et al., 2010; Eamus et al., 2009).

Complex terrain alters the energy and water distribution on the land surface (Gutiérrez-Jurado and Vivoni, 2013; Tromp-van Meerveld and McDonnell, 2006) and the nutrient conditions within the soil profile (Tokuchi et al., 1999). This results in differences in vegetation growth and species distribution as well as terrain mediated micrometeorology (Barij et al., 2007; Liu et al., 2012; Luizão et al., 2004). Therefore, investigating the coupling of terrain, vegetation and hydrological processes is a first step in deciphering the role of vegetation in the water balance of mountainous areas and the main controls on the distribution and adaptability of plants to a varying range of environmental conditions (Brooks and Vivoni, 2008; Gutierrez-Jurado et al., 2013; Vivoni et al., 2010). However, up to date only a few studies have compared tree water use and its response to environmental conditions as a function of the topographic positions (e.g., at different locations along a slope (Kumagai et al., 2008; Mitchell et al., 2012)). Limited information is available on tree water use and its environmental controls on contrasting slopes, which is a common arrangement of forests in mountainous areas. This is in part due to the

scarcity of comprehensive micrometeorological and tree water use measurements at these types of locations.

Heat-based sap flow measuring technique is a powerful tool for estimating tree water use at various spatiotemporal scales (Čermák et al., 2004; Vandegehuchte and Steppe, 2013). Sap flow measurements can be conducted in highly heterogeneous environments (Barrett et al., 1996; Wen et al., 2012), because the land surface heterogeneity does not limit its applicability (Ford et al., 2007; Wilson et al., 2001). Sap flow measurents can be performed on different individuals within a stand to estimate plant transpiration contributed by different species (Ewers et al., 2005; Pataki and Oren, 2003; Tang et al., 2006), thus provide information of species competition for water. Use of sap flow meters for ecohydrological studies involves the up-scaling of sap flow from individual trees to large scale transpiration. The up-scaling strategies have been extensively discussed in the literature using different scalars, for instance sapwood area (Cienciala et al., 2000; Granier, 1987), leaf area (Oren et al., 1999; Soegaard and Boegh, 1995), basal area (Teskey and Sheriff, 1996), and crown cover (Wullschleger et al., 1998). Sapwood area is the most common scalar. Sapwood area is usually estimated by measuring sapwood width from incremental wood cores (Pfautsch et al., 2010; Vertessy et al., 1997). In recent years, electrical resistivity tomography (ERT), which measures the cross-sectional electrical resistivity due to wood moisture, solute concentration and other factors, has been applied for quantifying sapwood width and hence sapwood area (Bieker and Rust, 2010; Guyot et al., 2013; Lin et al., 2012). ERT is relatively non-destructive and can be conducted throughout the sap flow measurement period rather than at the end of the period, which will benefit long-term tree water use study.

In South Australia, large areas of native trees were cleared and transformed to grazing pastures or grapevines in the last 5 decades (Bradshaw, 2012). Lying in between extensive pasture-lands and grapevines, the isolated forest stands function importantly as refugia for native wildlife and flora. Conservation of the trees within those stands is critical for the development of these natural communities. In this study, we measured tree water use, micrometeorology and soil water condition on two contrasting hill slopes in a remnant native forest stand in South Australia. Using the observations from a network of sensors, we aim to quantify the dynamics of tree water use, energy and soil water condition at the opposing slopes, and to characterize the environmental constraints on tree water use on the two slopes.

5.2. Methodology

5.2.1. Site description

The study site (Figure 5.1) is located in a mountainous catchment ($\sim$0.15 km^2) in McLaren Vale (35°12′48″, 138° 38′15″E), 45 km south of Adelaide, South Australia. There are two slopes with contrasting aspects in the catchment: north-facing (NFS) and south-facing (SFS). The dominant species on the NFS is *Eucalyptus leucoxylon*, while on the SFS is *Eucalyptus viminalis ssp. cygnetensis*. Both species are evergreen broadleaf trees. Trees of the two species at same age have similar leaf size and shape. At the scale of the hill slopes, the tree density and canopy cover is larger on the SFS than on the NFS.
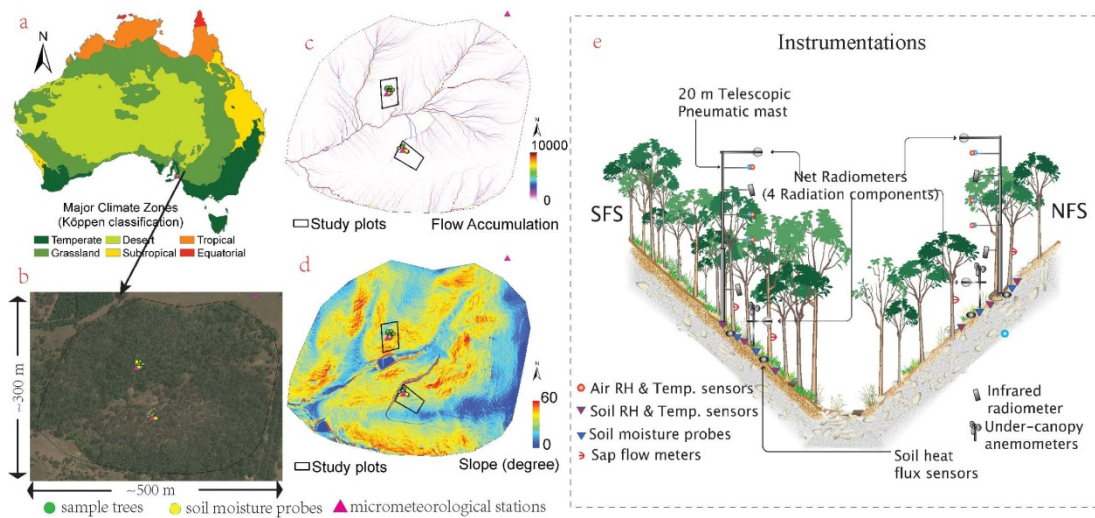
Figure 5.1 (*a*) Map of the Australian climate zones based on the Köppen classification method, from the Australian Bureau of Meteorology; (*b*) snapshot of the study site in Google Earth; (*c, d*) flow accumulation and slopes from LiDAR data, and (*e*) schematic plot of the site for instrumentations

One plot (20 m × 40 m) on each of the two slopes was delineated and instrumented for comparison of the micrometeorology and tree water use. Flow accumulation obtained from LiDAR derived digital elevation model of the catchment in ArcGIS shows that the two plots are located in areas devoid of clear drainage channels and terrain depressions, hence little surface runoff from the upper slopes contributing to the soil water storage in the study plots is expected (Figure 5.1*c*). Consequently, the trees in the plots have smaller canopy sizes relative to those located within the vicinity or along the flow pathways indicated by the LiDAR data. Some of the plot properties are listed in Table 5-1. Both the average slope calculated in ArcGIS and the soil porosity measured in laboratory using undisturbed soil samples in the NFS plot are smaller than those in the SFS plot. The porosity data indicate that the soil in the SFS plot should have higher saturated water content than the soil in the NFS plot.

Table 5-1 Comparison of the properties of the two plots on NFS and SFS in the catchment

Plot	Number of trees	Mean LAI[†]	Sapwood area (cm²)	Mean slope (º)	Topographic Index*	Mean soil porosity
NFS	78	1.4	3300.2	21	5.15	0.44
SFS	79	1.4	3396.0	26	5.06	0.51

*calculated following Tarboton (1997) using flow contributing area and slope. [†]LAI was estimated for 10 sample trees in each small plot using the method described in MacFarlane et al. (2007). For the entire slope the LAI is smaller on NFS than SFS due to meagre vegetation cover relative to that of SFS.

The estimated leaf area index (LAI), sapwood areas (A_s) and the number of trees within the plots are similar (Table 5-1). It should be noted that the LAI and A_s were estimated only on the trees inside the two small plots (Figure 5.1c-d); the values will be different for the two entire slopes. LAI and A_s are larger on SFS than NFS, as the vegetation cover on south facing slope is higher than that on north facing slope.

5.2.2. Instrumentation

Twenty four sets of compensation heat pulse sap flow meters (*Tranzflo NZ Ltd, New Zealand*) (Green et al., 2003) were installed on 12 trees of two dominant species. These trees have a range of stem sizes, from 100 to 350 mm in diameter at 1.3 m height. Thermo-sensors were embedded at the depths of 5, 15 and 25 mm from the bottom to tip of the sensor probes. We measured sapwood width by taking wood core samples with an increment borer (ϕ=5 mm) on 10 trees of each species. Electrical resistivity tomography was also applied on the same trees for sapwood width estimation. Tree diameter (DBH) at 1.3 m height was measured in order to establish the relationship with sapwood area for total sapwood area estimation in the plots. More details of the measurements and results comparison can be found in Chapter 2.

Two capacitance based soil moisture probes (*Sentek Sensor Technologies, Australia*) were installed in the plots for continuous measurement of volumetric water content at depths of 10, 30, 50 cm below the ground surface. Undisturbed soil samples at depths of 0-10, 10-30 and 30-50 cm were collected near the probes for gravimetric soil water content and bulk density measurements in laboratory. Particle size was also analysed using sedimentation method in laboratory (Marshall et al., 1996). Gravimetric soil water content was converted to volumetric content by bulk density to calibrate the soil moisture data collected from the probes. Mean soil water content at the depth of 0-50 cm was calculated as the equal weighted average of 10, 30 and 50 cm measurements (Miller et al., 2007), that is, (θ_{10cm} + θ_{30cm} + θ_{50cm})/3. Zone weighted depth-averaging method (Miller et al., 2007) was also applied, assuming that the measurements at 10,

30 and 50 cm from the probes represent soil water conditions of 0-10, 10-30 and 30-50 cm soil layers, i.e. ($10*\theta_{10cm} + 20*\theta_{30cm} + 20*\theta_{50cm}$)/50. The mean soil water content given by the two methods was similar. In this study, we used the equal-weighted average values for discussion.

Net radiometers and temperature and humidity sensors (*Environdata Weather Stations Pty Ltd, Queensland Australia*) were mounted on top of two masts above tree canopy. A third weather station was set up outside the catchment on the top of the hill at an open grassland site. When the sensors on masts on the two slopes did not record data due to sensor maintenance and battery power loss, the data (temperature, relative humidity and solar radiation mainly) from the hill-top weather station were used to fill up the gaps based on simple linear regressions of the relevant daily data. The linear regressions were also applied to the days before the two masts were set up for temperature, relative humidity and solar radiation estimates.

All loggers were configured to record data at 30-minute interval, except the net radiometer and hill-top weather station, which was at 10- and 15-minute intervals respectively. Note that the data of sap flow, micrometeorology and soil water content were not concurrent in time due to maintenance, so when analysing the relationship between transpiration and the environmental conditions, the days with all sap flow, micrometeorological and soil moisture data available were chosen. All data were aggregated to daily values for analysis.

5.2.3. Plot scale transpiration estimates from sap flow measurements

Transpiration rates in two plots were up-scaled following the strategy described in Kumagai et al. (2007): (1) total plot sapwood area (A_{splot}) estimation based on the relationship between the D_{130} and sapwood area (A_s) of the sampled trees in the plots; (2) mean plot scale sap flux density (J_S) estimation based on sap flux density (J) measured on the sampled trees in the plots; and (3) transpiration (E_c) of the whole plot, calculated from equations (5-1~5-5).

$$E_c = J_S \times \frac{A_{splot}}{A_G} \tag{5-1}$$

where E_c is the total transpiration of each plot (mm/d); A_G is the total ground area (800 m^2) of each plot.

The mean plot sap flux density (J_S) was calculated as follows:

$$J_S = \frac{J_{S1}\sum\limits_{i=1}^{N} A_{i,1} + J_{S2}\sum\limits_{i=1}^{N} A_{i,2} + J_{s3}\sum\limits_{i=1}^{N} A_{i,3}}{\sum\limits_{i=1}^{N}(A_{i,1} + A_{i,2} + A_{i,3})}, \tag{5-2}$$

$$J_{S1} = \frac{\sum\limits_{i=1}^{N} J_{i,1} A_{i,1}}{\sum\limits_{i=1}^{N} A_{i,1}}, \tag{5-3}$$

$$J_{S2} = \frac{\sum\limits_{i=1}^{N} J_{i,2} A_{i,2}}{\sum\limits_{i=1}^{N} A_{i,2}}, \tag{5-4}$$

$$J_{S3} = \frac{\sum\limits_{i=1}^{N} J_{i,3} A_{i,3}}{\sum\limits_{i=1}^{N} A_{i,3}} \tag{5-5}$$

where i stands for each sample tree; N is the total number of sample trees in the plots; $A_{i,1}$, $A_{i,2}$ and $A_{i,3}$ are areas of three sapwood bands where three sap flow sensors are located; J_{S1}, J_{S2} and J_{S3} are the mean sap flux density in three sapwood bands for all samples trees.

5.2.4. Parameterization of environmental controls on tree water use

Based on a modified model in Whitley et al. (2013) we correlated the tree water use in each plot with environmental variables including vapour pressure deficit (D) and net solar radiation (R_n), and soil water content (θ). The model is shown in equation (5-6), in which k_D and k_R are fitting parameters, D_p is the value of D at which E_c is maximized; θ_w and θ_c are wilting and critical points of the soil water content respectively. Note the critical point is the water content at which transpiration reaches its maximum, and it may or may not correspond to the field capacity. The parameter values were obtained using the DREAM optimization model (Vrugt et al., 2009; Wang et al., 2014).

$$E_c^m = E_{max} \cdot \exp\left[-\frac{k_D(D-D_p)^2}{D}\right] \cdot \left[\frac{R_n}{350} \times \frac{350+k_R}{R_n+k_R}\right] \cdot \min\left\{1, \frac{\theta-\theta_w}{\theta_c-\theta_w}\right\} \tag{5-6}$$

5.3. Results and discussion

5.3.1. Micrometeorology

Linear regression of daily temperature, relative humidity and solar radiation from the hill-top weather station and the masts is given in Figure 5.2. Data used for regression were from 6 April 2013 to 2 August 2014, covering 403 days for the NFS; and from 6 April to 24 November 2013 and 23 April to 22 June 2014, covering 215 days for the SFS. Data gaps were filled using the linear relationships. We did not use sub-daily (such as hourly) data to do the regressions, because the temporal dynamics of micrometeorological variables on the two slopes are different from those on hill-top weather station due to aspect effects, especially the solar radiation during the winter (June-August) time. Note that the radiation on the two masts was net solar radiation calculated from the four-component measurements (downward short/long wave radiation, upward short/long wave radiation), while the radiation on the hill-top weather station was global shortwave radiation. The temperature from three stations was highly linearly correlated; the regression slopes and coefficient of determination are close to one, and root mean square error is about 0.35°C. For relative humidity and solar radiation, the correlation between the SFS and the hill-top weather station was not as high as the NFS, especially when it was on more humid during cloudy days (i.e. days of high relative humidity and low radiation). Nonetheless, the relationships can be used to estimate relative humidity and net radiation in the period when data were missing.
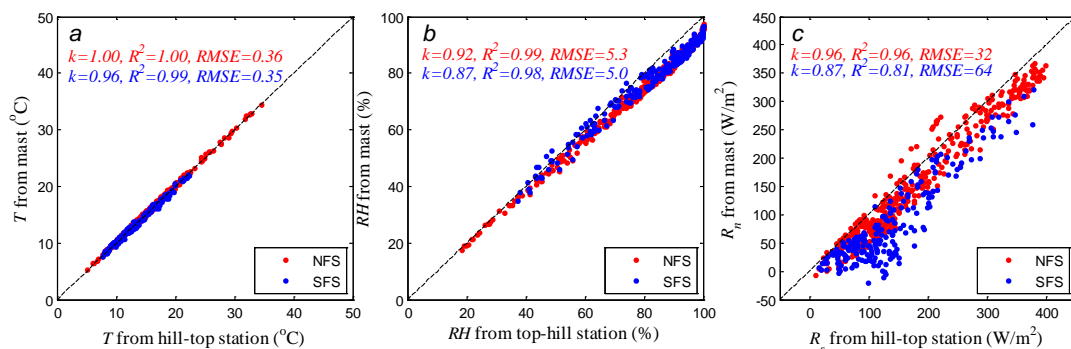
Figure 5.2 Linear regression between daily data from the hill-top weather station and from the two masts on the two slopes. (*a*) air temperature; (*b*) relative humidity (*RH*) and (*c*) solar radiation. *k*, R^2 and *RMSE* are the slope, coefficient of determination and root mean square error from the linear regression.

Daily *T*, *D* and R_n were compared and the differences between data on the two slopes are demonstrated in Figure 5.3. Rainfall was assumed to have no spatial variability at the study site, considering the short distance (~350 m) between the hill-top station and the two masts. Those variables had clear seasonal dynamics: *T*, *D*, R_n was low from May to September and high from October to April of the next year; rainfall had the contrary characteristics. Solar energy received

on the two slopes peaked about half a month earlier than temperature and vapour pressure deficit.

Throughout a year the temperature, vapour pressure deficit and solar radiation were higher on north facing slope than on the south facing slope, in particular the largest differences are observed in the solar radiation; the difference between air temperature and vapour pressure deficit on the two slopes although small shows consistently higher T and D on the NFS. The higher T, D and R_n resulted in higher atmospheric demand for evapotranspiration on NFS than SFS (Figure 5.4).
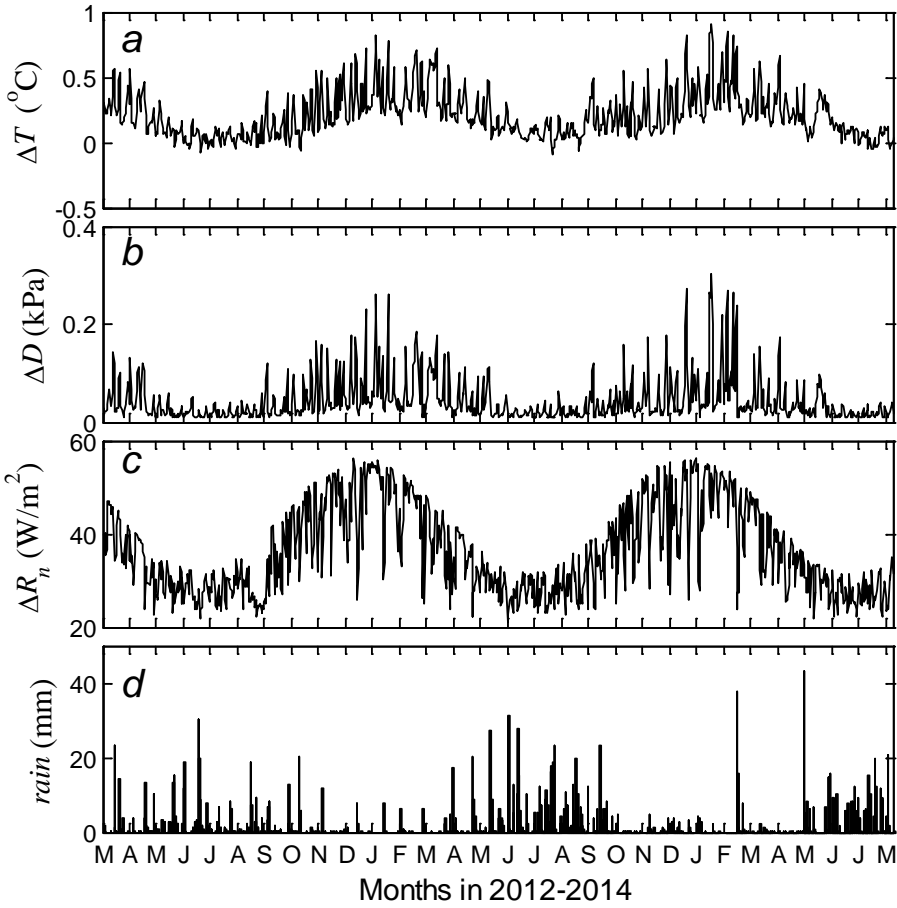
Figure 5.3 Comparison of micrometeorological variables on NFS and SFS in 2012-2014. (*a*) ΔT: temperature difference (NFS-SFS); (*b*) ΔD: vapour pressure deficit difference (NFS-SFS); (*c*) ΔR_n: net radiation difference (NFS-SFS) and (*d*) rainfall from hill-top station
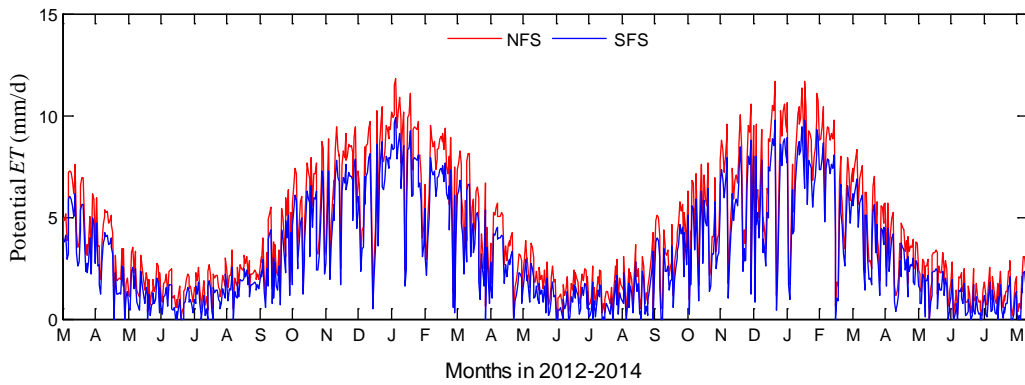
Figure 5.4 Daily potential evapotranspiration on the two slopes, calculated from the Priestley-Taylor (1972) method

5.3.2. Soil properties and water content

Particle size analysis results are given in Table 5-2. The soil on SFS had more sand and less clay compositions than soil on NFS almost at all surveyed depths. Infiltration experiments at three locations along each slope gave larger infiltration rates on SFS than NFS.

Table 5-2 Soil particle size analysis for the two slopes. Data for each depth range were averaged from 5 undisturbed soil samples

Depth (cm)	NFS			SFS		
	Clay (%)	Silt (%)	Sand (%)	Clay (%)	Silt (%)	Sand (%)
0-20	13.3	40.1	46.6	14.9	36.9	48.1
20-40	25.7	35.8	46.3	15.7	31.4	52.8
40-60	19.3	34.4	46.2	15.4	31.2	53.3

In accord with the rainfall seasonality, the volumetric soil water content showed high values in rainy season and low values in dry season on both slopes (Figure 5.5). In dry period, the deeper soil retained higher water content than the shallower soil, while in wet period the soil water content was similar at all depths, with the maximum soil water content on SFS slightly larger than NFS. Soil water content on both slopes reached the field capacity in rainy season, and the field capacity within the depth of 50 cm was around 0.344 m^3/m^3 on SFS and 0.329 m^3/m^3 on NFS. During the wet period, for example from days 160 to 180 (Figure 5.5), when there was little rainfall and a relatively long clear-day window, soil water content dropped quicker on NFS than SFS. This is likely due to the higher evapotranspiration rate on NFS than SFS during these days resulting from higher temperature and solar radiation. During the dry period, soil water content was more corresponsive to rainfall than during the wet period due to higher storage capacities of the oil in both slopes. Nevertheless, the same rainfall amount resulted in higher moisture storage increases on the SFS than on the NFS soils. Differences in infiltration capacities between the slopes (e.g., higher infiltration rates on the SFS than on the NFS) may be responsible for this.

78
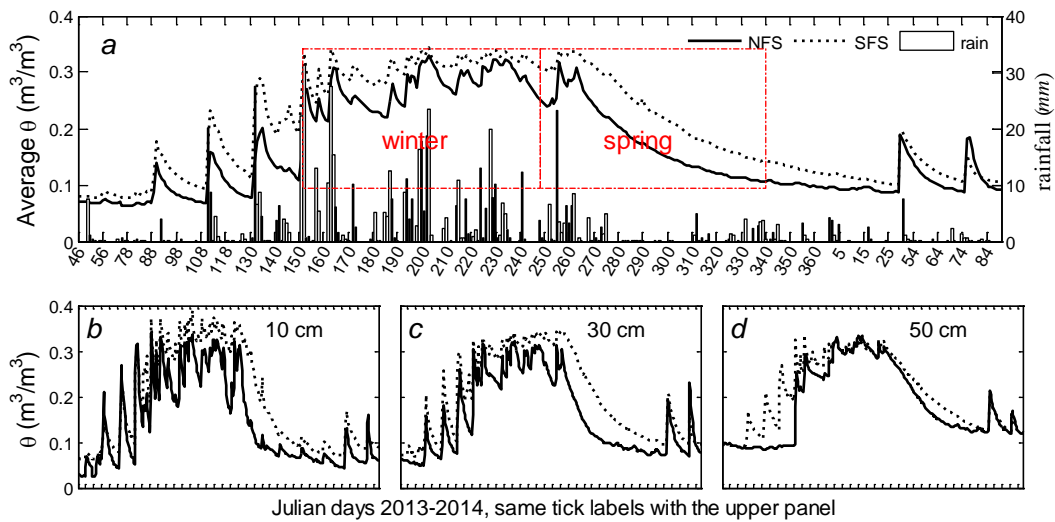
Figure 5.5 Volumetric soil water content on NFS and SFS and rainfall in 2013-2014. (*a*) equal weighted average volumetric soil water content in 0-50 cm soil layer following Miller et al. (2007) and rainfall; (*b-d*) water content measured at depths of 10 cm, 30 cm and 50 cm

5.3.3. Tree water use on two slopes

Mean sap flux density (J_S) in the sapwood area of all sampled trees in each plot was calculated from equations (5-2~5-5). Total tree water use in each plot was estimated using equation (5-1) and the relationship between sapwood area and D_{130}. Results are given in Figure 5.6 for the comparison of total transpiration in the plots on two slopes.
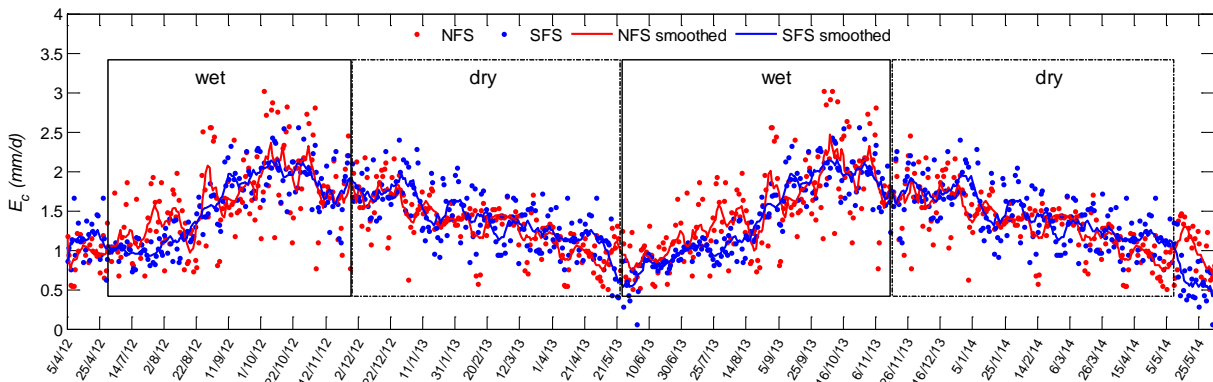
Figure 5.6 Tree water use estimated from sap flow measurements for the two plots on NFS and SFS. Rectangles enclose the relevant wet (winter and spring) and dry (summer and autumn) periods. Solid lines in the figure are smoothed tree water use by a 10-day moving average window.

Similar to the micrometeorological variables and soil water content, tree water use data showed clear seasonal dynamics on the two hill slopes. The transpiration rate was the largest in spring (September-November) throughout a year, and the smallest in autumn (March-May). Sap flow data in some winter (June-August) days were not recorded by the loggers because of flat batteries, so we were not able to determine exactly when the lowest sap flow value occurred;

however, from the trend in Figure 5.6, the minimum sap flow data tend to occur in late autumn. There was a phase shift among the potential *ET* (Figure 5.4), soil water content (Figure 5.5) and transpiration (Figure 5.6), that is, the maximum transpiration appeared (in October) after the soil water content reached its maxima (approximately in June), and before the potential *ET* approached the peak values (around January). This reveals a clear pattern of transpiration in response to water supply and evaporative demand. In wet period, transpiration was mainly limited by evaporative demand; while in dry period, the major limiting factor was soil water supply. The high leaf surface temperature and vapour pressure deficit in dry period would also cause the leaves to partly or fully close the stomata to prevent water loss.

Comparing the transpiration (E_c) rates on the two slopes, we observed different patterns throughout the measurement period. E_c on the NFS was larger than that on the SFS in winter and spring (marked as "wet" in Figure 5.6), while E_c on SFS slightly larger than that on NFS in summer and autumn (marked as "dry" in Figure 5.6). The total estimated transpiration during the measurement period in Figure 5.6 was similar for both plots, around 1000 mm in 710 days in 2012 to 2014. A parallel study at the site using the Maximum Entropy Production method (Wang and Bras, 2011) for evaporation and transpiration estimates showed that the total evapotranspiration on the NFS was larger than that on the SFS, and the main contributor to the difference was not transpiration from trees but evaporation from soil surface (Gutiérrez-Jurado et al., 2014).

5.3.4. Environmental controls on tree water use

The difference in topography (elevation, slope and aspect) and soil properties of the study site resulted in the difference in energy loading and soil water availability on the contrasting slopes throughout the measurement period. This, in turn, would have different effects on tree water use on the two contrasting slopes. The relationship between tree water use and vapour pressure deficit, net solar radiation and soil water content is shown in Figure 5.7 for comparison between the two slopes. Generally, the relationships between E_c and the environmental variables on the two slopes were similar at a daily scale, although the data ranges were slightly different. For example, the minimum solar radiation was smaller on SFS than NFS, and the maximum soil water content was higher on SFS than NFS.
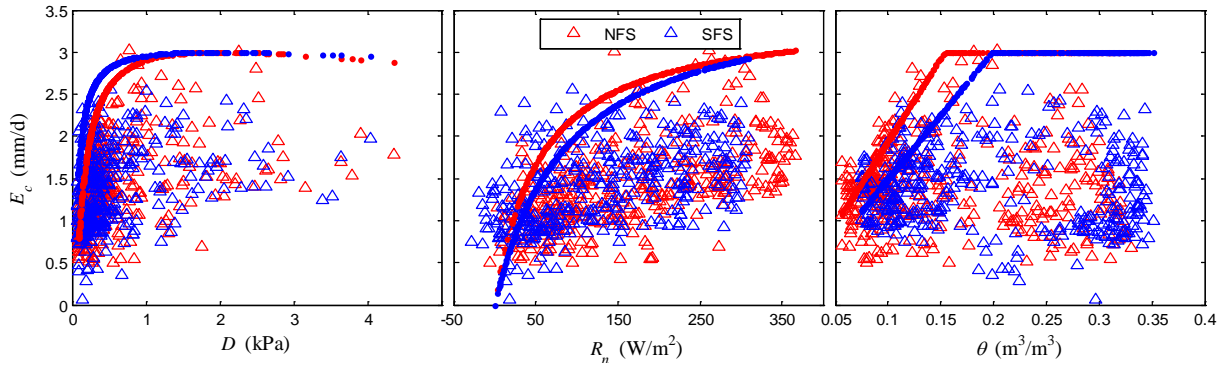
Figure 5.7 Relationship between daily tree water use and vapour pressure deficit (D), net solar radiation (R_n) and mean soil water content (θ). Dots in the figure are E_{max} multiplied by the response functions of the relevant environmental variables.

Using the DREAM optimization method (Vrugt et al., 2009), we obtained the parameter values (Table 5-3) for equation (5-6) on the NFS and SFS. The optimized maximum transpiration E_{max} is the same for the two slopes, about 3 mm/d. The vapour pressure deficit value (D_p) at which E_c was maximized was also similar on the two slopes. The main difference of parameter values was for k_R and critical point of soil water content. This implies that the optimal conditions of solar radiation and soil water supply for transpiration were different on the two slopes; specifically, the optimal amount of solar radiation and soil water content for the transpiration to reach its maximum rate was smaller on NFS than SFS.

Table 5-3 Parameter values for equation (5-6) obtained from the DREAM optimization model

	E_{max} [mm/d]	k_R [W/m²]	k_D	D_p [kPa]	θ_c [m³/m³]	θ_w [m³/m³]
NFS	3.0	53	0.03	1.99	0.153	0.0013
SFS	3.0	85	0.02	1.95	0.199	0.0016

To intuitively examine the response of transpiration to the environmental variables on the two slopes, the E_{max} was multiplied by the response functions of D, R_n and θ, results were plotted against the relevant environmental variables in Figure 5.7. The responses of E_c to D and R_n were similar on the two contrasting slopes, although the D_p value for SFS is slightly lower than for NFS. The response of E_c to θ had notoriously different characteristics on the two slopes. Transpiration approached the maximum rate at the critical point of 0.153 m³/m³ on the NFS and 0.199 on the SFS. Together with soil moisture data in Figure 5.5, results indicate that the trees on NFS suffered water stress longer than those on SFS when soil water content fell below the critical point (around 0.2 m³/m³), because soil on NFS drained up moisture faster than soil on SFS. The values of soil water content below which trees stopped transpiration were also different on the two slopes, but the difference was minor.

5.4. Conclusions

This study provides a close examination of tree water use and as it responds to environmental conditions modulated by topographic effects. The tree water use and environmental variables considered (i.e. temperature, vapour pressure deficit, solar radiation and soil water content) had clear seasonal variations at the study site. These variations are reflected in the trees' water use of the two slopes, specifically in the different dates that peak values occurred for daily soil water content, transpiration and potential *ET*. Our observations indicate that tree water use at the site was mainly controlled by soil water supply in summer and autumn and by evaporative demand in winter and spring. Despite the difference of transpiration in dry and wet periods, the total estimated transpiration during the study period was similar on both slopes. This is supported by a parallel study using the Maximum Entropy Production method for evaporation and transpiration estimation at the study site. The response of tree water use to vapour pressure deficit and solar radiation was similar on both slopes; while the response to soil water content was different. The maximum transpiration occurred at a lower critical point of soil water content on NFS than SFS. Trees on NFS suffered water stress longer than trees on the other slope when soil water content fell below the critical point.

5.5. References

Aranda, I., Forner, A., Cuesta, B. and Valladares, F., 2012. Species-specific water use by forest tree species: From the tree to the stand. Agricultural Water Management, 114: 67-77.

Asbjornsen, H., Goldsmith, G.R., Alvarado-Barrientos, M.S., Rebel, K., Van Osch, F.P., Rietkerk, M., Chen, J.Q., Gotsch, S., Tobon, C., Geissert, D.R., Gomez-Tagle, A., Vache, K. and Dawson, T.E., 2011. Ecohydrological advances and applications in plant-water relations research: a review. Journal of Plant Ecology, 4(1-2): 3-22.

Barij, N., Stokes, A., Bogaard, T. and Van Beek, R., 2007. Does growing on a slope affect tree xylem structure and water relations? Tree Physiology, 27(5): 757-764.

Barrett, D.J., Hatton, T.J., Ash, J.E. and Ball, M.C., 1996. Transpiration by trees from contrasting forest types. Australian Journal of Botany, 44(3): 249-263.

Bieker, D. and Rust, S., 2010. Non-Destructive Estimation of Sapwood and Heartwood Width in Scots Pine (Pinus sylvestris L.). Silva Fennica, 44(2): 267-273.

Bradshaw, C.J.A., 2012. Little left to lose: deforestation and forest degradation in Australia since European colonization. Journal of Plant Ecology, 5(1): 109-120.

Brooks, P.D. and Vivoni, E.R., 2008. Mountain ecohydrology: quantifying the role of vegetation in the water balance of montane catchments. Ecohydrology, 1(3): 187-192.

Čermák, J., Kučera, J. and Nadezhdina, N., 2004. Sap flow measurements with some thermodynamic methods, flow integration within trees and scaling up from sample trees to entire forest stands. Trees-Structure and Function, 18(5): 529-546.

Cienciala, E., Kucera, J. and Malmer, A., 2000. Tree sap flow and stand transpiration of two Acacia mangium plantations in Sabah, Borneo. Journal of Hydrology, 236(1-2): 109-120.

Damour, G., Simonneau, T., Cochard, H. and Urban, L., 2010. An overview of models of stomatal conductance at the leaf level. Plant Cell and Environment, 33(9): 1419-1438.

Dolman, A.J., Miralles, D.G. and de Jeu, R.A.M., 2014. Fifty years since Monteith's 1965

seminal paper: the emergence of global ecohydrology. Ecohydrology, 7(3): 897-902.

Eamus, D., Whitley, R., Medlyn, B., Zeppel, M. and Macinnis-Ng, C., 2009. Comparing the Penman-Monteith equation and a modified Jarvis-Stewart model with an artificial neural network to estimate stand-scale transpiration and canopy conductance. Journal of Hydrology, 373(1-2): 256-266.

Ewers, B.E., Gower, S.T., Bond-Lamberty, B. and Wang, C.K., 2005. Effects of stand age and tree species on canopy transpiration and average stomatal conductance of boreal forests. Plant Cell and Environment, 28(5): 660-678.

Ford, C.R., Hubbard, R.M., Kloeppel, B.D. and Vose, J.M., 2007. A comparison of sap flux-based evapotranspiration estimates with catchment-scale water balance. Agricultural and Forest Meteorology, 145(3-4): 176-185.

Granier, A., 1987. Evaluation of Transpiration in a Douglas-Fir Stand by Means of Sap Flow Measurements. Tree Physiology, 3(4): 309-319.

Green, S., Clothier, B. and Jardine, B., 2003. Theory and practical application of heat pulse to measure sap flow. Agronomy Journal, 95(6): 1371-1379.

Gutiérrez-Jurado, H.A., Huade Guan, Jingfeng Wang, Hailong Wang, Bras, R.L. and Simmons, C., 2014. Monitoring evapotranspiration and its partition over heterogeneous terrain and vegetation cover using the MEP model Geophysical Research Letters, under revision.

Gutiérrez-Jurado, H.A. and Vivoni, E.R., 2013. Ecogeomorphic expressions of an aspect-controlled semiarid basin: II. Topographic and vegetation controls on solar irradiance. Ecohydrology, 6(1): 24-37.

Gutierrez-Jurado, H.A., Vivoni, E.R., Cikoski, C., Harrison, J.B.J., Bras, R.L. and Istanbulluoglu, E., 2013. On the observed ecohydrologic dynamics of a semiarid basin with aspect-delimited ecosystems. Water Resources Research, 49(12): 8263-8284.

Guyot, A., Ostergaard, K.T., Lenkopane, M., Fan, J. and Lockington, D.A., 2013. Using electrical resistivity tomography to differentiate sapwood from heartwood: application to conifers. Tree Physiology, 33(2): 187-194.

Jarvis, P.G., 1976. The interpretation of the variations in leaf water potential and stomatal conductance found in canopies in the field. Philosophical Transactions of the Royal Society of London. B, Biological Sciences, 273(927): 593-610.

Kool, D., Agam, N., Lazarovitch, N., Heitman, J.L., Sauer, T.J. and Ben-Gal, A., 2014. A review of approaches for evapotranspiration partitioning. Agricultural and Forest Meteorology, 184(0): 56-70.

Kumagai, T., Aoki, S., Shimizu, T. and Otsuki, K., 2007. Sap flow estimates of stand transpiration at two slope positions in a Japanese cedar forest watershed. Tree Physiology, 27(2): 161-168.

Kumagai, T., Tateishi, M., Shimizu, T. and Otsuki, K., 2008. Transpiration and canopy conductance at two slope positions in a Japanese cedar forest watershed. Agricultural and Forest Meteorology, 148(10): 1444-1455.

Lin, C.J., Chung, C.H., Yang, T.H. and Lin, F.C., 2012. Detection of Electric Resistivity Tomography and Evaluation of the Sapwood-Heartwood Demarcation in Three Asia Gymnosperm Species. Silva Fennica, 46(3): 415-424.

Liu, H.Y., He, S.Y., Anenkhonov, O.A., Hu, G.Z., Sandanov, D.V. and Badmaeva, N.K., 2012. Topography-controlled soil water content and the coexistence of forest and steppe in northern China. Physical Geography, 33(6): 561-573.

Luizão, R.C.C., Luizão, F.J., Paiva, R.Q., Monteiro, T.F., Sousa, L.S. and Kruijt, B., 2004. Variation of carbon and nitrogen cycling processes along a topographic gradient in a central Amazonian forest. Global Change Biology, 10(5): 592-600.

Macfarlane, C., Hoffman, M., Eamus, D., Kerp, N., Higginson, S., McMurtrie, R. and Adams, M., 2007. Estimation of leaf area index in eucalypt forest using digital photography. Agricultural and Forest Meteorology, 143(3-4): 176-188.

Marshall, T.J., Holmes, J.W. and Rose, C.W., 1996. Soil physics. Cambridge University Press,

New York, USA, 21-28 pp.

Miller, G.R., Baldocchi, D.D., Law, B.E. and Meyers, T., 2007. An analysis of soil moisture dynamics using multi-year data from a network of micrometeorological observation sites. Advances in Water Resources, 30(5): 1065-1081.

Miralles, D.G., De Jeu, R.A.M., Gash, J.H., Holmes, T.R.H. and Dolman, A.J., 2011. Magnitude and variability of land evaporation and its components at the global scale. Hydrology and Earth System Sciences, 15(3): 967-981.

Mitchell, P.J., Benyon, R.G. and Lane, P.N.J., 2012. Responses of evapotranspiration at different topographic positions and catchment water balance following a pronounced drought in a mixed species eucalypt forest, Australia. Journal of Hydrology, 440: 62-74.

Oren, R., Phillips, N., Ewers, B.E., Pataki, D.E. and Megonigal, J.P., 1999. Sap-flux-scaled transpiration responses to light, vapor pressure deficit, and leaf area reduction in a flooded Taxodium distichum forest. Tree Physiology, 19(6): 337-347.

Pataki, D.E. and Oren, R., 2003. Species differences in stomatal control of water loss at the canopy scale in a mature bottomland deciduous forest. Advances in Water Resources, 26(12): 1267-1278.

Pfautsch, S., Bleby, T.M., Rennenberg, H. and Adams, M.A., 2010. Sap flow measurements reveal influence of temperature and stand structure on water use of Eucalyptus regnans forests. Forest Ecology and Management, 259(6): 1190-1199.

Priestley, C.H.B. and Taylor, R.J., 1972. On the Assessment of Surface Heat Flux and Evaporation Using Large-Scale Parameters. Monthly Weather Review, 100(2): 81-92.

Soegaard, H. and Boegh, E., 1995. Estimation of evapotranspiration from a millet crop in the Sahel combining sap flow, leaf area index and eddy correlation technique. Journal of Hydrology, 166(3–4): 265-282.

Stewart, J.B., 1988. Modeling surface conductance of pine forest. Agricultural and Forest Meteorology, 43(1): 19-35.

Tang, J.W., Bolstad, P.V., Ewers, B.E., Desai, A.R., Davis, K.J. and Carey, E.V., 2006. Sap flux-upscaled canopy transpiration, stomatal conductance, and water use efficiency in an old growth forest in the Great Lakes region of the United States. Journal of Geophysical Research-Biogeosciences, 111(G2).

Tarboton, D.G., 1997. A new method for the determination of flow directions and upslope areas in grid digital elevation models. Water Resources Research, 33(2): 309-319.

Teskey, R.O. and Sheriff, D.W., 1996. Water use by Pinus radiata trees in a plantation. Tree Physiology, 16(1-2): 273-279.

Tokuchi, N., Takeda, H., Yoshida, K. and Iwatsubo, G., 1999. Topographical variations in a plant-soil system along a slope on Mt Ryuoh, Japan. Ecological Research, 14(4): 361-369.

Tromp-van Meerveld, H.J. and McDonnell, J.J., 2006. On the interrelations between topography, soil depth, soil moisture, transpiration rates and species distribution at the hillslope scale. Advances in Water Resources, 29(2): 293-310.

Vandegehuchte, M.W. and Steppe, K., 2013. Sap-flux density measurement methods: working principles and applicability. Functional Plant Biology, 40(10): 213-223.

Vertessy, R.A., Hatton, T.J., Reece, P., Osullivan, S.K. and Benyon, R.G., 1997. Estimating stand water use of large mountain ash trees and validation of the sap flow measurement technique. Tree Physiology, 17(12): 747-756.

Vivoni, E.R., Rodriguez, J.C. and Watts, C.J., 2010. On the spatiotemporal variability of soil moisture and evapotranspiration in a mountainous basin within the North American monsoon region. Water Resources Research, 46.

Vrugt, J.A., ter Braak, C.J.F., Diks, C.G.H., Robinson, B.A., Hyman, J.M. and Higdon, D., 2009. Accelerating Markov Chain Monte Carlo Simulation by Differential Evolution with Self-Adaptive Randomized Subspace Sampling. International Journal of Nonlinear Sciences and Numerical Simulation, 10(3): 273-290.

Wang, H., Guan, H., Deng, Z. and Simmons, C.T., 2014. Optimization of canopy conductance models from concurrent measurements of sap flow and stem water potential on Drooping Sheoak in South Australia. Water Resources Research, 50(7): 6154-6167.

Wang, J.F. and Bras, R.L., 2011. A model of evapotranspiration based on the theory of maximum entropy production. Water Resources Research, 47.

Wen, M., Yang, S., Vintzileos, A., Higgins, W. and Zhang, R.H., 2012. Impacts of Model Resolutions and Initial Conditions on Predictions of the Asian Summer Monsoon by the NCEP Climate Forecast System. Weather and Forecasting, 27(3): 629-646.

Whitley, R., Taylor, D., Macinnis-Ng, C., Zeppel, M., Yunusa, I., O'Grady, A., Froend, R., Medlyn, B. and Eamus, D., 2013. Developing an empirical model of canopy water flux describing the common response of transpiration to solar radiation and VPD across five contrasting woodlands and forests. Hydrological Processes, 27(8): 1133-1146.

Wilson, K.B., Hanson, P.J., Mulholland, P.J., Baldocchi, D.D. and Wullschleger, S.D., 2001. A comparison of methods for determining forest evapotranspiration and its components: sap-flow, soil water budget, eddy covariance and catchment water balance. Agricultural and Forest Meteorology, 106(2): 153-168.

Wullschleger, S.D., Meinzer, F.C. and Vertessy, R.A., 1998. A review of whole-plant water use studies in trees. Tree Physiology, 18(8-9): 499-512.

6. Conclusions and future research interests

6.1. Conclusions

In the context of the need of accurate water balance study for water resources management, this thesis focused on the transpiration estimate and the response of transpiration to environmental conditions in order to enhance the understanding of interactions between vegetation and the atmosphere. Some of the challenges in ecohydrological studies have been discussed, e.g., the scale issues, information transferring across scales and the effects of complexity of land surface on transpiration estimation and the responses to environmental conditions.

In this thesis, models for transpiration estimation were divided into two groups, ″indirect″ (or Penman-Monteith method) and ″direct″, based on the way of linking with environmental variables. In Penman-Monteith equation, the term canopy conductance links the hydrology with plant physiology. The responses of canopy conductance to environmental variables are usually species and climate specific. The first part of this thesis rigorously determined the most appropriate canopy conductance model, taking a native Australian species as an example. The selection of proper response functions can substantially improve the canopy conductance simulation; in the meantime, the effect of temperature function in the canopy conductance modelling for the examined species is different from commonly used ones in other studies, which called for testing response functions before applying them in canopy conductance models. This most-appropriate-model selection procedure should be applied to more vegetation classifications under various climate conditions, to improve the land surface/atmospheric models for transpiration estimates.

The Penman-Monteith method and the ″direct″ models for transpiration estimates and the roles of soil water condition and air temperature functions in the transpiration modelling at different temporal scales were compared and tested comprehensively in the following section. The ″direct″ models gave better simulations than the Penman-Monteith method. Influence of both soil water condition and air temperature functions on transpiration modelling was more prominent at daily scale than hourly scale. At hourly scale, inclusion of a temperature function had negative impacts on transpiration modelling in autumn, positive impacts in spring and little impacts in summer; the influence of soil water condition function was stronger in autumn than in spring. Results indicated that for hourly transpiration modelling soil water condition and temperature functions can be omitted under wet and sunny periods when soil water is sufficient for vegetation transpiration. Parameters in each model varied across different time scales, calling

for attention to model applicability across various temporal scales. The major advantage of the 'direct' models is the simplicity in terms of measurements and parameter calibration. This allows for wide applications, for instance, replacing the current transpiration calculation scheme in land surface models, with increased computing efficiency and limited sacrifice of accuracy.

Reviewing the literature concerning the application of sap flow techniques for transpiration estimates at different spatial scales, we realised that the sapwood area is crucial for scaling the sap flow measurements on individual trees to large spatial scale such as catchment scale. In the third section of the thesis, we detailed the application of a newly developed geophysics based technique for tree cross-section water content mapping and quantification of sapwood width, which is one of the most common tree properties to extend sap flow measurements from individual trees to catchment scale transpiration. This technique has potential to determine preferential flow paths in trees and to quantify the diurnal and seasonal water storage change in trees by measuring multi-level tree electrical resistivity at different time in a day and in different seasons. Application of this technique is able to improve sap flow estimation in long term study compared to the one-off measurements of sapwood width at the end of sap flow measurement period using the traditional methods.

Due to topographic effects, difference in energy loading and hydrometeorology on contrasting slopes leads to differentiation of soil development, nutrient availability and vegetation distribution, which in turn will alter the topographic conditions in long term. The fourth part of this thesis is among the first to assess the tree water use and its response to environmental conditions on contrasting hill slopes. Transpiration on the north facing slope was higher than that on the south facing slope in winter and spring, but lower in summer and autumn, due to both energy allocation and water availability. Interestingly, the total transpiration during the study period on both slopes was similar. The result was also supported by a parallel study using the Maximum Entropy Production method for evaporation and transpiration estimation. Transpiration corresponded to soil water content differently on the two slopes, but similarly to vapour pressure deficit and solar radiation. Transpiration was controlled mainly by water availability in summer and autumn and by demand in winter and spring. Trees on NFS suffered longer water stress than trees on SFS when soil water content fell below the critical point. Understanding of the vegetation-topography-hydrology interactions will help clarify the role of vegetation in catchment water balance.

Last, when it comes to very large spatial scale, especially when there are not enough ground truth data; it can become difficult to carry out the water balance study. In this case, satellite data

can be a very useful and efficient source. In the last part of the thesis, we used remote sensing data for precipitation, evapotranspiration and terrestrial water storage change to examine the closure of water balance equation in continental Australia. We found in some regions in the Australian outback, it is quite possible to match the water budges under certain terrestrial hydrologic and climatic conditions. This provides the opportunity to improve water resources management in the data scarcity regions with the help of remote sensing data.

6.2. Future research interests

This thesis assessed the responses of transpiration to environmental variables including air temperature, vapour pressure deficit, solar radiation, plant stem water potential and volumetric soil water content, based on field measurements and optimization modelling. However, transpiration from vegetation is not only influenced by the factors discussed in this thesis, but also other important variables, for example, carbon dioxide concentration in the atmosphere (Leuning, 1995), and nutrients availability in the soil (Li et al., 2009). These factors are equally critical for trees to grow compared to the factors discussed, and should certainly be considered comprehensively. In addition, this thesis was mainly based on measurements on individual trees and in small plots, to make the research more meaningful for water resources management and policy making, it is necessary and important to extend knowledge to large spatial scales such as the ecosystem level, to enhance the understanding of the trade-offs between different components of the ecosystems.

In the context of global climate change, there is evidence for greenhouse gases enrichment in the atmosphere especially the carbon dioxide (Canadell et al., 2007; Solomon et al., 2009). Climate change has strong influences on terrestrial water and carbon cycles (Reichstein et al., 2013; Zeri et al., 2014), and has led to prolonged growing season (Menzel and Fabian, 1999) and vegetation mortality (McDowell et al., 2013). The effects and feedbacks between climate and vegetation can be considered as regulated by stomatal behaviour in the transpiration, photosynthesis and respiration processes (Figure 6.1). However, stomatal conductance and water use efficiency at leaf level usually vary with species and climate conditions, the study on coupled water-carbon cycle should emphasize on ecosystem instead of individual trees or species. The key issue is the physiological and physical understanding of water-carbon balance within and between ecosystems.
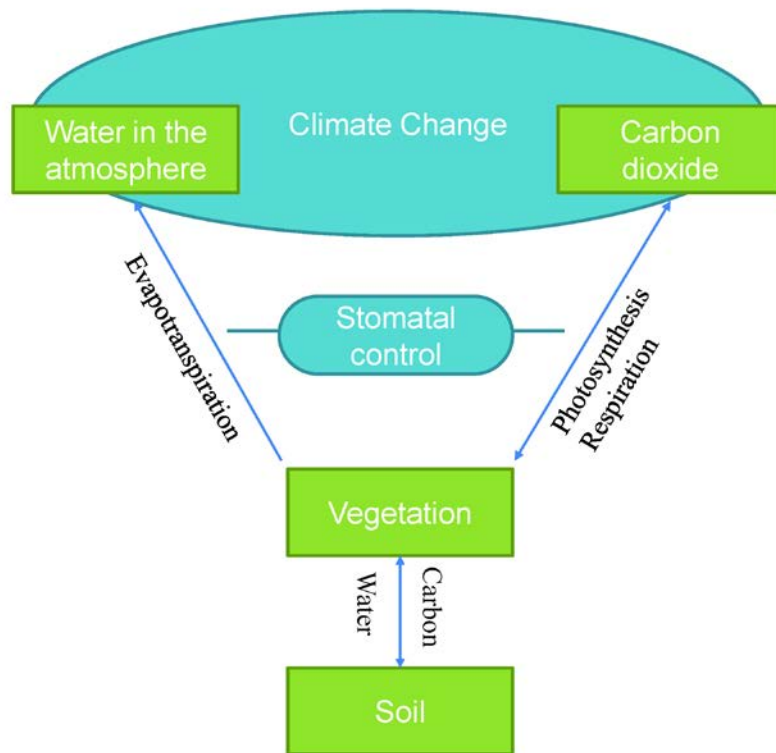
Figure 6.1 Simplified conceptualization of water and carbon coupling joined by stomatal behaviour

The abundant availability of remote sensing products, the integrated Eddy Covariance tower networks and the competent land surface, climate and biosphere models provide this age a great opportunity to explore the interactions between climate and vegetation in the earth systems. There are increasing research interests in the climate change (particularly the extreme events such as droughts, heatwaves and floods) impacts on ecohydrological process, for example the vegetation water use efficiency, mortality and productivity. Application of these data will boost the research and thus enhance our understanding of mechanisms of climate controls on ecosystem or vice versa.

As follow-ups of my thesis, I would be interested in doing the corresponding projects below. Note, these are only general ideas and personal opinions, and more specific research questions should come out.

[1] Vegetation water use and its interplay with main environmental drivers including carbon dioxide at different tempo-spatial scales

[2] Constraints of nutrients in soil on the vegetation growth and water use (efficiency)

[3] Coupled water-carbon balance study for different ecosystems within a distinctive climate

gradient (precipitation and temperature)

[4] Impacts of extreme climate events especially droughts on vegetation water use efficiency, productivity and mortality for different ecosystems and climate zones

6.3. References

Canadell, J.G., Le Quere, C., Raupach, M.R., Field, C.B., Buitenhuis, E.T., Ciais, P., Conway, T.J., Gillett, N.P., Houghton, R.A. and Marland, G., 2007. Contributions to accelerating atmospheric CO(2) growth from economic activity, carbon intensity, and efficiency of natural sinks. Proceedings of the National Academy of Sciences of the United States of America, 104(47): 18866-18870.

Leuning, R., 1995. A Critical-Appraisal of A Combined Stomatal-photosynthesis Model for C-3 Plants. Plant Cell and Environment, 18(4): 339-355.

Li, S.X., Wang, Z.H., Malhi, S.S., Li, S.Q., Gao, Y.J. and Tian, X.H., 2009. Nutrient and water management effects on crop production, and nutrient and water use efficiency in dryland areas of china. In: D.L. Sparks (Editor), Advances in Agronomy, Vol 102. Advances in Agronomy. Elsevier Academic Press Inc, San Diego, pp. 223-265.

McDowell, N.G., Fisher, R.A., Xu, C.G., Domec, J.C., Holtta, T., Mackay, D.S., Sperry, J.S., Boutz, A., Dickman, L., Gehres, N., Limousin, J.M., Macalady, A., Martinez-Vilalta, J., Mencuccini, M., Plaut, J.A., Ogee, J., Pangle, R.E., Rasse, D.P., Ryan, M.G., Sevanto, S., Waring, R.H., Williams, A.P., Yepez, E.A. and Pockman, W.T., 2013. Evaluating theories of drought-induced vegetation mortality using a multimodel-experiment framework. New Phytologist, 200(2): 304-321.

Menzel, A. and Fabian, P., 1999. Growing season extended in Europe. Nature, 397(6721): 659-659.

Reichstein, M., Bahn, M., Ciais, P., Frank, D., Mahecha, M.D., Seneviratne, S.I., Zscheischler, J., Beer, C., Buchmann, N., Frank, D.C., Papale, D., Rammig, A., Smith, P., Thonicke, K., van der Velde, M., Vicca, S., Walz, A. and Wattenbach, M., 2013. Climate extremes and the carbon cycle. Nature, 500(7462): 287-295.

Solomon, S., Plattner, G.K., Knutti, R. and Friedlingstein, P., 2009. Irreversible climate change due to carbon dioxide emissions. Proceedings of the National Academy of Sciences of the United States of America, 106(6): 1704-1709.

Zeri, M., Sa, L.D.A., Manzi, A.O., Araujo, A.C., Aguiar, R.G., von Randow, C., Sampaio, G., Cardoso, F.L. and Nobre, C.A., 2014. Variability of Carbon and Water Fluxes Following Climate Extremes over a Tropical Forest in Southwestern Amazonia. Plos One, 9(2).

Appendix: Examination of water budget using satellite products over Australia

A.1. Introduction

Quantification of water balance components over large regions is key in the investigation of water resources availability, the prediction of extreme hydrologic events and the understanding of land surface-atmosphere interactions (Sheffield et al., 2009). The general form of the water balance equation for a basin or a controlled volume is given as:

$$\Delta S = P - ET - Q , \qquad (A\text{-}1)$$

where ΔS is change in water storage, P is precipitation, ET is evapotranspiration, and Q is net runoff.

The conventional way to obtain the water balance terms is to establish ground-based measurement networks, as some developed countries have done, providing continuous estimates (Finnigan and Leuning, 2000; Sellers et al., 1992). However, in other parts of the world, ground truth data are still scarce (Swenson and Wahr, 2009). Some components of the water balance, such as evapotranspiration, are more problematic to measure over a large spatial range (Farahani et al., 2007; Rodell et al., 2004); and the heterogeneity of land cover and its consequent variability in land surface processes (Giorgi and Avissar, 1997) becomes an obstacle to the use of point-scale data for water resources assessments (Pan and Wood, 2006). Furthermore, calculating water balances at the regional and larger scales from ground-based measurements remains challenging due to the aggregation of error and inaccuracies (Allen et al., 2011; Sheffield et al., 2009), arising from their usually limited spatial representativeness.

Retrieval of water balance components from satellite observations can overcome the limited spatial coverage and representativeness issue of field measurements for large scale applications. Moreover, satellite products can provide ample spatial and temporal coverage data (Gowda et al., 2008; McCabe et al., 2008; Schultz and Engman, 2001) where no ground-measurements exist.

The increasing availability of satellite products provides opportunities to examine the water budgets and the different components of the water balance at the regional and continental scales. The idea of investigating water budget from space has already been explored in the literature (examples in Table A- 1) especially after the launching of the GRACE satellites in 2002. However, the majority of these studies were conducted in the northern hemisphere at the river

basin scale and under different climatic conditions from those of the arid Australian outback. Although a few studies in Australia focused on the Murray Darling basin, they may not entirely reflect the hydrology of the central and western part of the continent. On the other hand, these studies showed the difficulty of closing the water balance equation due to a number of factors such as data uncertainties, and temporal and spatial resolution mismatch between products. Another possible reason for the non-closure of the water budget in previous studies using GRACE data may lie in the way that GRACE satellites measure the Earth gravity change. GRACE data are integrated measure of the mass changes resulting from vertically transferred precipitation, evapotranspiration, and horizontally transferred stream and groundwater flow. Land surface modeling trying to reconcile the water balance in some of these studies such as Sheffield et al. (2009) and Gao et al. (2010) nevertheless was unable to account for groundwater flow between the grid cells of the model domain. For the same reason, the observed streamflow cannot adequately capture the subsurface water movement either.

Table A- 1 Remote sensing related water balance studies in recent years. For the abbreviations in the table refer to the reference sources in the last column. Note this is not a full list of studies, refer to the text for more.

Study area	Data sources				Reference
	P	*ET*	*Q*	*ΔS*	
Mississippi river basin	CMAP; GDAS	GLDAS/Noah; ECMWF; GDAS	gauging	GRACE	*Rodell et al. (2004)*
16 global river basins	GPCC	WGHM; LAD; GLDAS; ORCHIDEE	WGHM; LAD	GRACE	*Ramillien et al. (2006)*
southwestern United States	TRMM 3B42	SEBS + MODIS		AMSR-E for Soil Moisture	*McCabe et al.(2008)*
Murray Darling Basin, Australia	SILO (gauge-interpolated)	AVHRR; MODIS	-	-	*Guerschman et al. (2008)*
Mississippi river basin	TRMM 3B42RT; CMORPH	PM + MODIS;VIC; NARR	gauging	GRACE VIC simulated	*Sheffield et al. (2009)*
Lake Victoria, East Africa	TRMM 3B43	Multi-sensors including MODIS	gauging	GRACE	*Swenson and Wahr, (2009)*
pan-Arctic basin and Alaska	GPCP;GPCC	PM + AVHRR, MODIS, NASA/GEWEX	ArcticRIMS HYDAT GRDC	-	*Zhang et al. (2009)*
nine major river basins in US	CMORPH PERSIANN TRMM-3B42RT gauging	PM + MODIS; VIC	gauging	GRACE VIC simulated	*Gao et al. (2010)*
ten global river basins (including *MDB, Australia*)	GPCP; TRMM 3B42RT; CMORPH; PERSIANN	PM + MODIS, ISCCP PT + MODIS SEBS + MODIS	GRDC	GRACE	*Sahoo et al. (2011)*
Australia	SILO	AWRA	AWRA	GRACE AWRA	*van Dijk et al. (2011)*
seven global river basins	TMPA 3B42; ECMWF; CMAP	GLDAS; NLDAS;	GRDC	GRACE	*Rodell et al. (2011)*
Australia	TRMM 3B43	WGHM; GLDAS	gauging	GRACE; WGHM; GLDAS	*Awange et al. (2011)*

Many studies in Australia have discussed the application of remote sensing data in large scale hydrological studies. For instance, Guerschman et al. (2009) used MODIS and interpolated meteorological data to estimate actual *ET* across Australia, and then calculated the water budget by subtracting *ET* from precipitation. Evans (2009) evaluated the water balance in the Murray-Darling basin using the WRF model (Weather Research and Forecasting). King et al. (2009) introduced the capability of a water balance model based system for the delivery of weekly estimates of soil moisture storage and water fluxes at the continental scale over Australia. Glenn et al. (2011) reviewed various methods for *ET* estimation in Australian context, particularly different remote sensing techniques and water balance models. Furthermore, there are two distinguished operational systems: the Australian Water Availability Project (AWAP) (Raupach et al., 2009), and the Australian Water Resources Assessment (AWRA) system (van Dijk, 2010; van Dijk and Warren, 2010), both of which combine the ground based measurements and

satellite products, aiming at estimating soil moisture and other components of the water balance at multiple spatial and temporal scales across the whole country. Comparison of the two systems for *ET* estimation is available in King et al. (2011). We noticed that these studies combined ground based observations with satellite products to improve the water/energy/carbon fluxes estimation, while not much work examines the water budget with the emphasis on satellite products alone. It is worth exploring whether the similar spatial-temporal patterns can be reproduced comparable to the results using more comprehensive data.

In large regions of the Australian continent many rivers are ephemeral with rapid rise and decline in river level, low runoff coefficient and extended dry periods (Croke and Jakeman, 2001). In addition, limited precipitation, relatively flat topography (Australian Bureau of Statistics, 2012), and high transmission losses of rivers (Lloyd and Jacobson, 1987) result in very little or no streamflow in vast inland areas. Runoff data from both UNH/GRDC (University of New Hampshire/Global Runoff Data Center) (Fekete et al., 2002), http://www.compositerunoff.sr.unh.edu/) and AWAP (Raupach et al., 2009, http://www.csiro.au/awap/) provide evidence of little streamflow in many Australian regions. Furthermore, Rodell et al. (2004; 2011) suggested that in large basins considering the small ratio of perimeter to area and the slow movement of groundwater relative to surface water, the error of water balance examining associated with net groundwater flow should be small. Following this assumption and considering the context of Australian streamflow, we simplified the water balance equation to:

$$\Delta S = P - ET .$$
(A-2)

for areas where horizontal water transfer (surface runoff and groundwater flow) is minimal. When the assumption holds, both sides of the equation calculated from the satellite products should be comparable if the satellite products are reliable. Thus, equation (A-2) can be used to examine the consistency of data in use. However, if the horizontal water transfer is significant, the two sides of the equation would be imbalanced. Thus, equation (A-2) can also be used to examine whether the horizontal water transfer contributes to or depletes the water storage.

In hydrological studies, satellite products are widely used to assist in the interpolation of ground-based measurements (Journée and Bertrand, 2010), to serve as inputs for land surface and atmosphere models (Cheng et al., 2008) and to verify modeling results (Niu et al., 2007). In evaluating land surface modeling results in regions with limited or no ground-truth data, it is important to determine a proper time and spatial scale to obtain reasonable results. Therefore,

based on the simplified water balance (equation A-2), in this study we aim to (1) examine the large scale water balance over Australia using readily available satellite products for each component in equation (A-2); and (2) find the locations and time scales at which the water balance calculated from these satellite products is most consistent.

A.2. Data and Methods

A.2.1. Datasets description

There are many satellite data sources for each water component. The datasets we chose for this study (Table A- 2) are the ones that are easy to access, and more frequently discussed in the literature in terms of validation efforts and other applications, hence, widely used. Other data sources such as some described in Table A- 1 and cited above are acknowledged but not discussed, considering that comparison of different data sources is beyond the objectives of this study.

Table A- 2 Satellite products used in this study from 12/2002 to 01/2011

	Product	Resolution	Missing Period	Data Source
P	TMPA 3B43 V6	1°, monthly	-	NASA. http://disc2.nascom.nasa.gov/Giovanni/tovas/TRMM_V6.3B43.2.shtml
ET	MODIS_MOD 16	1km, monthly	-	University of Montana. http://ntsg.umt.edu/project/mod16#data-product
ΔS	GRACE	1°, monthly	06/2003 01/2011	Jet Propulsion Laboratory (JPL). ftp://podaac-ftp.jpl.nasa.gov/allData/tellus/L3/land_mass/RL05/ascii

TRMM Multi-Satellite Precipitation Analysis (TMPA) 3B43 combines the multiple independent estimates precipitation data (i.e. 3B42) and the Climate Anomaly Monitoring System (CAMS) global gridded rain gauge data, produced by NOAA's Climate Prediction Center and/or the global rain gauge product produced by the Global Precipitation Climatology Center (GPCC) (Huffman et al., 1997; Huffman et al., 2007). Validation of TMPA 3B43 and other TRMM precipitation products has been carried out worldwide (e.g. Greece (Feidas, 2010); Thailand (Chokngamwong and Chiu, 2008); Africa (Adeyewa and Nakamura, 2003); and Australia (Ebert et al., 2007; Fleming et al., 2011; Peña-Arancibia et al., 2013)). In Australia, much work has explored the production of gridded precipitation data by blending TRMM products with gauging data (Chappell et al., 2012; Chappell et al., 2013; Li and Shao, 2010; Oke et al., 2009).

Evapotranspiration is one of the most difficult hydrological variables to obtain, and global products are not as numerous as precipitation. The MOD16 *ET* is estimated with an algorithm

that uses MODIS products and GMAO (Global Meteorological Assimilation Office) climate data to solve the Penman-Monteith equation (Mu et al., 2011). MOD16 *ET* is the sum of daytime and nighttime evaporation from wet soil and canopy surfaces and transpiration from vegetation. The algorithm was evaluated against eddy covariance tower data over a winter wheat field in North China Plain (Sun et al., 2007), and MOD16 *ET* data were validated at 17 eddy covariance tower locations distributed in Asia, with the two datasets showing good agreement (Kim et al., 2012). *ET* estimates based on this algorithm are comparable to Variable Infiltration Capacity model (Liang et al., 1994) simulated *ET* (Sheffield et al., 2009). These results prove that MOD16 can provide reasonable *ET* estimations over large areas.

GRACE provides gravity anomaly data that can be used to infer water storage on Earth. Although the coarse resolution of GRACE data (monthly and 1°) limits their application for water resources assessment in small regions, the data are still able to reflect the hydrological signals (Awange et al., 2009) and does provide useful information for water resources management at larger scales. GRACE data have been widely used to validate modeling results of terrestrial water storage change (Rodell and Famiglietti, 2001; van Dijk et al., 2011), soil moisture variations (Niu et al., 2007), and groundwater table fluctuations (Henry et al., 2011). GRACE data have also been incorporated to assist in parameterization and model performance improvement (Zaitchik et al., 2008).

We retrieve three satellite products at a monthly scale from 12/2002 to 01/2011, and aggregate them into seasonal and annual datasets, resulting in 32 seasons and 8 years. GRACE data are missing in 06/2003 and 01/2011, and filled with average values calculated using the data from a month before and a month after. MOD16 *ET* data are re-sampled to 1° resolution using the nearest neighbor method via the MODIS Re-projection Tool (Dwyer and Schmidt, 2006).

A.2.2. Methods

Each GRACE monthly grid (*G* below) represents the mass anomaly, that is, the difference in the masses for that month (*m*) and the average over 01/2004 to 12/2009 ($\overline{m}$) (http://grace.jpl.nasa.gov/data/gracemonthlymassgridsland/).   This   can   be   expressed mathematically as:

$$G_{j} = m_{j} - \overline{m} . \qquad \text{(A-3)}$$

$$G_{j+1} = m_{j+1} - \overline{m} . \qquad \text{(A-4)}$$

where the subscript j stands for the jth month. Thus, by subtracting equation (A-3) from equation (A-4), the difference of GRACE data in two successive months is equivalent to the water storage change (Δm) at a monthly interval as follows:

$$\Delta m_j = m_{j+1} - m_j = G_{j+1} - G_j \ . \tag{A-5}$$

GRACE measurements do not cover all days in each nominal month (for details about missing days refer to http://gracetellus.jpl.nasa.gov/data/GraceMonths), hence the data may not reflect the effect of rainfall and evapotranspiration on gravity change during these days. If we assume the water storage at the start of month j is $S_{j,s}$ and at the end of next month j+1 is $S_{j+1,e}$; the cumulative precipitation and evapotranspiration in these two months are P_j, P_{j+1} and ET_j, ET_{j+1} respectively, then storage change in these two consecutive months ($S_{j+1,e}$-$S_{j,s}$) should equal (P_j+P_{j+1})-(ET_j+ET_{j+1}) based on equation (A-2). In order to minimize the effect of time mismatch of the three datasets and make the components comparable at monthly step, we use the monthly average of (P_j+P_{j+1})-(ET_j+ET_{j+1}) to account for their contribution to the mass change:

$$\Delta w_j = \frac{P_{j+1} + P_j}{2} - \frac{ET_{j+1} + ET_j}{2} . \tag{A-6}$$

For areas where equation (A-2) applies, Δw provides a reasonable approximation of Δm, refer to Rodell et al. (2004; 2011) for a more detailed explanation. For these areas, the discrepancy between the two quantities indicates inconsistencies and errors among the three remote sensing products. For example, in areas where runoff occurs in large quantities, such as northern and eastern coastal regions of Australia, Δw should be theoretically larger than Δm. Note, however, that the difference between Δw and Δm includes both surface and subsurface runoff. To remove potential errors in the analysis due to significant amounts of runoff, we mask out the areas where annual runoff is more than 10 mm based on UNH/GRDC composite runoff data. On top of this, the satellite data are analyzed based upon three metrics for comparison: residual of the simplified water balance equation (Δ), precipitation-normalized absolute residual (β), and correlation coefficient (r) between Δw and Δm:

$$\Delta_{ij} = \Delta w_{ij} - \Delta m_{ij} , \tag{A-7}$$

$$\beta_{ij} = \frac{1}{n}\sum_{j=1}^{n}\frac{|\Delta_{ij}|}{P_i} , \tag{A-8}$$

$$P_i = \frac{1}{n}\sum_{j=1}^{n} P_{ij} \, , \qquad\qquad\qquad (A\text{-}9)$$

$$r_i = \frac{\sum\limits_{j=1}^{n}\left[(\Delta m_{ij} - \frac{1}{n}\sum\limits_{j=1}^{n}\Delta m_{ij})(\Delta w_{ij} - \frac{1}{n}\sum\limits_{j=1}^{n}\Delta w_{ij})\right]}{\sqrt{\sum\limits_{j=1}^{n}(\Delta m_{ij} - \frac{1}{n}\sum\limits_{j=1}^{n}\Delta m_{ij})^2 \cdot \sum\limits_{j=1}^{n}(\Delta w_{ij} - \frac{1}{n}\sum\limits_{j=1}^{n}\Delta w_{ij})^2}} \, , \qquad (A\text{-}10)$$

where i is the ith grid cell (pixel), j is the jth month/season/year, and n is the total number of months/seasons/years. In this study besides the data error, the signs (+/-) of residuals (Δ) reflect the net water flow directions based on the water balance equation in the following manner: positive values indicate net water flowing out of the relevant pixels and negative values indicate net water flowing into the pixels from their neighbours.

A.3. Results and discussion

A.3.1. Water budget over runoff-limited regions

Mean and median values of Δw, Δm, Δ, and correlation coefficients (r) are calculated for all the locations with mean annual surface runoff less than 10 mm, and given in Table A- 3. The overall average residuals for monthly, seasonal and annual time scales are 7.6, 22.6 and 90.4 mm; the median values are 5.2, 16.6 and 66.4 mm respectively; and the correlation coefficients between Δw and Δm are 0.58, 0.73 and 0.50 for the three time scales. GRACE inferred water storage change (Δm) is smaller than Δw at all time-scales because of the existence of runoff flowing out of the region. Theoretically, the residual is a combination of the integrated error of the three products in the form of equation (A-7) and the net water flowing out of (or into, for negative values) this region through surface and/or subsurface. Knowledge of one will help to evaluate the other.

Table A- 3 Statistics for comparison of water balance components over areas of $Q < 10$ mm/year

	Δm (mm)		Δw (mm)		Δ (mm)		Correlation Coefficient between Δw and Δm
	mean	median	mean	median	mean	median	
Monthly	0.6	0.3	8.4	5.3	7.6	5.2	0.58
Seasonal	0.6	0.0	23.7	15.1	22.6	16.6	0.73
Annual	2.2	0.2	94.8	60.3	90.4	66.4	0.50

Spatially, the monthly, seasonal and annual residuals show the same pattern, but with different amplitudes due to the method employed to obtain seasonal and annual estimates from monthly data; therefore, only monthly residuals are demonstrated in Figure A. 1. The distribution coincides with the annual precipitation and runoff patterns. Larger positive residuals appear in

98

the northern and eastern areas; smaller residuals, which imply that three datasets close the water balance equation better, appear in the central part of Western Australia, where rainfall amounts to 300-400 mm annually, the average aridity index (potential *ET* over *P*) is close to 15 (Figure A. 2*a*), and the elevation is high but relief is low (Figure A. 2*b*). Lake Eyre Basin in the Central Lowlands shows more negative values, suggesting that these areas receive water from neighbouring locations.
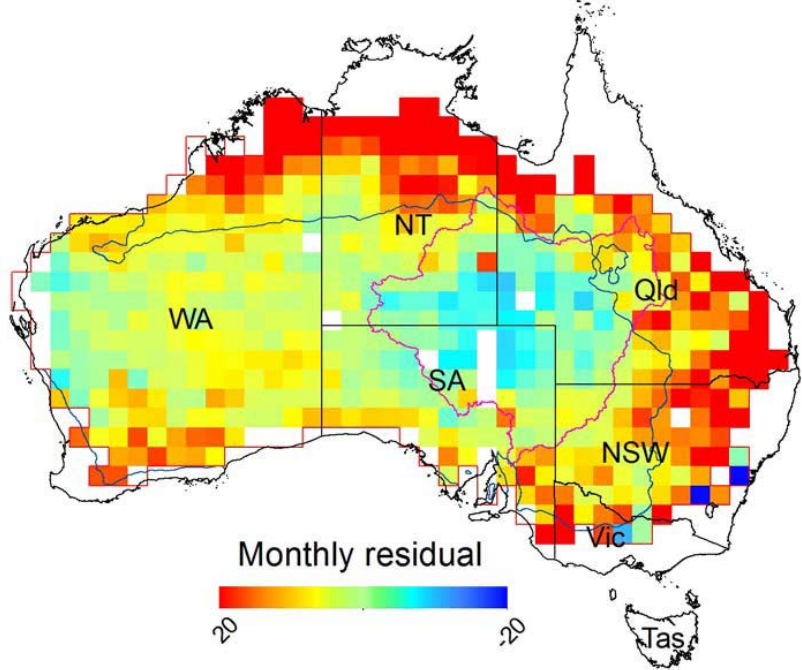
Figure A. 1 Spatial distribution of monthly difference (Δ) between Δ*w* and Δ*m* over areas with *Q*<10mm/year (red boundary). Seasonal and annual residuals share the same spatial pattern with monthly data, and are not shown in this paper. WA-Western Australia; NT-Northern Territory; SA-South Australia; Qld-Queensland; NSW-New South Wales; Vic-Victoria; Tas-Tasmania. White color corresponds to no data. Black, blue and pink lines are boundaries of states, rainfall-limited region and Lake Eyre Basin respectively. Scale bar is in mm.

Figure A. 2 (a) Rainfall distribution and index of aridity (*ET_P/P*, data are from MOD16 and TRMM,

respectively). Labels and curves in the map are the 30-year mean annual rainfall in corresponding regions (in mm/year. data is from Bureau of Meteorology, Australia). (b) DEM overlaid with hill shades (from GMTED2010 30sec data). Pink line is boundary of Lake Eyre Basin. Scale bar for DEM is in meter above sea level.

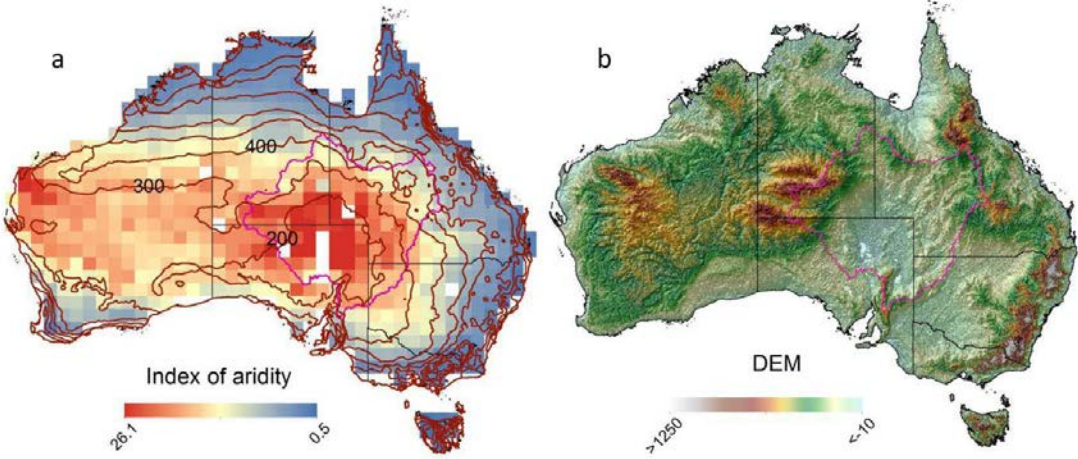To examine the relationship between the water balance residual and each component, we plotted them at three time scales over the whole runoff-limited region in Figure A. 3. The analysis shows that the residuals are better correlated with *P* than with *ET* and Δ*S,* which is consistent with previous studies (Sahoo et al., 2011; Sheffield et al., 2009). It should be noted that it is not necessarily true that the three datasets are inconsistent and inappropriate for water budget studies for areas with large residuals, because the non-closure may be ascribed to runoff due to large amount of rainfall in those areas. Therefore, we use the index *β* in equation (A-8) to examine the residuals in relation to precipitation (Figure A. 4). The index increases as time scale decreases. At the annual scale this runoff-limited region shows very small *β* values except in the locations near Lake Eyre, where *β* is around 1.0. At the seasonal scale, the values increase slightly, but in most areas are still smaller than 1.0. At the monthly scale, however, we find that larger values extend to cover most areas, particularly in the west and central-south locations. In the lower Lake Eyre Basin, the *β* values are consistently large at all time-scales. This may reflect the effects of net water inflow to the basin.
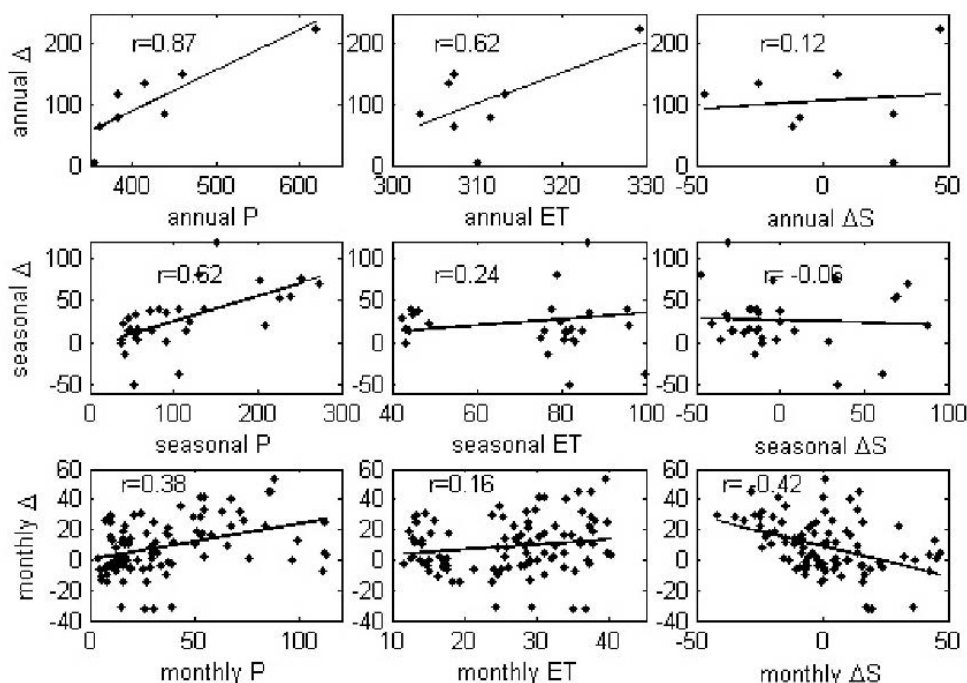

Figure A. 3 Relation between residuals and precipitation, evapotranspiration and storage change at three time scales over runoff-limited regions. Lines in figures are linearly fitted between each two variables. Units of both axes are mm.
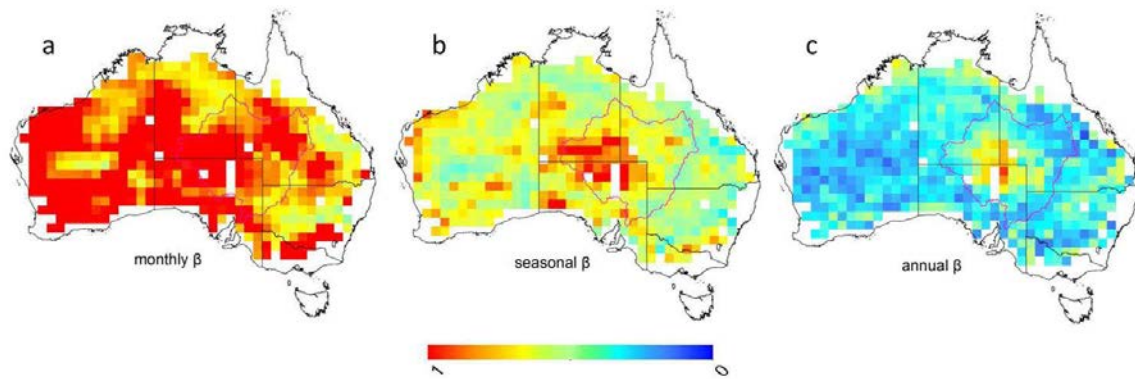
Figure A. 4 Precipitation-normalized absolute residuals for monthly, seasonal and annual time scales ($|\Delta|/P$, dimensionless). Pink line in the map shows the boundary of Lake Eyre Basin. White color corresponds to no data.

Correlation coefficients of the monthly, seasonal and annual Δw and Δm for each pixel are shown in Figure A. 5. Monthly and seasonal correlation coefficients share the same spatial pattern. They decrease from north (monthly $r > 0.6$ and seasonal $r > 0.9$) to south. The smaller correlation coefficients appear in South Australia and New South Wales. At the annual scale, the centers of high correlation coefficients evolve southwardly in the west, east and southeast. The correlation coefficients are persistently lower in the northwestern part of South Australia at all time-scales, where the western part of Lake Eyre is located with relatively large slopes (Figure A. 2*b*). A study on the relation between *P* and surface mass changes (*SMCs*, from GRACE) (Rieser et al., 2010) gave a similar spatial pattern of correlation coefficients, and suggested that it generally takes about 1-2 months for a GRACE observation to detect preceding precipitation events, and even longer (e.g. up to four months) in low correlated areas. One possibility for this low correlated behaviour may be due to the fact that the water storage changes inferred by GRACE at a pixel are not only contributed by *P* and *ET*, but also by water moving into that pixel laterally from surrounding pixels through surface and/or subsurface flow. In other words, TRMM and MODIS detect the vertical water transfer on Earth, but GRACE reflects the integrated vertical and horizontal water movements. This could cause the asynchronous temporal variation of Δw and Δm.
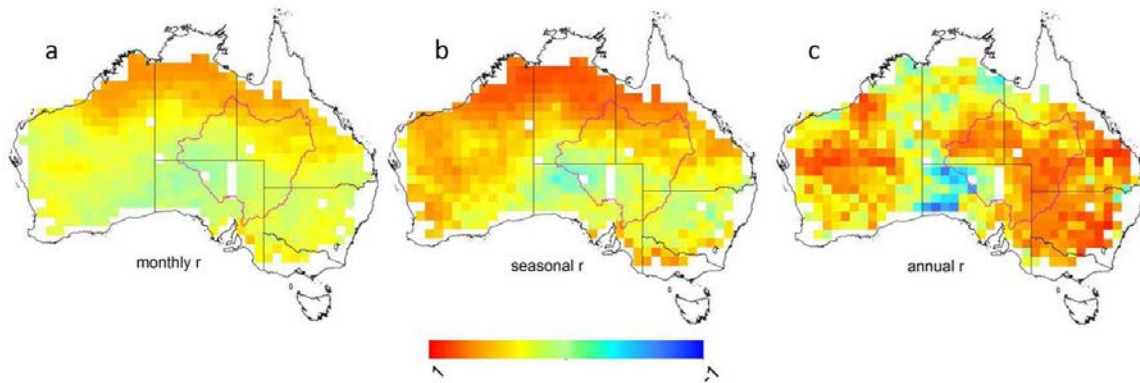
Figure A. 5 Correlation coefficients between Δw and Δm at different time scales (97 months, 32 seasons, 8 years). Pink line shows the boundary of Lake Eyre Basin. White color corresponds to no data.

The preceding analyses demonstrate that water budgets derived from remote sensing products show better closure and consistency in central areas of Western Australia. Regarding the effect of time scales on the water budget residuals, in central areas of Western Australia the correlation coefficients increase and the correlation of residuals with precipitation decreases from monthly to annual time scales. Therefore, only seasonal and annual time scales should be considered for water budget studies using the methods proposed in this work. Nevertheless, due to the seasonality of some terms in the water balance equation, annual scale may be too long to be useful for water resources management purposes (Pearson, 2008).

A.3.2. Water budget in rainfall-limited regions and its implications

Data in the regions of $P<400$ mm/year is extracted and analyzed for each austral season (summer: Dec-Jan-Feb; autumn: Mar-Apr-May; winter: Jun-Jul-Aug; spring: Sep-Oct-Nov). Similarly, mean and median values of Δw, Δm, Δ and r for each time scale are calculated and given in Table A- 4. Temporally, mean values of Δw and Δm over the entire rainfall-limited region are calculated for each season from austral summer 2003 (comprised of Dec 2002 and Jan, Feb 2003), and seasonal time series plots of the two quantities are given in Figure A. 6, showing a correlation coefficient of 0.38, about half the correlation coefficient (0.73) over the $Q<10$mm/year region. Δw and Δm follow the same temporal trend most of the time, except during the year 2008 to 2009 when a severe drought occurred (Leblanc et al., 2009; McGrath et al., 2012), slowing down the temporal response of storage change to rainfall events.

Table A- 4 Statistical indices for comparison of water balance components over areas of $P<400$mm/year

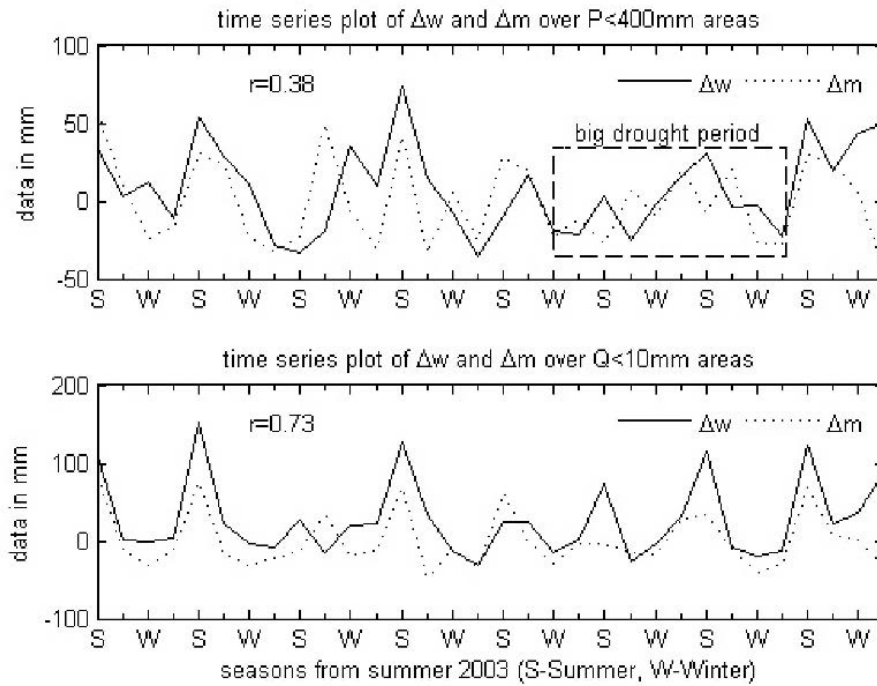|	Δm (mm)		Δw (mm)		Δ (mm)		Correlation Coefficient between Δw and Δm
	mean	median	mean	median	mean	median	
Monthly	0.2	0.1	2.9	2.6	2.8	2.5	0.29
Seasonal	-0.4	-0.2	7.7	7.3	8.6	7.8	0.38
Annual	-1.8	-0.9	30.7	29.2	34.2	31.4	0.39

Figure A. 6 Time series plots of Δ*w* and Δ*m* over 32 seasons for rainfall limited regions (top) and runoff limited regions (bottom).

Spatially, within this area distinct variations can be observed across the four seasons (Figure A. 7). Generally the western part shows a mean residual closer to zero, while the eastern part gives more negative residuals in all seasons, especially in summer and autumn within the Lake Eyre Basin (LEB). LEB is one of the world's largest internal draining systems. It receives about 200 mm annual rainfall, the least in Australia; northeast part is dominated by the monsoon (Croke et al., 1999). None of the rivers and creeks in this basin flows permanently (McMahon et al., 2008a; McMahon et al., 2008b). The mean annual water balance residual in this work for the whole LEB is -6.2 mm/year. The negative sign indicates net water inflow to the relevant area. This is consistent with the regional water flow direction in this area, as is shown in previous studies on the hydrology of the Great Artesian Basin (GAB) (Costelloe et al., 2008; Herczeg et al., 1991). Since LEB is a closed drainage basin with no external streamflow coming in from the adjacent basins, the 6.2 mm/year seems to be the maxima of groundwater inflow across the northeast basin boundary. Given that the lateral groundwater inflow to the basin is very likely smaller than 6.2 mm/year; this result also indicates that the absolute value of integrated error of the three products in terms of equation (A-7) should not exceed 6.2 mm/year. This is about 2.1% of the annual precipitation in the basin during the study period.
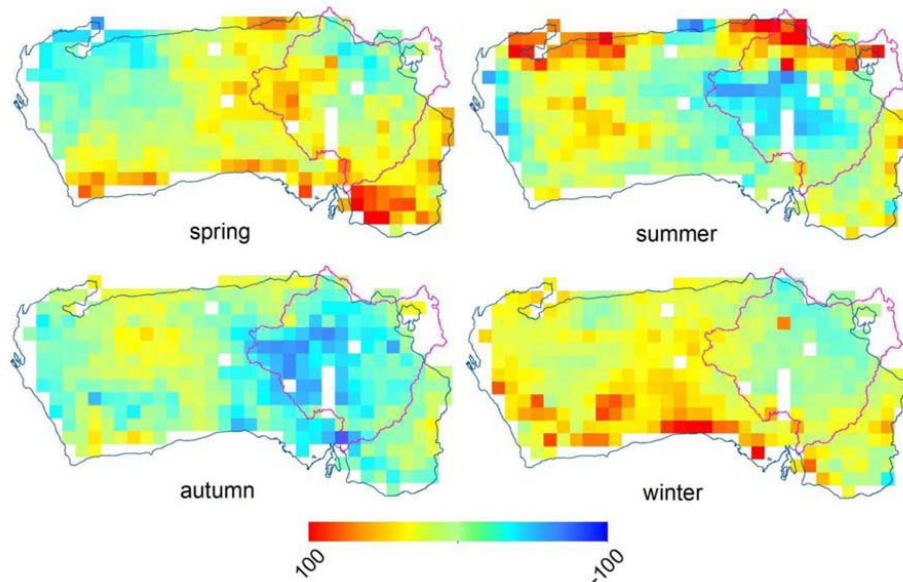
Figure A. 7 Spatial distributions of the average residuals of Δw and Δm for each season in the region of P < 400 mm/year. Pink line is the boundary of Lake Eyre Basin. White colour corresponds to no data. Scale bar is in mm.

Assuming that the integrated error of the three products relative to the annual precipitation applies to the entire Australian continent, we calculated the mean annual residual of three water balance components, which is 144.7±11.3 mm/year. This number is within the reported range of total runoff in Australia, as the mean annual rainfall during 2003-2010 was 502 mm/year (from *Annual Climate Summary Reports* by Bureau of Meteorology, http://www.bom.gov.au/climate/annual_sum/annsum.shtml); of which 10%~30% becomes runoff into rivers or recharge into groundwater aquifers (Chiew and McMahon, 2002; National Water Commission, 2007). This results in 50.2 to 150.6 mm/year during the 8-year period.

A.4. Conclusions

The relationship of three commonly used satellite products defining the water balance were investigated over Australia based on a simplified water balance equation. Our results show that depending on the time scale (i.e., seasonal or annual) and the hydro-climatology patterns of large regions, using only satellite products has the potential to close the water budget. This has been demonstrated in regions of Australia, (e.g., the central part of Western Australia) having high altitude and low relief, little annual rainfall (300-400 mm) and high aridity indices (~15), as these conditions hold the assumption of negligible runoff in the water balance calculation. More precise areas can be mapped out by setting filters on the applied indices using geographical information systems. Though the coarse temporal and spatial resolution (monthly and 1°) makes the data less informative for water resources management purposes in small regions, the consistency between the datasets can give us useful information for analysis of hydrologic

104

variations and modelling validation using these satellite products at large scales. Application of the satellite products for the water balance in Lake Eyre Basin reflects well the seasonal hydrological processes in terms of net groundwater flow, and gives a reasonable estimation of the maximum possible integrated error of the three products as well as the maximum net groundwater inflow to the basin. However, this assessment needs further verification with other methods. If the precipitation-relative maximum error can be extrapolated to the entire Australian continent, the net annual water loss through streamflow and groundwater flow into the surrounding oceans is estimated to be 144.7±11.3 mm/year, comparable to the estimate from the Australian National Water Commission and Bureau of Meteorology. Anticipated improvements in the retrieval algorithms of satellite data are expected to increase the accuracy of their products. For example, the version 7 TMPA 3B43 of rainfall products is now available and considered better than version 6 (Prakash et al., 2013). These advances are expected to improve the feasibility and accuracy of large scale water balance analyses using satellite data alone in the near future.

A.5. References

Adeyewa, Z.D. and Nakamura, K., 2003. Validation of TRMM radar rainfall data over major climatic regions in Africa. Journal of Applied Meteorology, 42(2): 331-347.

Allen, R.G., Pereira, L.S., Howell, T.A. and Jensen, M.E., 2011. Evapotranspiration information reporting: I. Factors governing measurement accuracy. Agricultural Water Management, 98(6): 899-920.

Australian Bureau of Statistics, 2012. 2012 Year Book Australia, Catalogue No. 1301.0, ABS., Canberra, Australia. pp. 71-74.

Awange, J.L., Fleming, K.M., Kuhn, M., Featherstone, W.E., Heck, B. and Anjasmara, I., 2011. On the suitability of the 4 degrees x 4 degrees GRACE mascon solutions for remote sensing Australian hydrology. Remote Sensing of Environment, 115(3): 864-875.

Awange, J.L., Sharifi, M.A., Baur, O., Keller, W., Featherstone, W.E. and Kuhn, M., 2009. GRACE Hydrological Monitoring of Australia: Current Limitations and Future Prospects. Journal of Spatial Science, 54(1): 23-36.

Chappell, A., Renzullo, L. and Haylock, M., 2012. Spatial uncertainty to determine reliable daily precipitation maps. Journal of Geophysical Research-Atmospheres, 117.

Chappell, A., Renzullo, L.J., Raupach, T.H. and Haylock, M., 2013. Evaluating geostatistical methods of blending satellite and gauge data to estimate near real-time daily rainfall for Australia. Journal of Hydrology, 493: 105-114.

Cheng, F.Y., Kim, S. and Byun, D.W., 2008. Application of high resolution land use and land cover data for atmospheric modeling in the Houston-Galveston Metropolitan area: Part II Air quality simulation results. Atmospheric Environment, 42(20): 4853-4869.

Chiew, F.H.S. and McMahon, T.A., 2002. Modelling the impacts of climate change on Australian streamflow. Hydrological Processes, 16(6): 1235-1245.

Chokngamwong, R. and Chiu, L.S., 2008. Thailand daily rainfall and comparison with TRMM products. Journal of Hydrometeorology, 9(2): 256-266.

Costelloe, J., Irvine, E., Western, A., Matic, V., Walker, J. and Tyler, M., 2008. Quantifying near-surface, diffuse groundwater discharge along the south-west margin of the Great Artesian Basin, Proceedings of Water Down Under 2008 incorporating 31st Hydrology

and Water Resources Symposium & 4th International Conference on Water Resources and Environment Research, pp. 831-840.

Croke, B.F.W. and Jakeman, A.J., 2001. Predictions in catchment hydrology: an Australian perspective. Marine and Freshwater Research, 52(1): 65-79.

Croke, J.C., Magee, J.W. and Wallensky, E.P., 1999. The role of the Australian Monsoon in the western catchment of Lake Eyre, central Australia, during the Last Interglacial. Quaternary International, 57-8: 71-80.

Dwyer, J. and Schmidt, G., 2006. The MODIS reprojection tool. Earth Science Satellite Remote Sensing: Data, Computational Processing, and Tools, Vol 2. Springer, New York, 162-177 pp.

Ebert, E.E., Janowiak, J.E. and Kidd, C., 2007. Comparison of near-real-time precipitation estimates from satellite observations and numerical models. Bulletin of the American Meteorological Society, 88(1): 47-+.

Evans, J.P., 2009. Water Balance in the Murray-Darling Basin and the recent drought as modelled with WRF. 18th World Imacs Congress and Modsim09 International Congress on Modelling and Simulation: Interfacing Modelling and Simulation with Mathematical and Computational Sciences. Univ Western Australia, Nedlands, 2790-2797 pp.

Farahani, H.J., Howell, T.A., Shuttleworth, W.J. and Bausch, W.C., 2007. Evapotranspiration: Progress in measurement and modeling in agriculture. Transactions of the Asabe, 50(5): 1627-1638.

Feidas, H., 2010. Validation of satellite rainfall products over Greece. Theoretical and Applied Climatology, 99(1-2): 193-216.

Fekete, B.M., Vörösmarty, C.J. and Grabs, W., 2002. High-resolution fields of global runoff combining observed river discharge and simulated water balances. Global Biogeochemical Cycles, 16(3): 15-1-15-10.

Finnigan, J.J. and Leuning, R., 2000. Long term Flux Measurements-Coordinate Systems and Averaging. Proceedings of the International Workshop for Advanced Flux Network and Flux Evaluation, 27-29 September 2000, Sapporo Japa, Center for Global Environmental Research, National Institute for Environmental Studies, Tsukuba, Japan.

Fleming, K., Awange, J.L., Kuhn, M. and Featherstone, W.E., 2011. Evaluating the TRMM 3B43 monthly precipitation product using gridded raingauge data over Australia. Australian Meteorological and Oceanographic Journal, 61(3): 171-184.

Gao, H.L., Tang, Q.H., Ferguson, C.R., Wood, E.F. and Lettenmaier, D.P., 2010. Estimating the water budget of major US river basins via remote sensing. International Journal of Remote Sensing, 31(14): 3955-3978.

Giorgi, F. and Avissar, R., 1997. Representation of heterogeneity effects in earth system modeling: Experience from land surface modeling. Reviews of Geophysics, 35(4): 413-437.

Glenn, E.P., Doody, T.M., Guerschman, J.P., Huete, A.R., King, E.A., McVicar, T.R., Van Dijk, A., Van Niel, T.G., Yebra, M. and Zhang, Y.Q., 2011. Actual evapotranspiration estimation by ground and remote sensing methods: the Australian experience. Hydrological Processes, 25(26): 4103-4116.

Gowda, P.H., Chavez, J.L., Colaizzi, P.D., Evett, S.R., Howell, T.A. and Tolk, J.A., 2008. ET mapping for agricultural water management: present status and challenges. Irrigation Science, 26(3): 223-237.

Guerschman, J.P., Van Dijk, A., Mattersdorf, G., Beringer, J., Hutley, L.B., Leuning, R., Pipunic, R.C. and Sherman, B.S., 2009. Scaling of potential evapotranspiration with MODIS data reproduces flux observations and catchment water balance observations across Australia. Journal of Hydrology, 369(1-2): 107-119.

Guerschman, J.P., Van Dijk A.I.J.M , McVicar T.R. , Van Niel T.G. , Li L, Liu Y and J., P.-A., 2008. Water balance estimates from satellite observations over the Murray-Darling Basin.

Henry, C.M., Allen, D.M. and Huang, J.L., 2011. Groundwater storage variability and annual recharge using well-hydrograph and GRACE satellite data. Hydrogeology Journal, 19(4): 741-755.

Herczeg, A.L., Torgersen, T., Chivas, A.R. and Habermehl, M.A., 1991. Geochemistry of ground waters from the Great Artesian Basin, Australia. Journal of Hydrology, 126(3-4): 225-245.

Huffman, G.J., Adler, R.F., Arkin, P., Chang, A., Ferraro, R., Gruber, A., Janowiak, J., McNab, A., Rudolf, B. and Schneider, U., 1997. The Global Precipitation Climatology Project (GPCP) Combined Precipitation Dataset. Bulletin of the American Meteorological Society, 78(1): 5-20.

Huffman, G.J., Adler, R.F., Bolvin, D.T., Gu, G.J., Nelkin, E.J., Bowman, K.P., Hong, Y., Stocker, E.F. and Wolff, D.B., 2007. The TRMM multisatellite precipitation analysis (TMPA): Quasi-global, multiyear, combined-sensor precipitation estimates at fine scales. Journal of Hydrometeorology, 8(1): 38-55.

Journée, M. and Bertrand, C., 2010. Improving the spatio-temporal distribution of surface solar radiation data by merging ground and satellite measurements. Remote Sensing of Environment, 114(11): 2692-2704.

Kim, H.W., Hwang, K., Mu, Q., Lee, S.O. and Choi, M., 2012. Validation of MODIS 16 global terrestrial evapotranspiration products in various climates and land cover types in Asia. Ksce Journal of Civil Engineering, 16(2): 229-238.

King, E.A., Paget, M.J., Briggs, P.R., Trudinger, C.M. and Raupach, M.R., 2009. Operational Delivery of Hydro-Meteorological Monitoring and Modeling Over the Australian Continent. Ieee Journal of Selected Topics in Applied Earth Observations and Remote Sensing, 2(4): 241-249.

King, E.A., T.G. van Niel, A.I.J.M. van Dijk, Z. Wang, M.J. Paget, T. Raupach, J. Guerschman, V. Haverd, T.R. McVicar, I. Miltenburg, M.R. Raupach, L.J. Renzullo and Zhang., Y., 2011. Actual Evapotranspiration Estimates for Australia Inter-comparison and Evaluation, Canberra, Australia.

Leblanc, M.J., Tregoning, P., Ramillien, G., Tweed, S.O. and Fakes, A., 2009. Basin-scale, integrated observations of the early 21st century multiyear drought in southeast Australia. Water Resources Research, 45.

Li, M. and Shao, Q.X., 2010. An improved statistical approach to merge satellite rainfall estimates and raingauge data. Journal of Hydrology, 385(1-4): 51-64.

Liang, X., Lettenmaier, D.P., Wood, E.F. and Burges, S.J., 1994. A Simple Hydrologically Based Model of Land-Surface Water and Energy Fluxes for General-Circulation Models. Journal of Geophysical Research-Atmospheres, 99(D7): 14415-14428.

Lloyd, J.W. and Jacobson, G., 1987. The hydrogeology of the Amadeus Basin, Central Australia. Journal of Hydrology, 93(1-2): 1-24.

McCabe, M.F., Wood, E.F., Wojcik, R., Pan, M., Sheffield, J., Gao, H. and Su, H., 2008. Hydrological consistency using multi-sensor remote sensing data for water and energy cycle studies. Remote Sensing of Environment, 112(2): 430-444.

McGrath, G.S., Sadler, R., Fleming, K., Tregoning, P., Hinz, C. and Veneklaas, E.J., 2012. Tropical cyclones and the ecohydrology of Australia's recent continental-scale drought. Geophysical Research Letters, 39: 1-6.

McMahon, T.A., Murphy, R.E., Peel, M.C., Costelloe, J.F. and Chiew, F.H.S., 2008a. Understanding the surface hydrology of the Lake Eyre Basin: Part 1 - Rainfall. Journal of Arid Environments, 72(10): 1853-1868.

McMahon, T.A., Murphy, R.E., Peel, M.C., Costelloe, J.F. and Chiew, F.H.S., 2008b. Understanding the surface hydrology of the Lake Eyre Basin: Part 2 - Streamflow. Journal of Arid Environments, 72(10): 1869-1886.

Mu, Q.Z., Zhao, M.S. and Running, S.W., 2011. Improvements to a MODIS global terrestrial evapotranspiration algorithm. Remote Sensing of Environment, 115(8): 1781-1800.

National Water Commission, 2007. Australian Water Resources 2005 - A baseline assessment of water resources for the National Water Initiative, National Water Commission, Canberra, Australia. pp. 17-22.

Niu, G.Y., Yang, Z.L., Dickinson, R.E., Gulden, L.E. and Su, H., 2007. Development of a simple groundwater model for use in climate models and evaluation with Gravity Recovery and Climate Experiment data. Journal of Geophysical Research-Atmospheres, 112(D7).

Oke, A.M.C., Frost, A.J. and Beesley, C.A., 2009. The use of TRMM satellite data as a predictor in the spatial interpolation of daily precipitation over Australia. 18th World Imacs Congress and Modsim09 International Congress on Modelling and Simulation: Interfacing Modelling and Simulation with Mathematical and Computational Sciences. Univ Western Australia, Nedlands, 3726-3732 pp.

Pan, M. and Wood, E.F., 2006. Data assimilation for estimating the terrestrial water budget using a constrained ensemble Kalman filter. Journal of Hydrometeorology, 7(3): 534-547.

Pearson, C., 2008. Short- and medium-term climate information for water management. WMO Bulletin, 57(3): 173-177.

Peña-Arancibia, J.L., van Dijk, A.I.J.M., Renzullo, L.J. and Mulligan, M., 2013. Evaluation of Precipitation Estimation Accuracy in Reanalyses, Satellite Products, and an Ensemble Method for Regions in Australia and South and East Asia. Journal of Hydrometeorology, 14(4): 1323-1333.

Prakash, S., Mahesh, C. and Gairola, R.M., 2013. Comparison of TRMM Multi-satellite Precipitation Analysis (TMPA)-3B43 version 6 and 7 products with rain gauge data from ocean buoys. Remote Sensing Letters, 4(7): 677-685.

Ramillien, G., Frappart, F., Guntner, A., Ngo-Duc, T., Cazenave, A. and Laval, K., 2006. Time variations of the regional evapotranspiration rate from Gravity Recovery and Climate Experiment (GRACE) satellite gravimetry. Water Resources Research, 42(10).

Raupach, M.R., Briggs, P.R., Haverd, V., King, E.A., Paget, M.J. and Trudinger, C.M., 2009. Australian Water Availability Project (AWAP): CSIRO Marine and Atmospheric Research Component: Final Report for Phase 3. CAWCR Technical Report No. 013.

Rieser, D., Kuhn, M., Pail, R., Anjasmara, I.M. and Awange, J., 2010. Relation between GRACE-derived surface mass variations and precipitation over Australia. Australian Journal of Earth Sciences, 57(7): 887-900.

Rodell, M. and Famiglietti, J.S., 2001. An analysis of terrestrial water storage variations in Illinois with implications for the Gravity Recovery and Climate Experiment (GRACE). Water Resources Research, 37(5): 1327-1339.

Rodell, M., Famiglietti, J.S., Chen, J., Seneviratne, S.I., Viterbo, P., Holl, S. and Wilson, C.R., 2004. Basin scale estimates of evapotranspiration using GRACE and other observations. Geophysical Research Letters, 31(20).

Rodell, M., McWilliams, E.B., Famiglietti, J.S., Beaudoing, H.K. and Nigro, J., 2011. Estimating evapotranspiration using an observation based terrestrial water budget. Hydrological Processes, 25(26): 4082-4092.

Sahoo, A.K., Pan, M., Troy, T.J., Vinukollu, R.K., Sheffield, J. and Wood, E.F., 2011. Reconciling the global terrestrial water budget using satellite remote sensing. Remote Sensing of Environment, 115(8): 1850-1865.

Schultz, G.A. and Engman, E.T., 2001. Present use and future perspectives of remote sensing in hydrology and water management. Remote Sensing and Hydrology 2000(267): 545-551, 610.

Sellers, P.J., Hall, F.G., Asrar, G., Strebel, D.E. and Murphy, R.E., 1992. An overview of the 1st International Satellite Land Surface Climatology Project (ISLSCP) Field Experiment (FIFE). Journal of Geophysical Research-Atmospheres, 97(D17): 18345-18371.

Sheffield, J., Ferguson, C.R., Troy, T.J., Wood, E.F. and McCabe, M.F., 2009. Closing the terrestrial water budget from satellite remote sensing. Geophysical Research Letters, 36.

Sun, Z.G., Wang, Q.X., Ouyang, Z., Watanabe, M., Matsushita, B. and Fukushima, T., 2007.

Evaluation of MOD16 algorithm using MODIS and ground observational data in winter wheat field in North China Plain. Hydrological Processes, 21(9): 1196-1206.

Swenson, S. and Wahr, J., 2009. Monitoring the water balance of Lake Victoria, East Africa, from space. Journal of Hydrology, 370(1-4): 163-176.

van Dijk, A.I.J.M., 2010. The Australian Water Resources Assessment System. Technical Report 3. Landscape Model (version 0.5) Technical Description. CSIRO: Water for a Healthy Country National Research Flagship.

van Dijk, A.I.J.M., Renzullo, L.J. and Rodell, M., 2011. Use of Gravity Recovery and Climate Experiment terrestrial water storage retrievals to evaluate model estimates by the Australian water resources assessment system. Water Resources Research, 47.

van Dijk, A.I.J.M. and Warren, G., 2010. The Australian Water Resources Assessment System Technical Report 4.Landscape Model (version 0.5) Evaluation Against Observations.

Zaitchik, B.F., Rodell, M. and Reichle, R.H., 2008. Assimilation of GRACE terrestrial water storage data into a Land Surface Model: Results for the Mississippi River basin. Journal of Hydrometeorology, 9(3): 535-548.

Zhang, K., Kimball, J.S., Mu, Q.Z., Jones, L.A., Goetz, S.J. and Running, S.W., 2009. Satellite based analysis of northern ET trends and associated changes in the regional water balance from 1983 to 2005. Journal of Hydrology, 379(1-2): 92-110.